University of Southampton

An analysis of drivers of seawater temperature in Kuwait Bay, Arabian Gulf

By

Thamer Badi Al-Rashidi

This thesis is submitted for Doctor of Philosophy

Faculty of Engineering, Science and Mathematics

School of Ocean and Earth Sciences

November 2009

UNIVERSITY OF SOUTHAMPTON

ABSTRACT

FACULTY OF ENGINEERING, SCIENCE AND MATHEMATICS
SCHOOL OF OCEAN AND EARTH SCIENCES

Doctor of Philosophy

AN ANALYSIS OF DRIVERS OF SEAWATER TEMPERATURE IN KUWAIT BAY, ARABIAN GULF

By Thamer Al-Rashidi

Kuwait Bay presents a unique ecosystem and a significant nursery ground for many fish and shrimp species. In the last three decades, the bay has been under pressure from urbanization as well as from development from the entire region of the Arabian Gulf. Seawater temperature has an important impact on the marine environment. The aim of this study is to evaluate the drivers of seawater temperature in Kuwait Bay over the last two decades. Moderate Resolution Imaging Spectro-radiometer (MODIS) and Landsat satellites images were used to describe the spatial and temporal distribution of sea surface temperature (SST) in the Arabian Gulf and Kuwait Bay. Hourly temperature measurements collected during the winter, 2007 and summer, 2008 were used to define the vertical temperature gradient in the water column, sea-bed and the intertidal flats of Kuwait Bay. Advanced Very High Resolution Radiometric (AVHRR) satellite data collected between 1985 and 2007 was also used to study the trends and drivers of increasing SST in Kuwait Bay over the last two decades.

Satellite imaging showed that generally SST of Kuwait Bay is higher in the south than in the north. Highest SST was recorded near local human activities especially close to power and desalination plants due to thermal discharges. The field measurements showed that the water temperature is well-mixed in the bay. Seawater temperature reached 37 ºC in summer and dropped to 15.2 ºC in winter. Measurements beneath the sea-bed and within the intertidal flats showed that the temperature increased with depth in winter and decreased in summer. In winter, the sea-bed and intertidal flats are a source of heat to the water column, during summer

the opposite is true. AVHRR data showed that the seawater temperature increased in Kuwait Bay by 0.62 (± 0.01) ºC/decade in the last two decades. This trend is three times greater than the global average. The defined trends were substantiated by routine *in situ* monthly measurements of SST made by the EPA in the bay, and were also similar in pattern and trend to air temperature recorded at Kuwait airport. Temperature trends have been affected by drivers, conveniently sub-divided into global (which contributes 37% of the change), regional (which contributes 50% of the change) and local (which contributes 13% of the change). SST measurements showed peaks in summer temperature coincident with El Niño events in 1998 and 2003. The measurements also showed a relatively-low summertime peak during 1991 in the aftermath of Iraqi invasion of Kuwait due to atmospheric dimming brought about by dense smoke that persisted in the region for most of that year. The long term trend also showed a drop in temperature after 2004 as a result of increasing dust storm frequency in the region. Air temperature was found to be the most dominant driver of seawater temperature in Kuwait Bay and operates at a regional scale. At the local scale the seawater temperature of Kuwait Bay is influenced by intertidal flat exposure time and the thermal discharge from power and desalination plants.

ACKNOWLEDGEMENTS

First of all I would like to thank Professor Carl Amos, for all of his constant help, support, motivation, and guidance throughout every stage of my PhD study until the completion of this thesis. Also, thanks to Professor Robert Nicholls, Professor Ian Robinson, and Professor Andrew Bradbury for the helpful advice and support. I would like to give special thanks to Dr. Hamdy El-Gamily for the invaluable guidance, encouragement and friendship. I am also very appreciative of the massive help and support I have received from Dr. Karim Rakha. I am indebted to Dr. Khalid Al-Baana for assistance during the field work in Kuwait Bay.

I would like to say a word of gratitude to the National Oceanography Centre (NOC) for the use of facilities and the library. Also I would like to give thanks to Dr. Paolo Cipollini, Dr. Charlie Thompson, Dr. Simon Josey and Dr. Lisa Marsh for useful suggestions and discussions during my PhD study. I must also thank Mrs. Kate Davis for help with the thesis graphics. Dr. Mohammad Qurban needs to be acknowledged for his support through my study. Also I would like to thank my friends Amr Deaf and Turki Al-Raddidi.

I am grateful to Kuwait Institute for Scientific Research for use of the facilities and the help with the field work. I am truly grateful to the Kuwait Navy for the financial support and the scholarship that made it possible for me to obtain this degree. A special word of thanks should go to Dr. Peter Petrov and Fahad Alawadi in the Regional Organization for the Protection of the Marine Environment for providing MODIS satellite images of the study area. Also thanks to Hasan Al-Dashti in the Meteorological Department in Kuwait Airport for providing air temperature data. Thanks to the Environment Public Authority in Kuwait for providing me with seawater temperature data. Thanks to AVHRR Oceans Pathfinder project at NASA Jet Propulsion Laboratory, Physical Oceanography Distributed Active Archive Centre for the sea surface temperature data.

Finally I would like to give special thanks to my parents and my wife for support and encouragement during my study. This thesis would not have been possible without their support and encouragement.

GRADUATE SCHOOL OF THE SOUTHAMPTON OCEANOGRAPHY

This PhD dissertation by
Thamer Badi Al-Rashidi

has been produced under the supervision of the following persons;

Supervisor/s

Prof. Carl Amos
Prof. Robert Nicholls
Prof. Ian Robinson
Dr. Hamdy El-Gamily
Dr. Karim Rakha

Chair of Advisory Panel

Prof Andrew Bradbury

DECLARATION

This thesis is the result of work done wholly while under registered postgraduate candidature.

THESIS CONTENT

LIST OF FIGURES

LIST OF TABLES

LIST OF ABBREVIATIONS

AVHRR	Advanced Very High Resolution Radiometer
DN	Digital Number
EOS	Earth Observing System
ERSST	Extended Reconstructed Sea Surface Temperature data set
EPA	Environment Public Authority
ETM	Enhanced Thematic Mapper
GCP	Ground control point
GIS	Geographical Information System
ICOADS	International Comprehensive Ocean Atmosphere
JPL	Jet Propulsion Laboratory
KISR	Kuwait Institute for Scientific Research
MODIS	Moderate Resolution Imaging Spectrometer
MSS	Multispectral Scanner
NASA	National Space Agency
NCDC	National Climate Data Centre
ROPME	Regional Organization for the Protection of the Marine Environment
SST	Sea Surface Temperature
TM	Thematic Mapper
UNEP	United Nations Environment Program
USGS	US Geological Survey
UTM	Universal Transverse Mercator
WGS	World Geodetic System

LIST OF PUPLICATIONS

- Al-Rashidi, T. B., El-Gamily, H. I., Amos, C. L. and Rakha, K. A. (2009) Sea surface temperature trends in Kuwait Bay, Arabian Gulf. Natural Hazards, 50, 73-82.

- Al-Rashidi, T. B., El-Gamily, H. I., Amos, C. L. and Rakha, K. A. An early warning system for the potential impact of increasing the sea water temperature in Kuwait Bay. *Proc*. of First Regional Conference on Geoinformatics: Disaster Management and Early Warning Systems 24-26 November, 2008 State of Kuwait.

- Al-Rashidi, T. B., Amos, C. L. El-Gamily, H. I., and Rakha, K. A. Effects of regional drivers on the sea water temperature in Kuwait Bay, northern Arabian Gulf *Proc*. of International Symposium on Effects of Climate Change on the World's Oceans, 19-23 May 2008**.** Gijón, Spain.

- Al-Rashidi, T. B., Amos, C. L. and El-Gamily, H. I. (2007) Utilization of remotely sensed data to detect anthropogenic impacts on sea surface temperature of Kuwait Bay, Kuwait. Oceans 2007 - Europe, Vols 1-3, 94-98

Chapter 1: Introduction

1.1 Scientific contents and justification

Seawater temperature is a fundamental parameter in the marine environment (Stenseth et al., 2002), which has an important effect on species and marine habitats (Mahiko ABE, 2008). This thesis reports on the trends observed for seawater temperature in Kuwait Bay, northern Arabian Gulf (Figure, 1.1). The trend of seawater temperature is affected by a number of drivers at global, regional and local scales. Most of the work, to date, on the drivers of seawater temperature trends have been focused at the global level. However, within the Arabian Gulf, local and regional effects may be far more important in terms of future trends of seawater temperature than would be suggested by global trends. In view of this, all scales are analysed in this thesis from global to local in order to determine the relative contribution of each scale to the temperature change observed in Kuwait Bay.

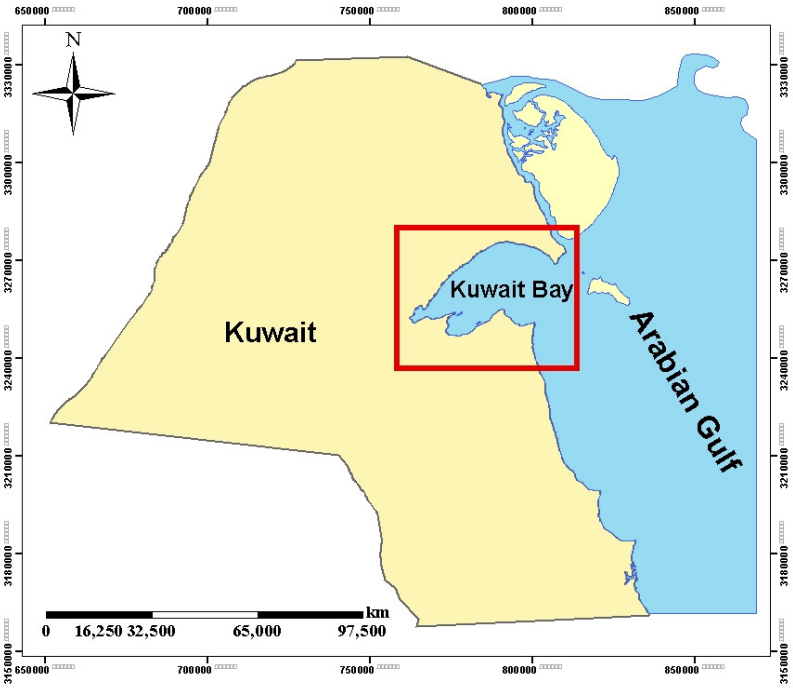

Figure 1.1: Kuwait Bay (the study area) located in the northern Arabian Gulf

Over the last century, global surface temperature has increased by 0.8 ºC due to the increase of anthropogenic greenhouse gases concentrations (IPCC, 2007). In

the last three decades, global warming has been estimated to be 0.2 ºC/decade over the land and ocean (GISS, 2005; IPCC, 2007). 0.27 ºC/ decade on the land and 0.13 ºC/decade in the ocean (Trenberth et al., 2007). Figure (1.2) shows the future scenarios of global surface temperature predicted in the IPCC Final Report. It shows that the expected temperature will increase by 1.8 to 4 ºC by the end of this century. The graph also shows that the range of predictions is very wide due to the different used scenarios.

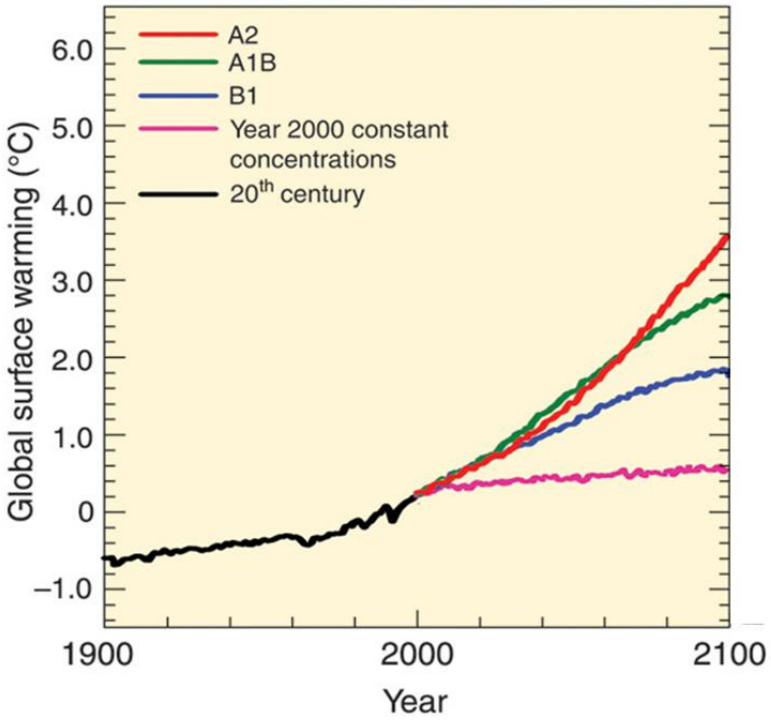

Figure 1.2: Observed and projected global mean temperature change according to different scenarios (IPCC, 2007). The solid lines are multi-model global averages of surface warming for scenarios A2, A1B and B1.

IPCC scenarios have been used to guide climate projections; but they have limitations when used for the projection at local scales (Ziervogel et al., 2003). Global monitoring of future climate change remains uncertain for specific regional impacts (Kabat et al., 2005). Warming due to global climate change differs from one location to another (Nature, 2006). So far, nobody has provided an analysis of various contributions of the temperature drivers at different scales. Indeed, it's proposed that local and regional drivers are dominant in regions of high population. The manifestation of the heat island effect is well documented for urban cities.

London, for example, is predicted to be 10 ºC higher than its surrounding areas by 2080 (Leake, 2009). In some coastal tropical cities such as Los Angeles and Mexico City, air temperature has increased by 0.6 ºC/decade in the last three decades (González et al., 2005). Gregory and Walling, (1980) divided the human source of heat that may influence the earth radiation balance into local, regional and global spatial scales. At the local scale, the activities are taking place within cities and are due mainly to urban heat effects. At the regional scale, the artificial heat source takes place at 100- 200 km: They refer to the heat sources across the regional scale to a global scale.

Seawater temperature trends have been found also to differ from location to location. Pearce and Feng (2007) found that the sea surface temperature (SST) has increased by 0.2 ºC/decade on the Western Australia coast, over the last 50 years. Khan et al., (2004) studied the variation of SST in the Arabian Sea and Bay of Bengal, from 1985 to 1998. They found that SST had increased by 0.2 ºC/decade in the Arabian Sea, NW Indian Ocean (in keeping with global averages), but had increased by 0.5 - 0.6 ºC/decade along the Southern coast of Oman (a rate much higher than the global average). This latter observation suggests that regional and local effects were at work on SST that was dominating over the global trends in temperature. It also suggests that local trends may exceed the global indicator. Yanagi (2008) used seawater temperature measurements from 1976 to 1997 in Tokyo Bay of Japan and found that the seawater temperature increased by 1.5 ºC/decade: He foud that high local anthropogenic activities are greater than the global warming effect in the bay. The scientific objective of this thesis is thus to quantify the contribution of the global, regional and local drivers of seawater temperature trends in Kuwait Bay, for the purposes of better predictions.

1.2 Background to measurements of seawater temperature

The British Challenger Expedition of 1873-1876 was the first to measure seawater temperature (Sverdrup, 1945). Seawater temperature was measured with instruments such as:

1. accurate thermometers of standard type, for measuring the sea surface temperature;

2. reversing thermometers, used for measuring the temperature at subsurface levels;
3. bathythermographs, to record temperature variations with depth;
4. In additional recently, CTD (conductivity, temperature and depth) recorders; or
5. satellites, by converting infrared radiation to an electrical signal.

The global seawater temperature ranges from -2 ºC to +30 ºC, the upper limit depends on the radiation and the heat exchange with the atmosphere, whereas the lower limit depends on the formation of ice (Sverdrup, 1945). Figure 1.3 showed the global distribution of seawater temperature at the surface. The warmest temperature is near the equator and the coldest temperature is near the poles.

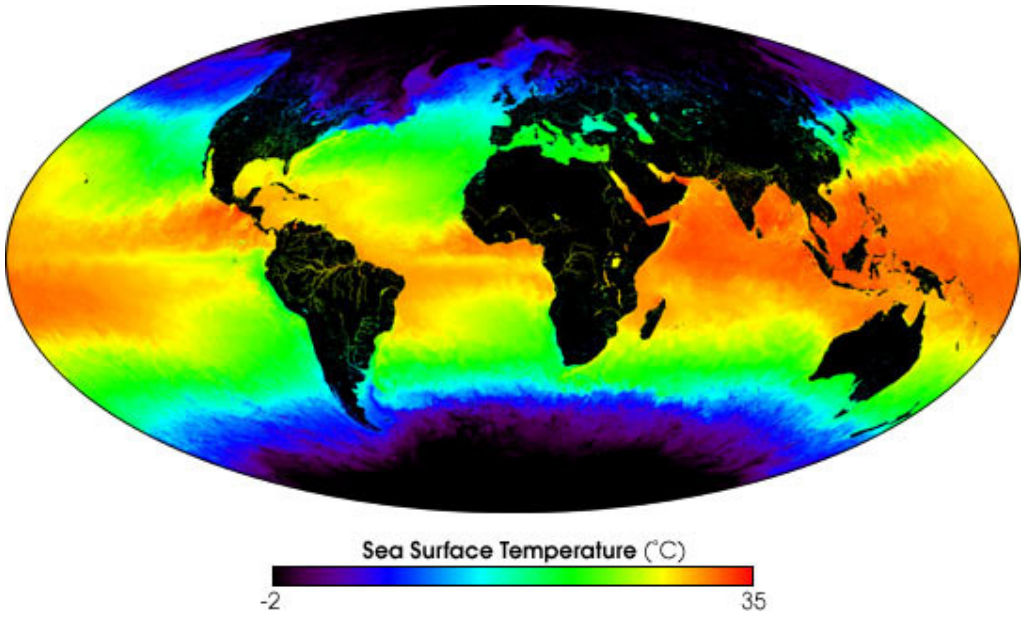

Figure 1.3: MODIS SST for May 2001 describes the Global distribution of seawater temperature at the surface. The warmest temperature is near the equator and the coldest temperature is near the poles (NASA, 2009b)

The freezing point of sea water is -1.9 ºC and depends on the salt content (Devries et al., 1970). About 75% of the ocean temperature lies between 0 and 4 ºC (Knauss, 1997). Figure 1.4 shows typical vertical temperature profiles in the open Ocean. In the low and middle latitudes, surface water is warm and it decreases with increasing depth. In the high latitudes, the temperature is low from the surface to the bottom. The seawater temperature is an important control on water circulation. Ocean currents are driven by density, wind and tide (Knauss, 1997). The density is determined by temperature, salinity and depth (Sverdrup et al., 1942). Therefore,

temperature and salinity are two fundamental parameters to understand transport, mixing and stratification of the coastal ocean. Temperature provides information about the heat exchange in the seawater, whilst salinity provides information about movements and dilution (Al-Yamani et al., 2004). Thus, the temperature of seawater is fundamental for the thermohaline circulation of the ocean. The thermohaline circulation is a central factor in climate variability (Jayne and Marotzke, 1999).

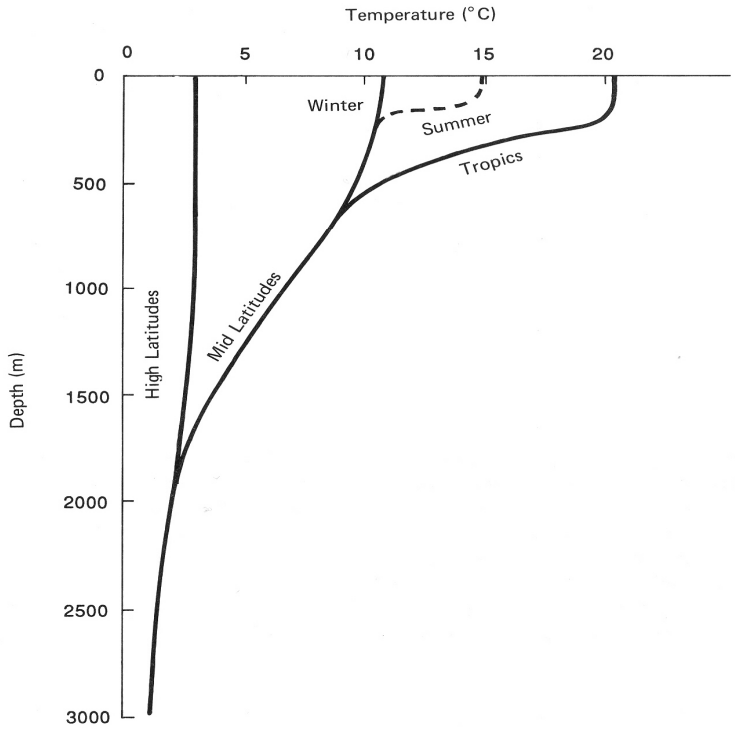

Figure 1.4: Typical temperature profiles in the open ocean. The temperature is warm at the surface and it decreases with increasing depth in the middle and low latitudes. In the high latitudes the temperature is low from the surface to the bottom (After Knauss, 1997).

1.3 Impact of seawater temperature rise on habitats

Seawater temperature is considered as an important factor in controlling propagation, metabolism and species diversity in the marine environment (Stenseth et al., 2002). Seawater temperature is also an important controlling factor in the ecological balance (Etnoyer et al., 2004). Marine habitats such as coral reefs, seagrasses and mangroves are restricted to specific ranges of water temperature (Campbell et al., 2006). In general, the rise of seawater temperature is linked to

losses in marine habitats (Sheppard and Rayner, 2002). Changes of temperature could have serious and rapid effects on species mortality, as well as on their geographic distribution. Seawater temperature increase is considered to be the primary cause of coral bleaching (Coles and Brown, 2003). Coral mortality has largely taken place in the Indian Ocean due to an increase in seawater temperature of 1-2 ºC, for the duration of only a few weeks (Wilkinson, 2000). Also, seawater temperature affects the growth of seagrasses (Lécuyer et al., 1996). A temperature above 35 ºC, for example, is considered to be the thermal stress threshold for *Halophila ovalis* (Ralph, 1998). Campbell et al., (2006) found that seawater temperatures between 40-45 ºC, even for a short period of time, significantly affect the mortality in seven tropical species of seagrasses (*Cymodocea rotundata, Cymodocea serrulata, Halodule uninervis, Halophila ovalis, Syringodium soetifolium, Thalassia hemprichii and Zostera capricorn*). Variability in the seawater temperature could also have a major impact on mangrove mortality. Paula et al., (2003) found that seawater temperatures above 35 ºC could effect the survival of mangrove larval developments in South Africa. Temperature affects also the amount of dissolved oxygen in seawater. The optimal aquatic range of dissolved oxygen in seawater for growth activity is 5.0 to 6.0 mg/L. Decreasing dissolved oxygen in seawater can harm aquatic animals such as fish (Burton et al., 1980). Matthews and Berg, (1997) found that, if the level of dissolved oxygen is lower than 3 mg/L it can be stressful to fish. Table 1.1 illustrates the relationship between dissolved oxygen and seawater temperature. As seawater temperature increases, the concentration of dissolved oxygen decreases (Morton et al., 1997; Weiss, 1970). Seawater temperature has been considered the dominant factor controlling fin-fish dynamics and has been associated recently with massive fish kills of wild mullet (*Liza klunzingeri*) in Kuwait Bay, in August, 2001 (Glibert et al., 2002). Thus, seawater temperature is one of the main limiting factors controlling ecosystems 'well-being' in the marine environment of the Arabian Gulf.

Table 1.1: Relationship between dissolved oxygen and seawater temperature in still water (Salinity=40‰) (Weiss, 1970)

Temperature (°C)	O_2 (ml/L)
0	7.77
5	6.86
10	6.12
15	5.52
20	5.02
25	4.59
30	4.24
35	3.93

1.4 Drivers of seawater temperature

Within the context of this thesis, changes in the seawater temperature are considered to arise from three scales of drivers: global, regional, and local. Global drivers are those sources of heat that may be considered to have an impact on seawater temperature that is the same everywhere. One such driver is global warming, due to the increase of greenhouse gas concentration and thermal insulation due to CO_2 in the atmosphere (Cox et al., 2000; IPCC, 2007; Jenkinson et al., 1991; Manabe and Stouffer, 1980). Whilst it is clear that a global average is only significant in the long-term and may not be appropriate at smaller scales, it is considered to be the effect that could, in theory, be evident once the impact of regional and local drivers has been accounted for.

Regional drivers lie between local and global scales; they are the sum total effect of a number of peripheral drivers. Regional drivers are those that may be considered to influence the Gulf region, as a whole. These drivers include: changing weather patterns; circulation and mixing in the Arabian Gulf; fresh water discharge from the Euphrates and Tigris rivers, into the northern Arabian Gulf; and dust storms. The source of heat at the regional scale is considered to come from global and local drivers. Regional drivers are manifested by seawater temperature changes

of water masses largely away from the shoreline; these are distinct in character from those at smaller and larger scales. The source of the regional drivers is a sum of local sources in the Gulf region. Shelf water masses may be considered as an example of this, which collectively are defined as the Coastal Ocean.

Local drivers are those sources of heat that may be detected and defined from a clearly-defined adjacent source, which may be traced without interruption from that source. Local drivers are manifested by thermal plumes from point sources at the shoreline and the warming of intertidal waters by conduction from the land mass. In Kuwait Bay, local drivers of seawater temperature rise are largely anthropogenic and are found along the coastline. These include urban development of the coastline, thermal discharge from power and desalination plants, and sewage discharge (Al-Zaidan et al., 2003; Al Bakri and Kittaneh, 1998).

Figure 1.4 is a schematic diagram of the interactions considered to link local, regional and global drivers. In this thesis, a cascading approach has been taken to analyse the drivers of temperature change. Local sources refer largely to the smallest spatial and temporal scales, that is, the coherent events that can be distinguished reasonably, from either satellite thermal imagery or ground measurements. The sum total of local heat sources combine to yield the regional (and, thus, non-local) trends in temperature change. While it is clear that regional drivers (such a weather patterns) operate also at the local scale, this has not been included in the discrimination of drivers. Global source can be defined only after considerable data compilation and analysis.

In Kuwait Bay, local drivers of temperature change are typically found within 30 km of the shoreline; they can change in intensity in periods from hours to days. Whilst it is likely that some local sources of heat are apparent in the open Gulf (oil production platforms, network gas seeps, ground water escape), these are more clearly visible in satellite imagery and so it is assumed that temperature trends defined beyond the detected influences of shoreline are controlled by regional drivers.

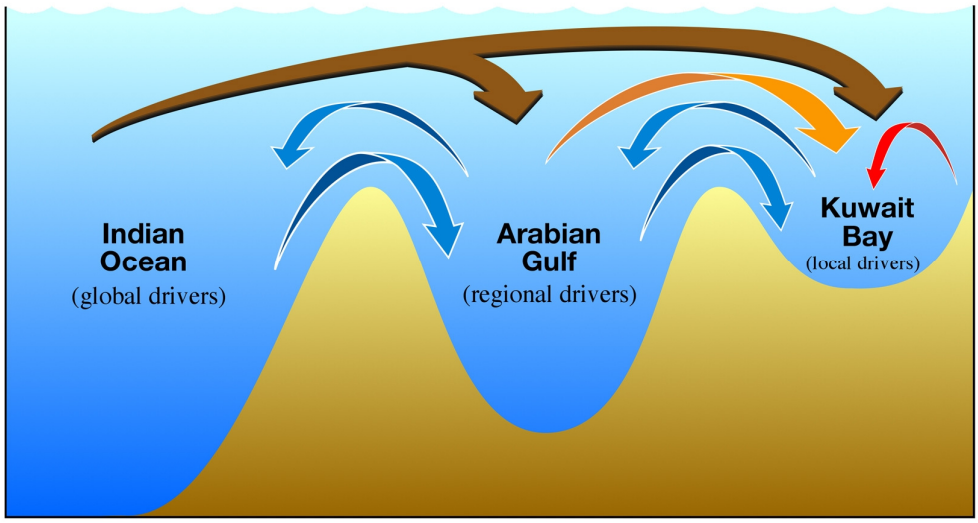

Figure 1.5: A schematic diagram of the drivers of seawater temperature trends in the Arabian Gulf. Local drivers (red arrow) have small spatial scales (typically less than 30 km) and have temporal scales (hours to days), and can be traced directly to the source of heat forming them. Global drivers (Brown arrow) operate at larger scales and have been defined from the literature (IPCC, 2007). Regional drivers are those that operate between local and global scales (orange arrow) they are typical seasonal temporal scales and reflect trends that operate through the Gulf region, for example. The blue arrows represent the heat exchange between Kuwait Bay and Arabian Gulf, also, heat exchange between Arabian Gulf and Indian Ocean. For simplicity we do not consider exchanges in heat at local to local scales or regional into regional scales.

1.5 Statement of the Problem

The Arabian Gulf has recently suffered habitat degradation (Khan, 2006). Coral reefs in the southern part of the Arabian Gulf have measurably deteriorated, in response to increasing seawater temperature (Sheppard and Rayner, 2002). An hypothesis to explain the damage of the coral reefs is the high fluctuation of the heating/cooling of seawater temperature in the region (Riegl, 2003). Recent research in the southern part of the Arabian Gulf identified two positive seawater temperature anomalies in the summer of 1996 and 1998 that resulted in high coral reef mortality off Dubai (Riegl, 2002; Sheppard and Loughland, 2002). Rezai et al., (2004) found that the Arabian Gulf is one of the areas worst affected by coral bleaching. Today, less than 1% of the original coral cover is still living in many coastal areas. They also found a direct effect of human activity on coral reef mortality. Gischler et al., (2005) showed also that coral reefs are practically or completely dead off Kuwait. Thus, the problem of coral bleaching is widespread in the Gulf. The fresh water discharge to the Gulf has been reduced from the Euphrates and Tigris Rivers (through the Shatt

Al-Arab), resulting in higher temperatures. Also, the Gulf War has impacted marine ecosystems through oil spills to the region and atmospheric smoke that blanketed the region and blocked out sunlight, for several months.

The state of Kuwait has experienced an increase in environmental degradation of the coastal zone due to limited controls on waste discharge, aquaculture, oil transportation, desalination, the construction of marinas, resorts, and the expansion of commercial as well as residential developments (Al-Zaidan et al., 2003). The proximity of industrial activities and recreational areas, to the coasts, is likely to lead to further deterioration of environmental quality. The capacity of coastal waters in Kuwait to absorb the impact of coastal development is strongly influenced by the physical and chemical oceanography of the local marine environment, as well as in the rate and magnitude of coastal impacts (Al-Yamani et al., 2004). Seagrasses and mangroves have also disappeared from the Kuwait coastal zone over the last 20 years, in response to rapid human development (Al-Awadhi pers.com; El-Sammak, pers.com). The lack of mangroves in Kuwait Bay is notable, rather surprisingly given that the region is macrotidal (4 m spring tidal range) and has wide, well-flushed and muddy intertidal flats, which provide suitable habitats. Seagrass is absent, despite the presence of intertidal, ventilated and hard substrates on which they normally attach. Turbidity is a possible factor limiting the growth of coral in the Kuwait Bay, as they are particularly sensitive to light and turbidity (Jones et al., 2002). Pollution has also been postulated as a cause of the impoverished habitats of the region (Al-Zaidan et al., 2000). However, it has only recently come under development and water pollution is a relatively recent phenomenon (Khan, 2006). By default, it would appear that increasing seawater temperature is contributing to the loss of key species in the region. The purpose of this thesis is to address the effect of global, regional and local drivers on the seawater temperature in Kuwait Bay, in order to examine their influence on habitats losses.

1. 6 Aims and objectives

The main aim of this research is to understand the factors influencing the seawater temperature in Kuwait Bay. The detailed objectives are as follows:

1. to define the distribution patterns of the seawater temperature in Kuwait Bay;

2. to define the trends in seawater temperature of Kuwait Bay over the last 20-30 years;
3. to evaluate the influence of global, regional and local drivers of seawater temperature in Kuwait Bay;
4. to determine the influence of seawater temperature in the Arabian Gulf on that in Kuwait Bay;
5. to evaluate the influence of human activities on seawater temperature in Kuwait Bay; and
6. to examine factors controlling the drivers of seawater temperature, and thus examine future scenarios of temperature change in the region.

The approach of this study is to use time-series observations of seawater temperature, from a variety of sources, to define trends in seawater temperature in Kuwait Bay. These data source are:

- thermal (AVHRR, MODIS, Landsat) satellite images to define spatial trends in the Gulf region over the last 20 years;
- Kuwait Environment Public Authority (EPA) seawater temperature measurements, to validate the seawater temperature derived from the satellite images; and
- *in situ* measurements of seawater, sea-bed and intertidal flat sediments temperature, in order to examine the high frequencies, variation and fluctuations in vertical temperature.

1. 7 Thesis outline

This thesis contains seven Chapters. The first Chapter provides a general introduction, a statement of the problem, the purpose of the study, and the main aims and objectives of the research. Chapter 2 provides a general description of the study area, from the literature. Chapter 3 is a literature review of the use of satellites in the prediction of sea surface temperature (SST). Chapter 4 defines the current state for seawater temperature in the study region. In this Chapter, remotely sensed data are used to demonstrate the distribution of SST in the study area. Field measurements are used to define the vertical variation in seawater temperature. This Chapter provides

also a description of the heat flow into the sea-bed and into the intertidal flats of Kuwait Bay from the overlying water mass. Chapter 5 examines the long-term trends in seawater temperature in the study region. Chapter 6 defines the most important regional drivers that affect seawater temperature in Kuwait Bay, and how these drivers influence seawater temperature in the study region. Chapter 7 defines the most significant local drivers of seawater temperature in Kuwait Bay, and how these drivers influence seawater temperature. Finally, Chapter 8 provides a general discussion, conclusions and recommendations for future work.

Chapter 2: The study region

2.1 Arabian Gulf

2.1.1 Geophysical setting

The Arabian Gulf is a shallow semi-enclosed water body; it is a marginal sea separated from the Arabian Sea of the Indian Ocean by the Strait of Hormuz (Figure 2.1). It is located within the arid region of the Middle East between latitudes 24 º and 30 º N and longitudes 48 º and 56 º E (Al-Ghadban et al., 1998; Elshorbagy, 2005; Robinson and Brink, 2006). The Arabian Gulf is bordered by Iran and seven Arab countries, namely, Iraq, Kuwait, Saudi Arabia, Bahraini, Qatar, the United Arab Emirates and Oman (Figure 2.1). Kuwait is located in the north-western part of the Arabian Gulf. It extends nearly 1000 km from the Shatt Al-Arab (a river formed by the confluence of the Tigris and Euphrates Rivers) to the Strait of Hormuz and has a maximum width of 370 km. The greater part of the Gulf is shallow with an average depth of 35 m, however the maximum depth is 100 m (K¨ampf and Sadrinasab, 2006).

The geomorphological character of the Arabian Gulf and its coastline configuration were created by Plio-Pleistocone tectonic movements (Robinson and Brink, 2006). Later tectonic activities were responsible for only minor adjustments of its present shape (Al-Asfour, 1981). The Arabian Gulf is a sedimentary basin due to its enclosed topographic conditions and favours production of biogenic sediments, especially by foraminifera and other micro-organisms (Al-Ghadban, 2002). The majority of fresh water supply to the Arabian Gulf comes from the Shatt Al-Arab waterway, containing the waters from the Tigris, Euphrates and Karun rivers; s mean flow of 1456 m^3 /s (Al-Yamani et al., 2007; Reynolds, 1993). Therefore, the sediment supplies from the Euphrates, Tigris and Karun rivers affect wide areas in the northern part of the Gulf, including the Bay of Kuwait (Al-Ghadban, 2002).

Figure 2.1: Location map of the Arabian Gulf. The Gulf is separated from the Arabian Sea of the Indian Ocean by the Strait of Hormuz. The Arabian Gulf is surrounded by Iran and seven Arab countries. Kuwait is located in the northern part of the Gulf

2.1.2 Climate

The Arabian Gulf is located in a typical north-temperate tropical climatic region, surrounded by deserts. The climate in the Arabian Gulf area is very cold in winter and very hot in summer (Al-Yamani et al., 2004). The maximum air temperature in summer is 50 °C and it can vary by as much as 20°C during the day, with relative humidity ranging from 40 to 100% (Al-Gahtani and Maslehuddin, 2002). The annual rainfall is low in the Gulf, providing only 7 cm yr^{-1}. The net evaporation is higher than both inflow from rivers and precipitation (Reynolds, 2002). Hence, the salinity in the northern Arabian Gulf ranges from 40 to 41 psu. However, it sometimes exceeds 50 psu due to the high rates of evaporation (Al-Yamani et al., 2004). Cool air originates from Turkey and enters the northern part of the Arabian Gulf via the Tigris-Euphrates valley (Robinson and Brink, 2006), which produces the well-known phenomenon in the Arabian Gulf region called the *shamal* (Arabic for North). The average wind speeds in the Gulf range between 30 and 40 knots, with high wind speeds reaching 50 knots. The *shamal* wind causes hot and dry dust storms particularly in July and August (Elshorbagy, 2005; Reynolds, 2002;

Robinson and Brink, 2006). Figure (2.2) shows a dust storm driven by *shamal* winds in the northern part of the Arabian Gulf (June 2008), as revealed from Moderate Resolution Imaging Spectroradiometer (MODIS) data provided by the Regional Organization for Protection of the Marine Environment in Kuwait (ROPME). Dust storm frequency has been increasing rapidly in the last few years and is now present over 25% of the year in Kuwait (Alsharhan, 2009). Most of these come from Iraq, in response to limited rainfall and increased desertification (Al-Haddad, 2009; Khalaf et al., 1985). Recently, military operations have made some contribution to the increasing dust storms in the region; in particular, the US invasion of Iraq in 2003 (Tharp, 2009).

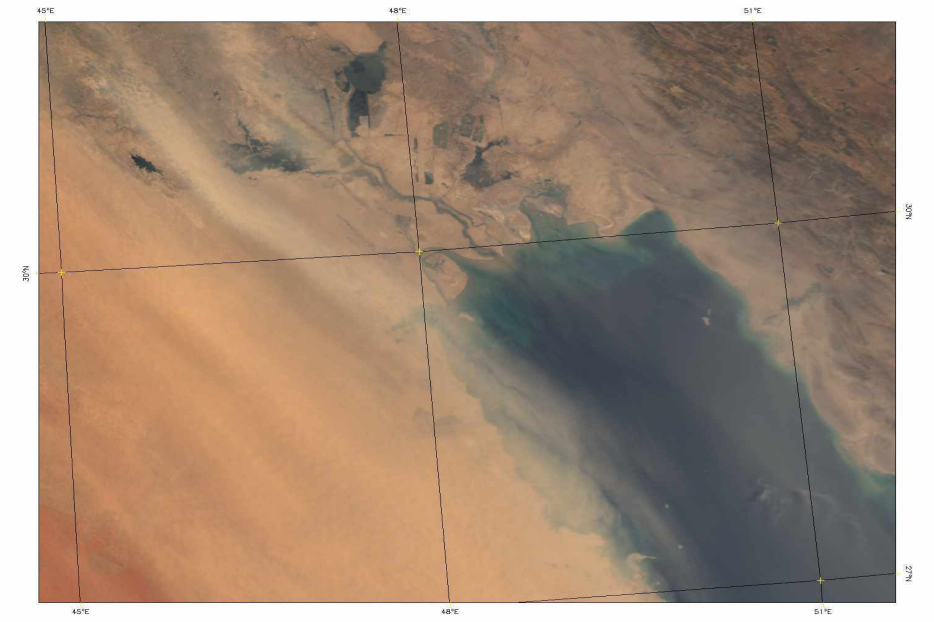

Figure 2.2: MODIS satellite image on 17th June 2008 shows one of the heavy dust storm in the northern part of the Arabian Gulf (data supplied by ROPME receiving station).

2.1.3 Oceanography: Tides, water circulation, and mixing

Tides, winds and waves are the three major factors affecting the mixing of the water column in the Arabian Gulf (Robinson and Brink, 2006). Tides in the Arabian Gulf are complex and vary from semi-diurnal to diurnal (Reynolds, 1993). The tidal range in the Gulf varies from about 1 m (during neap tides) to 4 m (during spring tides) in the north of the Gulf (Rakha et al., 2007). Figure (2.3) illustrates the maximum tidal range in the Arabian Gulf. It increases from the centre to the south and the north with the highest tidal range situated in the study area. The average

velocity of the surface and bottom residual current in the Arabian Gulf is about 6 cm s^{-1} (Abdelrahman and Ahmad, 1995). The general circulation of the water in the Arabian Gulf is anticlockwise due to the Coriolis Effect (Figure 2.3). Due to the shallow nature of the Gulf, wind has a significant effect on the water circulation and mixing (Swift and Bower, 2003). The northern part of the Arabian Gulf is dominated by north-westerly winds which force the currents southwards. This flow drives the river plume southwards along the Kuwaiti and Saudi coasts (Figure 2.3). According to (Reynolds, 2002), the water mass in the Arabian Gulf is stratified, particularly in the south, throughout the year. In the northern Gulf, the water column is well mixed in winter and stratified in summer. The stratification in summer is driven by high evaporation that leads to higher saline water that flows beneath surface water to the south. According to (Reynolds, 2002), upwelling occurs only along the southern coast of Iran. The mean annual water temperature in the Arabian Gulf is 25 ºC; it ranges from 10 ºC to 12.5 ºC in January and from 34 ºC to 35.5 ºC in July (Sheppard and Loughland, 2002).

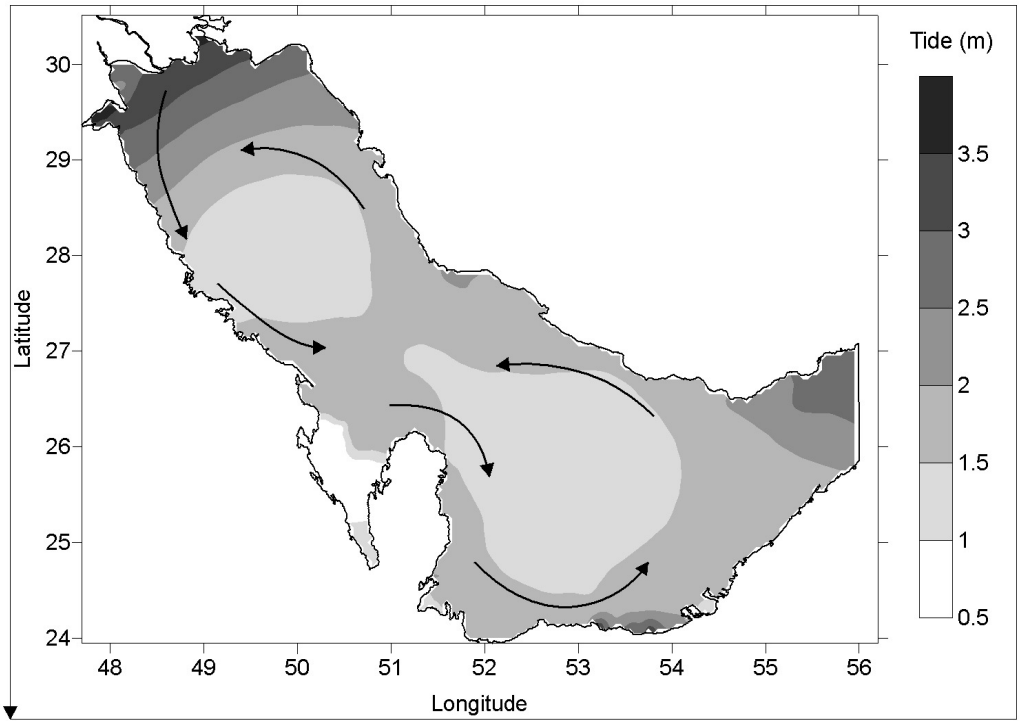

Figure 2.3: The maximum tidal range in the Arabian Gulf. The greatest variation is in the northern part of the Gulf (4 m in Kuwait Bay). The arrows show general circulation patterns in the Gulf (Rakha et al., 2007a; Robinson and Brink, 2006).

2.1.4 Human impact on seawater in the Arabian Gulf

Over the last four decades, rapid coastal industrial development has taken place around the Arabian Gulf. Development has brought desalination, power and petroleum refining plants (Khan, 2006). The construction of desalination plants has increased in the Arabian Gulf, due to the increased population and is the sole source of fresh water, for human use. The total production capacity was estimated at 5.075 million m^3/day, which represents 58% of the capacity of all desalination plants worldwide (Smith et al., 2007). The thermal pollution plume from industrial development has led to rises in seawater temperature which may affect the marine ecosystems in the Gulf (Al-Muzaini et al., 1997). Oil spills are among the major pollutants to affect the marine environment in the Arabian Gulf (Al-Muzaini et al., 1997). Oil absorbs heat and, hence, has the capacity to increase seawater temperature (Habib and Fakhral-Deen, 2001).

The fresh water discharge from the Shatt Al-Arab to the Arabian Gulf has decreased over the last century due to man-made dams and projects along the Euphrates and Tigris rivers. Turkey has constructed 22 dams and 19 power plants in the early 1980's along the Euphrates and Tigris rivers (El-Fadel et al., 2002). The discharge from the Shatt Al-Arab has been also used for marshland restoration south of Iraq, since April 2003 (Maxwell, 2006), because the marshlands were dried after construction of the third River in1990 (Al-Yamani et al., 2007). Reduction in the fresh water discharge from the Shatt al-Arab has led to increased salinity in the Gulf. High turbidity was recorded in the northern Arabian Gulf during the 2003 marshland restoration programme (Al-Yamani et al., 2007).

2.2 Kuwait Bay

2.2.1. Physical environment

a. Background and geophysical setting

Kuwait Bay is a relatively large embayment in the north-western corner of the Arabian Gulf (Figure, 2.4), which covers an area of about 720 km^2 (Al-Shemmari et al., 2002). Its maximum length is about 45 km in an east-west direction and its maximum width is about 25 km. The bay is relatively shallow, with an average water depth of 5 m (Al-Zaidan et al., 2006). Kuwait Bay is a semi-enclosed basin (semi-

sheltered), characterized by low wave energy and wide intertidal mud flats (Anderlini et al., 1982). Previous surveys have shown that the intertidal mudflats are the most prominent features of the bay (Al-Asfour, 1982; Al-Ghadban and El-Sammak, 2005; Anderlini et al., 1982), however the southern coast is sandy-mud or gravelly-sand (Al-Majed and Preston, 2004) rather than classical muds of other regions.

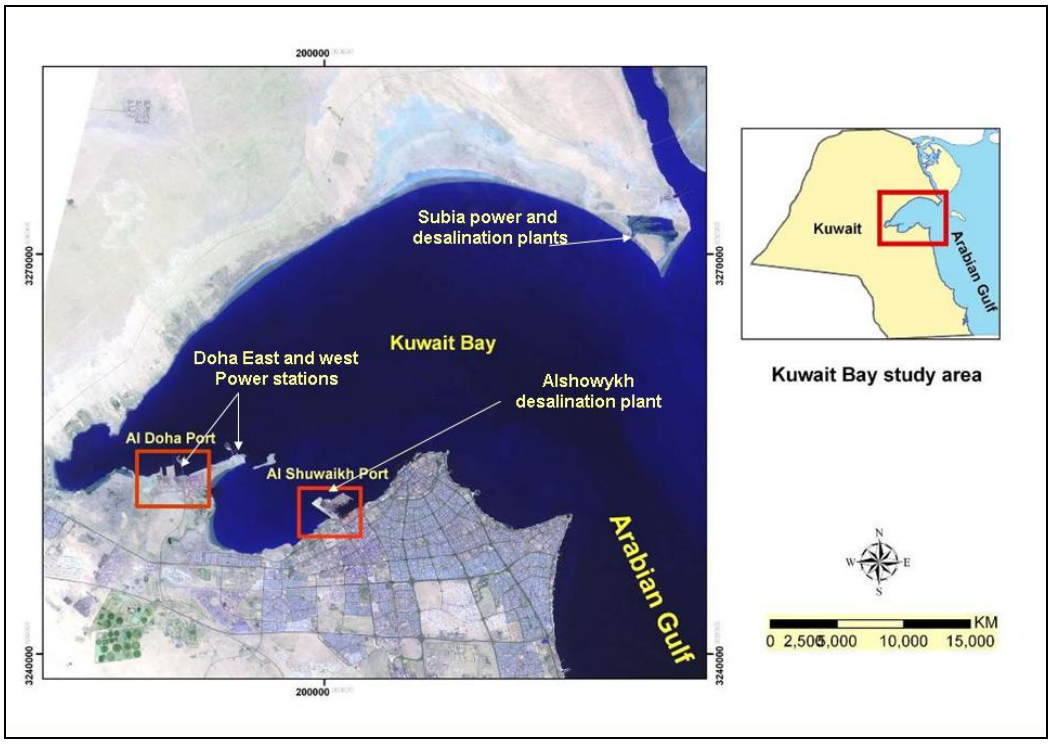

Figure 2.4: Location map of Kuwait Bay. The bay hosts two main ports, three power stations, and four desalination plants. Most of population resides along the south side of the bay.

Most of the population of Kuwait lives close to the coastline, on the southern side of the bay; there are no residents on the north side. Kuwait Bay hosts the major ports of Shuwaikh and Doha, and has three major power generating stations: Doha East; Doha West (west of the bay); and Subia (Figure 2.4). Also, it is the site of four desalination plants: Doha East; Doha West; Subia; and Alshoykh. In addition, there are many types of coastal development along the south side of the bay, such as marinas and tourist activities (Al-Ghadban et al., 1998; Al-Mussalam, 1999).

b. Weather

Kuwait Bay is subject to a hot and arid desert climate, with little rainfall (less than 120 mm/year) (Kwarteng et al., 2000). 80% of this rainfall falls in winter

between December and March (Nasrallah et al., 2004). Thus salinity is greatest during the summertime. Air temperature reaches 50 ºC in summer and can be as low as to -2 ºC in winter (Al-Bassam et al., 2009; Al-Zaidan et al., 2006; and AlFahed et al., 1997). The *shamal* wind is the dominant wind over Kuwait Bay which enhances water column mixing and also increases evaporation. These winds cause the re-suspension of bottom sediments in the bay and bring airborne dust to the region (Al-Asfour, 1981; Al-Yamani et al., 2004; and Al Bakri, 1996). Evaporation in Kuwait Bay is much higher than precipitation (Al-Yamani et al., 2004; Reynolds, 2002), resulting in the evaporative cooling of these waters, and resulting in hypersaline conditions, in particular over the intertidal flats.

c. Oceanographic Characteristics

- **Tides and currents**

The tides in Kuwait Bay are semidiurnal and range from 4 m during spring tide to 0.5 m during neap tide (Al-Yamani et al., 2004; Rakha et al., 2007). Figure (2.5) illustrates a tide gauge record for Al-Shuwaikh port (southern Kuwait Bay) during May 2009. The figure shows that the tide in Kuwait Bay has a large diurnal inequality. Tidal currents are the major source of water movement in Kuwait Bay (Anderlini et al., 1982). According to Al-Sarawi et al., (1988) and Rakha et al., (2007), the tidal currents are generally counter-clockwise in Kuwait Bay and have a peak current velocity of about 0.5 m s^{-1}. However, in some areas, the maximum currents can reach 1 m s^{-1} (Abouseida and Alsarawi, 1990; Rakha et al., 2007).

- **Water temperatures**

Previous research has shown that the water column is well mixed (Al-Yamani et al., 2007; Dames and Moore, 1983; and Khalaf et al., 1982) and the water temperature is high in August and low in January (Anderlini et al., 1982). The published mean annual temperature of Kuwait Bay surface water is 23.8 °C. The lowest seawater temperature recorded in Kuwait Bay was 11.9 °C in January 1993 and the highest water was 36 °C in August, 2001 (Al-Yamani et al., 2004; Glibert et al., 2002). This indicates that the seasonal fluctuation in the seawater temperature is about 25°C, whereas the daily fluctuation is about 7 °C (Dames and Moore, 1983).

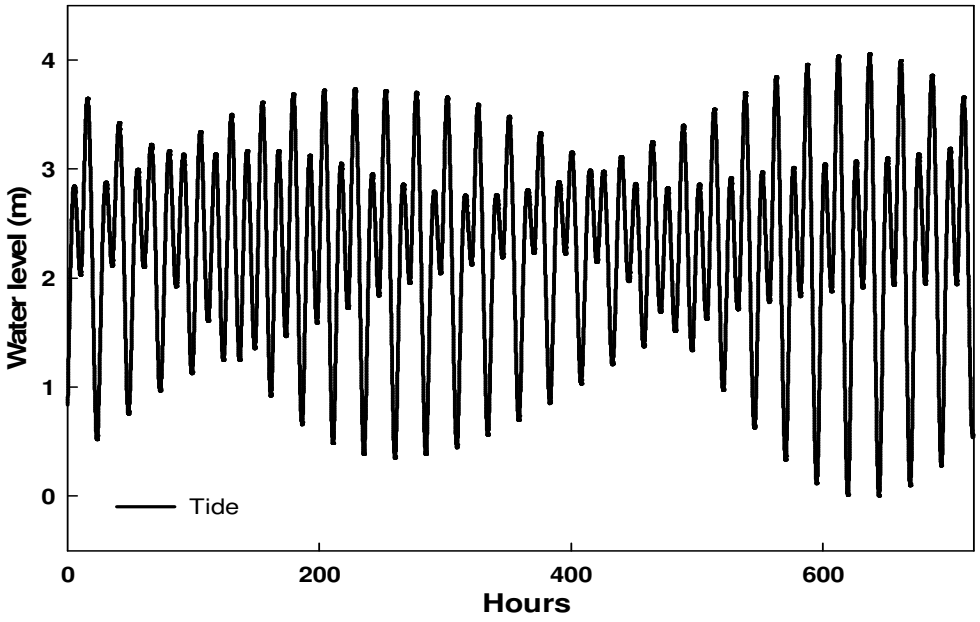

Figure 2.5: Water level fluctuations at Al-Shuwaikh port (Kuwait Bay), during May, 2009. The Figure shows that the tide in Kuwait Bay has a large diurnal inequality and a wide spring-neap variation.

- **Salinity**

The salinity of seawater in Kuwait Bay is affected by high atmospheric temperatures, high evaporation and the fresh water inflow from the Shatt Al-Arab (Anderlini et al., 1982). In general, the salinity in Kuwait Bay ranges from approximately 37 psu to 50 psu, with highest concentrations occurring in December (at the end of the dry season) and lowest values during February (at the end of the wet season) (Al Bakri and Kittaneh, 1998).

- **Sediment and sediment transport**

According to Khalaf et al., (1982) and Al-Ghadban and Salman, (1993), Kuwait Bay may be divided into two main zones: a low-energy zone located in the northern part, which is underlain by bottom mud and muddy-sand sediments; and a moderate to high energy zone, restricted to an area covered by sand and sandy sediment, in the southern part. Due to its shallowness, it is affected strongly by wind generated waves.

The flood waters of the Tigris and Euphrates Rivers, which enter the northern end of the Gulf through the Shatt Al-Arab, bring sediment into the bay by longshore (eastward) residual flows (Al-Ghadban and El-Sammak, 2005; Anderlini et al., 1982;

Elsayed and Albakri, 1994; and Saad and Al-Azmi, 2002). The turbidity in Kuwait Bay is higher than any other location in the Arabian Gulf (Saad and Al-Azmi, 2002). Figure 2.6 illustrates a turbid plume from the Shatt Al-Arab imaged by the MODIS satellite on 8th August, 2006. This image, provided by the Regional Organization of Protection the Marine Environment (ROPME), shows that the turbidity is higher in the northern part of Kuwait Bay.

Figure 2.6: MODIS satellite image of 8th August, 2006 in the northern part of the Arabian Gulf. The image shows the turbid plume from Shatt Al-Arab as well as from the north of Kuwait (data supplied by ROPME receiving station).

Al-Ghadban and El-Sammak (2005) investigated the source of marine sediments in Kuwait Bay. They identified five major sources of suspended sediments in its waters: (1) dust fallout; (2) biogenic production; (3) Shatt Al-Arab alluvial sediments; (4) re-suspension of bottom sediments; and (5) particles contributed from construction and engineering works. They constructed a conceptual model for the suspended sediment transport pattern in Kuwait Bay (Figure, 2.7). This sediment contributes to the intertidal flats and accumulates on the seabed, thus influencing the physical properties of these substrates. This, in turn, affects the thermal capacity and transmissivity which influences water temperature (Cho et al., 2005). However, sandy intertidal flats respond much more to heat, than do muddy sediments (Abu-Hamdeh and Reeder, 2000; Newson and Brunning, 2004).

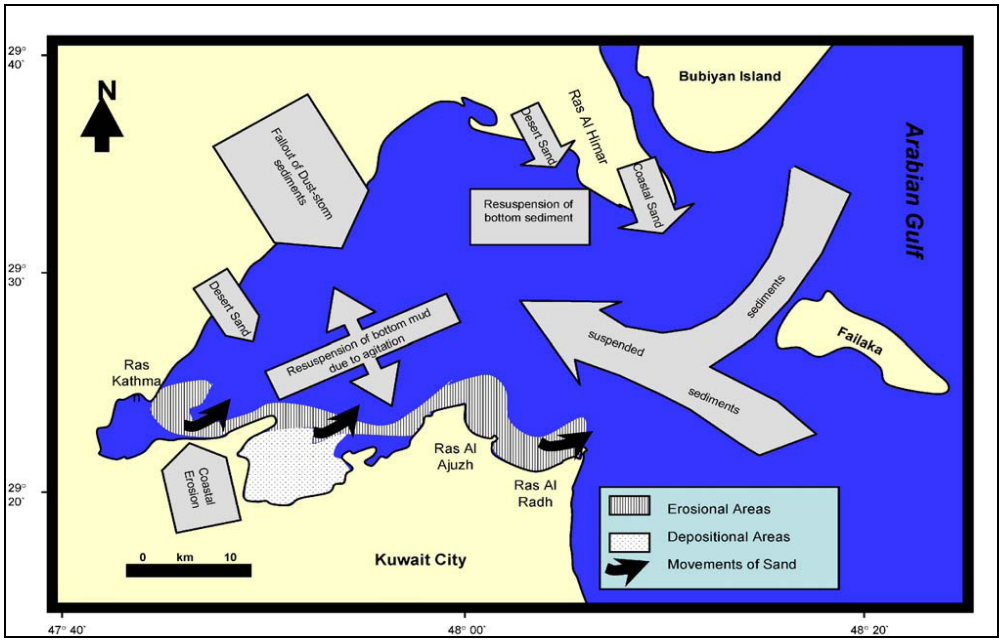

Figure 2.7: Conceptual model for the suspended sediment transport pattern in Kuwait Bay (Al-Ghadban and El-Sammak, 2005).

2.2.2 Ecological environment

The Kuwait coastline is described as a rich marine environment (Al-Yamani et al., 2004; Alabdulrazzaq et al., 1982). Alabdulrazzaq et al., (1982) studied the distribution and abundance of several species found in the sands of the bottom sediments in Kuwait Bay. They identified shell fragments, micro-bivalves, micro-gastropods, foraminifera, ostracods, echinoid fragments, corals, serpulid worms, holothurians, bryozoans, sponge spicules and alcyonarian spicules. Dames and Moore (1983) conducted a study in Kuwait Bay, as part of a multidisciplinary investigation and found planktonic (zooplankton, larval fish, and Crustacea), nektonic (fish and squid) and epigenetic (shrimp, carbs and sea urchins) assemblages in Kuwait Bay. The bay fauna was once rich and diverse, but recent studies suggest that many species are disappearing as they reach the limit of heat tolerance (Al-Zaidan et al., 2003; Gischler et al., 2005; Glibert et al., 2002; and Sheppard and Rayner, 2002).

Red tides were reported in Kuwait Bay in 1999 (Rao et al., 1999). A high water temperature was recorded at the time of the massive fish kills of wild mullet (*Liza klunzingeri*), which took place in Kuwait Bay during the summer of 2001 (Glibert et al., 2002). Gischler et al., (2005) reported that the coral reefs off Kuwait exist only in the open Gulf and not in Kuwait Bay itself; most of these corals reefs are dead or partially damaged. Mangroves and seagrassess are also absent from Kuwait Bay. However, planted mangroves have been grown in Kuwait Bay (Bhat et al., 2004). It is proposed here that the absence of coral, seagrasses and mangroves is as a result of the temperature changes as evident in southern Kuwait (Gischler et al., 2005).

2.2.3. Socio-economic environment

Kuwait's coastal zone is considered to have special importance because most of the country's urban, industrial, commercial and recreational activities are concentrated there (Abouseida and Alsarawi, 1990). Urban settlement along the coast of Kuwait has increased rapidly in the last 30 years (Al Bakri, 1996). The population of Kuwait is about 3 million; 1.5 million reside in the southern part of Kuwait Bay, unlike the north of the bay, where no-one lives (Ministry of Planning, 2005).

In Kuwait, the fisheries remain one of the major sources of nutrition, and fishing is an important economic activity. The local production of fish is about 50% of local demand. According to Al-Yamani et al., (2004) there is a large stock of fish in Kuwait Bay, due to the shallowness of the water and the plentiful food supplies from the Shatt Al-Arab delta in the northern part of Arabian Gulf.

Kuwait Bay is under pressure from urbanisation and development around its coastline. Figure 2.8 illustrates the type of human activity along this coastline. It is expected that water circulation, and consequently physical and biological processes will be affected by coastal development (Marmoush, 1999). Sediment resulting from coastal development can increase turbidity. Benthos, which is the main source of food for fish, can also be affected by dredging at the coast (Al-Ghadban and El-Sammak, 2005).

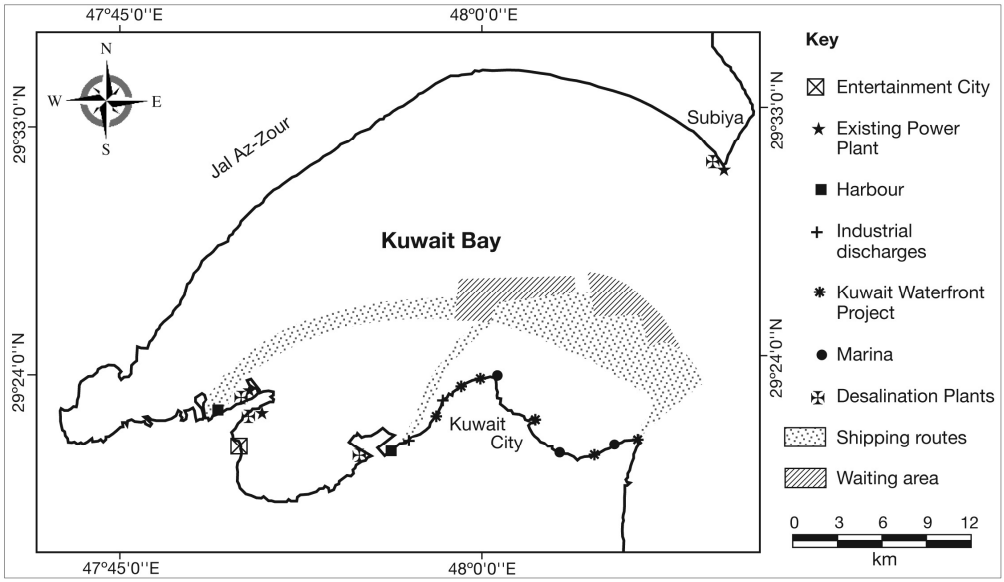

Figure 2.8: Human activities along the coastline of Kuwait Bay. Most of the activities are taking place along the south side of the bay. Only Subia power station is in the northern part of the bay (adapted after Al-Musalam, 1999).

The demand for fresh water and electricity has increased in the Arabian Gulf countries, due to the increase of population and changes in life style (Smith et al., 2007). In Kuwait, there are 11 power and desalination plants, 7 of them are located in Kuwait Bay (see Figure, 2.8). The thermal discharge from the power and desalination plants is leading to increased seawater temperatures in Kuwait Bay (Al Bakri and Kittaneh, 1998).

Kuwait's drainage system consists of storm water outfalls and emergency sewage outfalls. The southern coast of Kuwait Bay is subject to sewage pollution, due to the over discharge of sewage through emergency rainwater sewers, in particular from the port of Al-Shuwaikh (Al-Mussalam, 1999; Al Bakri, 1996). Figure 2.9 illustrates the sewage and storm water discharge into the bay, during heavy rains. It shows the region likely to be affected by thermal pollution from sewage. The sewage is the same temperature as the air temperature (approaching 50 ºC in summer); hence, it raises the seawater temperature in the coastal zone.

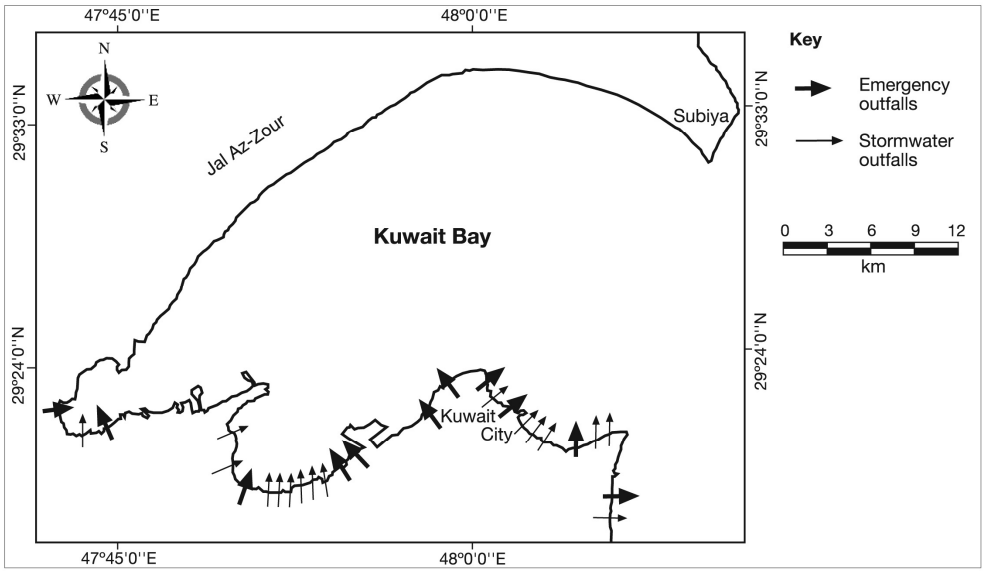

Figure 2.9: Discharge of sewage into the sea in Kuwait Bay (adapted after Al-Musalam, 1999).

On 2nd August, 1990, Kuwait was invaded by Iraqi troops. The environmental damage resulting from the invasion and the subsequent war of liberation has affected all the existing ecosystems, as well as human health (Al-Sarawi et al., 1988; Price, 1998). The coastal, marine, terrestrial and atmospheric sub-environments have all been affected by military operations. Spilling of oil into the marine and terrestrial environment and the burning of more than 730 oil wells in Kuwait are major sources of pollution (El-Gamily, 2007; UNEP, 1991; and Osman, 1997). This event is described as one of the largest marine environmental pollution incidents in history (Literathy, 1993; Readman et al., 1992). The impact of marine pollution as a result of the Gulf War has damaged critical habitats, not only in Kuwait waters but also along the Saudi Arabian coast (Gerges, 1993).

3. Chapter 3: Remote sensing and seawater temperature

3.1 Definition of remote sensing

Remote sensing is defined basically as the science and art of obtaining information about the objects or features on earth, without being in contact with them (Lillesand and Kiefer, 1987). Remote sensing technology has been used in ocean science to determine water colour and suspended sediments whilst water masses, since 1970 (Nelson et al., 2003). It depends on the interaction of the electromagnetic radiation with the water mass, land and atmosphere to obtain instantaneous information about these "themes" (Lillesand and Kiefer, 1987). Remote sensing techniques have developed rapidly in the last two decades, as the sensors which capture the data have been improved to provide better spectral and spatial resolutions (Robinson and Donlon, 2003). It has been identified as a powerful tool, producing information in spatial and temporal dimensions, instead of conventional *in-situ* measurement that is usually limited in space (Nelson et al., 2003). Remote sensing is a valuable tool not only for monitoring and examining water mass characteristics, but also for managing the coastal zone environment through routine monitoring (Sanderson, 2009).

There are two types of remote sensing sensor: passive and active. The passive sensor depends on the interaction of electromagnetic radiation from the sun with the Earth's surface. Basically, passive remote sensing techniques depend on measuring the energy which is reflected, transmitted, or emitted from any of the Earth's features. This kind of emitted, reflected, or transmitted energy is a function of the physical properties of the feature and the wavelength of the electromagnetic radiation (Lillesand and Kiefer, 1987). Therefore, optical remote sensing techniques are based on the electromagnetic energy from the Sun's light. However, active remote sensing, in contrast, depends on an artificial light source (Boyd and Danson, 2005). In this kind of remote sensing the active sensor uses outsourcing of radiation, which could be radar or microwave (Lillesand and Kiefer, 1987).

3.2 Remote sensing systems

A multispectral satellite sensor acquires multiple images of the same area (i.e. features of the Earth's surface), at different wavelengths (channels). Each channel measures unique spectral characteristics of the target. A spectral channel is a data set collected by the sensor with information from discrete portions of the electromagnetic spectrum (Green et al., 2000). Multispectral sensors focus on ranges within the electromagnetic radiation (EM) spectrum where radiation penetrates the air, with little or no loss by absorption of the target. Remote sensors on space platforms are programmed to operate in these optical windows and make measurements using detectors, tuned to the specific wavelength frequencies that pass through the atmosphere. Spectral reflectance characteristics of common earth surface materials are located within the visible and near-to mid-infrared range (Richards, 1986). However, thermal heat patterns are detected within the thermal infrared range.

Digital remote sensing systems convert electromagnetic energy (colour, light, heat, etc…) to digital form. Spatially, the data are composed of discrete picture elements, or pixels, and they are quantities radiometrically into discrete brightness levels (ERDAS, 1999). The great advantage of having data available digitally is that it can be processed by computer, either for machine-assisted information extraction or for enhancement by an image interpreter.

Resolution is an important term used commonly to describe remotely sensed imagery. However, there are four distinct types of resolution to be considered: spatial, spectral, radiometric, and temporal (NASA, 2009a). These resolution characteristics help to describe the functionality of both remote sensing sensors and remotely sensed data. To describe them in greater detail, the four resolutions are as follows:

A) Spatial resolution is the minimum size of a terrain feature that can be distinguished on the Earth by a satellite image, or the ability to differentiate between two closely spaced features in an image. It is also defined by the area on the ground that a pixel represents in a digital image file. "Large scale" in remote sensing refers to imagery in which each pixel represents a small area on the ground (e.g. Landsat). "Small scale" refers to imagery in which each pixel represents a large area on the ground (e.g. NOAA and MODIS);

B) spectral resolution refers to the number and dimension of specific wavelength intervals in the electromagnetic spectrum, in which a sensor or detector can record. Wide intervals in the electromagnetic spectrum are referred to as high spectral resolution, whilst narrow intervals are referred to as low spectral resolution. For example, Landsat is a high spectral resolution sensor with 9 channels, compared with NOAA, which has only four channels;

C) radiometric resolution refers to the dynamic range, or number of possible data-file values in each band. This is referred to by the number of bits into which the recorded energy is divided. For example, 8-bit data is broken down into 256 brightness levels; and

D) temporal resolution is a measure of how often a given sensor system obtains the imagery of a particular area, or how often an area can be revisited by the satellite. The temporal resolutions of satellites are on a fixed schedule. Temporal resolution is an important factor to consider in studies of change detection as well as monitoring our environment. For example, the NOAA satellite visits any given part of the Earth twice a day, compared with Landsat satellite, which revisits the same location once in 16 days (Wilkie and Finn, 1996).

3.3 Thermal remote sensing

The remote sensing sensors which operate in the thermal infrared range of the electromagnetic spectrum record the energy emitted from the Earth, in the wavelength range from 3 μm to 5 μm and from 8 μm to 14 μm (NASA, 2009a). The former range is related to high temperature phenomena such as forest fires, whilst the latter with general earth features having lower temperatures.

3.4 Thermal properties of water

Compared with land, water has very dark to medium grey tones in day-time thermal IR images, with moderately light tones in night-time thermal images. The interpretation of this means simply that it is cooler in the day and warmer at night, than most of the other materials in the scene (Notarstefano et al., 2006). This response is due, in part, to the retention by water of relatively high thermal energy,

compared with the land. It is due also to the fact that water is not a solid and is likely to experience disruption of its thermal gradient by convection (upwelling) and turbulence (wave action), which tend to mix the water mass (Al-Yamani et al., 2004). Consequently, the water temperature during thermal imaging is controlled by the time of the day when the image is captured.

Thermal infrared remote sensing has been an efficient tool for both oceanographers and meteorologists, in obtaining sea surface temperature measurements (Smith et al., 1996). It has been applied not only to the open ocean and coastal waters, but also to the surface temperature of inland waters and associated circulation patterns (Anderson et al., 1995; Garrett and Hayes, 1997), as well as heat dispersion in effluent plumes (Davies et al., 1997). It is a useful application for oil spill detection, since oil shows a number of thermal properties, which are clearly distinguishable from seawater. These include a unique heat capacity and thermal conductivity, since the oil acts as a black body absorbing heat and becoming warmer than the surrounding seawater. The difference in the thermal properties of oil and seawater allow potential discrimination within the thermal channels (Alawadi et al., 2008; Brekke and Solberg, 2005).

3.5 Satellites and water temperature

Satellite infrared radiometers measure indirectly the temperature of a very thin layer (skin temperature) about 10 micrometres thick (Robinson and Donlon, 2003). Sea surface temperature (SST) is the temperature of the water in the topmost layer of the sea. For stratified conditions, the temperature at the surface is different from that below. This condition is clearly observed in the southern part of the Arabian Gulf, whereas the northern part of the Gulf is thermally stratified in summer only (Reynolds, 2002). The temperature of the water is constant with depth when the waters are well mixed; this is the case in Kuwait Bay (Al-Yamani et al., 2007; Dames and Moore, 1983; and Khalaf et al., 1982).

Measuring SST from space over the whole Earth has been performed routinely since the early 1980s (Robinson and Donlon, 2003). In this study, SST was estimated from Advanced Very High Resolution Radiometer (AVHRR), Moderate

Resolution Imaging Spectroradiometer (MODIS) and Landsat Thematic Mapper (TM). These sensors are described below:

3.5.1 AVHRR

The NOAA satellite and its Advanced Very High Resolution Radiometric (AVHRR) sensor have collected data globally since 1981, and are still operational. The satellite orbits the Earth twice a day, once during the day and once during the night. The AVHRR passes over the Arabian Gulf at 02:00 and 14:00 hours every day, and has operated since 1985 (except for the period from January 2003 to June 2005, when it passed at 10:00 and 22:00). Five thermal channels of calibrated data are available for analysis (NOAA, 2009). Thus, AVHRR is the most widely used thermal infrared (IR) remote sensor for measuring SST and in this sense, is the most successful space platform (Robinson, 2004).

Khan et al., (2004) used the AVHRR dataset of the monthly SST at 9 km resolution from 1985 to 1998 to study the variations of the SST in the Arabian Sea and Bay of Bengal. They found that SST had increased by 0.2 ºC per decade in the Arabian Sea and by 0.5 ºC to 0.6 ºC along the coast of Muscat and Salalah (two cities in Oman). Stuart-Menteth et al., (2003) used 10 years of AVHRR pathfinder project data to look at the day-night SST difference, to investigate the distribution of global diurnal warming. They found that large regions of the oceans are affected frequently by diurnal warming, particularly at mid-latitudes, as well as in the tropics.

3.5.2 MODIS

The Moderate Resolution Imaging Spectroradiometer (MODIS) is an Earth Observing System (EOS) satellite designed to measure biological and physical processes on a global basis, every one to two days. The MODIS TERRA satellite was launched in December, 1999 and the MODIS AQUA satellite in May, 2002 (NASA, 2009b). MODIS has 36 spectral bands with wavelengths ranging from 412 to 14200 nm and 16 thermal emissive bands, covering the middle wave infrared (MWIR: bands 20-25) and long wave infrared (LWIR: bands 27-36) (NASA, 2009b). Reinart and Reinhold (2008) used MODIS SST to study the variations of SST for large lakes in Sweden; they discovered that the auto-generation of SST from the

MODIS satellite varies greatly in space and time, but it can be used to monitor SST over the globe.

3.5.3 LANDSAT

The history of Landsat began with the launch of ERTS-1 (Earth Resources Technology Satellite) by the National Space Agency (NASA), on 23rd July, 1972. Landsat imageries have been found to be appropriate for studying inland water bodies, due to the reasonable cost and the 16 days coverage (Álvarez-Robles et al., 2006). Landsat data have been collected regularly since that time. Landsat 5 and 7 satellites are still operational (Glasgow et al., 2004) , (Table 3.1).

The first 5 Landsat Satellites carried MSS sensors, with four spectral channels (2 visible, 2 near-infrared). The Landsat Thematic Mapper (Landsat 5) carried a more advanced scanning system. The Landsat TM sensor scans the Earth in seven spectral bands of the electromagnetic spectrum, of which three channels are in visible light, three channels are in the infra-red, and one is in the thermal infrared band. The spatial resolution of the visible and infra-red channels is 30 m whilst the thermal band is 120 m (Glasgow et al., 2004; USGS, 2009). The Landsat 5 Thematic Mapper (TM) and Landsat 7 Enhanced Thematic Mapper (ETM+) bands are listed in Table 3.1.

Table 3.1: Landsat 5 (TM) and Landsat 7 (ETM+) instrument bands (adapted from USGS, 2009).

Bands	Channel	Spectral resolution (micrometres)	Spatial resolution (metres)
1	Visible blue	0.45-0.52	30
2	Visible green	0.52-0.60	30
3	Visible red	0.63-0.69	30
4	Near infrared	0.76-0.90	30
5	Mid-infrared	1.55-1.75	30
6	Thermal infrared	10.4-12.5	120 (TM) 60 (ETM+)
7	Mid-infrared	2.08-2.35	30
8	Pan-chromatic	0.52-0.9	15 (ETM)

The Enhanced Thematic Mapper Plus (ETM+) on Landsat 7 is similar to the earlier TM, but it has enhanced spatial resolution of the thermal band to 60 m. There is also an extra 15 m band (pan-chromatic) which was added to the ETM+ sensor (USGS, 2009). This thermal infrared channel is useful for studying changes in sea surface temperature, which could be related to thermal coastal pollution (Fisher and Mustard, 2004).

Many techniques have been developed in the use of satellite imagery for studying water mass characteristics. Most of these techniques are based on spectral band algorithms and can detect changes in water quality. For example, Amos and Alfoldi (1979) used Landsat data to determine suspended sediment concentration in a macrotidal system in the Bay of Fundy, Canada. They concluded that the thematic maps generated from Landsat images could be used quantitatively to determine circulation patterns, sources of materials and volumes of suspended sediment; they may be applied to other, similar marine environments. Han and Jordan (2005) use Landsat ETM+ data to map the chlorophyll-a concentration in Pensacola Bay; they found that the ratio of ETM+1/ETM+3 could be used to estimate and map chlorophyll-a concentration. Álvarez-Robles et al., (2006) integrated statistical models and observed samples of Trophic State Index (TSI), with Landsat imagery, (bands 1 and 2) to establish a relationship with the two bands. The authors found a linear relationship between the observed and predicted TSI, which could be used for predicting TSI. Ahn et al.,(2006) used thermal infrared sensors (band 6) of Landsat TM, to measure the sea surface temperature on the south coast of Korea. They found that Landsat SST could provide information about thermal plumes from nuclear power plants

To detect the sea surface temperature from Landsat, the following digital image processing techniques need to be carried out. This approach of predicting the SST from satellite images is standard and is approved by the USGS (USGS, 2009):

(1) Pre-processing techniques

A- Image restoration:

- **Geometric corrections:** The satellite imagery needs to be in the correct grid reference system. Geometric correction is the process

required to put the satellite images into the Kuwaiti grid system. This is based on ground control points from topographic base maps or on using the Global Positioning System (GPS) ;

- **radiometric and atmospheric corrections:** The atmospheric conditions affect usually the quality of images and their information content, i.e. the digital number (DN) of each pixel. The presence of water vapour, dust, CO_2 and many other parameters in the atmosphere can affect the value of reflected light (Green et al., 2000). Thus, radiometric and atmospheric corrections are essential, to remove error and to calibrate the DN values of any image, before extracting information. In this study, radiometric and atmospheric corrections were carried out for all Landsat images; and

B- conversion to radiance:

The satellite data need to be converted to radiance, before they can be used for computation. In this process, the digital numbers (DN) are scaled to brightness numbers (i.e. from 0-255, which is known as absolute radiance), essential transformation for comparative and accurate analysis.

(2) Post-processing techniques

A- Image enhancement:

Spatial and spectral enhancement techniques are carried out to improve the visual interpretation of the water masses in Kuwait Bay. For example, the Histogram Equalization Technique (spectral enhancements) redistributes normally the pixel digital number (DN) values non-linearly, resulting in a broad histogram (NASA, 2009a). This enhancement re-assigns and distributes the DN values of the image pixels, on a scale from 0 to 255. This means that the contrast is high between objects in the image. This enhancement helps the visual interpretation of satellite images;

B- image classification:

The different image classifications, such as unsupervised, supervised and hybrid classification techniques are used mostly to extract the information needed from the remotely sensed data. In this study, supervised

classification techniques are used to classify the Landsat images of Kuwait Bay and its coastal zone; and

C- sea surface temperature:

The Landsat TM sensor has a spatial resolution of 120 x 120 m for the thermal infrared band (band 6), whereas other bands (bands 1, 2, 3, 4, 5 and 7) have 30 x 30 m resolution. The spectral resolution of band 6 is 10.4 -12.5 μm (Table 3.1); it is very useful in mapping the thermal pattern of water masses (NASA, 2009a). Predicting SST from Landsat images is discussed in more detail in Chapter 7.

4. Chapter 4: Properties of seawater temperature in Kuwait Bay

Abstract

This Chapter provides a description of seawater temperature distribution in the study area. MODIS and Landsat satellite images are used to describe the spatial and temporal distribution of the sea surface temperature (SST) in the Arabian Gulf and Kuwait Bay. Field measurements are used also to define the vertical temperature gradient over the sea-bedsediments and on the intertidal flats sediments as well as the thermal energy fluxes. Hourly temperature measurements were collected throughout the water column during winter, 2007 and summer, 2008 in Kuwait Bay. The temperature was measured at three levels: surface; mid-depth; and at the bottom of the water column. At the same time, the temperature was measured at selected depths below the sea-bed. Finally, hourly field measurements of temperature at different depths below the sea-bed were conducted on the intertidal flats of southern Kuwait Bay.

Satellite imaging showed that generally SST of Kuwait Bay is higher in the south than in the north. The field measurements showed that the water column was well-mixed in the bay. Seawater temperature reached 37 ºC in summer and dropped to 14 ºC in winter. Measurements beneath the sea-bed showed that the temperature increased with depth in winter and decreased in summer. In winter, the sea-bed and intertidal flats are a source of heat to the water column, during summer the opposite is true. In general, SST of Kuwait Bay is influenced by intertidal flat exposure time, air temperature and wind speed. On the intertidal flats, air temperature is considered the most important factor controlling sea-bed temperature. Frequency analysis of the time-series of temperature recorded show peaks with periods of 24, 12.4, 8 and 6.2 hours. The peaks are due mainly to diurnal inequality in atmospheric temperature variations and tidal variations.

4.1 Introduction

The aim of this Chapter is to measure the temperature patterns in Kuwait Bay and the temperature gradients in the water column, as well as in the upper 1 m of the sea-bed and intertidal flat sediments in the study region. These measurements were made in order to define the heat flux of the bay. Firstly, it is important to describe the seawater temperature in the Arabian Gulf, in order to understand the factors influencing the seawater temperature in Kuwait Bay. High tide in the north of the Gulf (4 m spring tidal range) results in complete vertical mixing of the water column, and strong horizontal exchanges of water between Kuwait Bay and the northern Arabian Gulf (Reynolds, 2002). Thus, water temperatures in Kuwait Bay are influenced by those of the northern Arabian Gulf. Due to the high degree of vertical mixing, the thermal character of the water in the Arabian Gulf can be described adequately by the sea surface temperature measurements from satellites such as MODIS (Reinart and Reinhold, 2008), which provides regional coverage of the entire Gulf, on a daily basis. Ground-truthing of the satellite has been undertaken using surface measurements of temperature made by the Environment Public Authority of Kuwait (EPA), at 12 monitoring stations in the northern Arabian Gulf. These measurements provide fundamental data for estimating the accuracy and resolution of the thermal sensor and measure any temperature drift of the sensor over time. The temperature distribution in Kuwait Bay (the study region) has been examined in greater detail than that of the Arabian Gulf, using data from the Landsat Enhanced Thematic Mapper Plus (ETM+). This satellite has a spatial resolution of 60 m for the thermal band (band 6), but has much less frequency of imaging (16 days) than the lower resolution MODIS satellite. Thus, information on the spatial patterns of SST is provided by satellite imagery. However, it is less useful in defining temporal trends. For this reason, monthly EPA measurements taken in Kuwait Bay are included in the analysis and used to calibrate the Landsat SST. Trends in the seawater temperature at diurnal or lower frequencies, can be defined from the satellite or monthly EPA measurements. In order to examine the temperature trends at frequencies higher than 24 hours, field measurements were made to assess the temperature of the water column and the topmost metre of the sea-bed sediments.

The heat fluxes across the sea-bed and intertidal flats could play a key role in the thermal character of the overlying water masses (Cho et al., 2005). Understanding the thermal properties of sediment in contact with seawater is very important for engineering design in the area (Abu-Hamdeh and Reeder, 2000; Newson and Brunning, 2004), as well as in the ultimate formulation of the thermal budget of the region. Several studies have been made on the vertical temperature gradients in sediments along the coastal zone, to understand the transfer of heat to and from the water column. Harrison and Phizacklea (1985) investigated the vertical thermal structure of muddy sediments, by measuring the ground temperature at three depths in the Forth Estuary, Scotland. They found a marked seasonal change in the direction and magnitude of gradients, indicating heat transfer into the bed in summer and from the bed in winter. Cho *et al.* (2005) deployed temperature loggers at six levels below the sediment surface on the Baeksu tidal flats, Korea. They found that the sediment temperatures decrease with increasing depth during summer, and increased during winter. They concluded that the surface temperatures significantly increased during tidal exposure when the solar radiation was strong, particularly during summer. Also, they found peaks in temperature at 24, 8 and 6 hour periods. They ascribed the peaks at 24 and 6 hours to the diurnal effect of solar radiation. The peak of 8 hours was considered to be an influence due to the unequal duration of day and night, at the time of measurements.

4.2 Methodology

4.2.1 Long term SST

Smith et al., (2008) produced an Extended Reconstructed Sea Surface Temperature data set (ERSST) of the world's ocean, from 1854 till the present. These data were constructed using the International Comprehensive Ocean Atmosphere (ICOADS) SST data set. ICOADS observation records sea surface temperature from the World Ocean database (ships, buoys, and other platform types) (Rayner et al., 2006). The set is available online as ASCII text files at the National Climate Data Centre (NCDC), on a monthly Basis at 2° ×2° resolution (NCDC, 2009).

4.2.2 Seasonal temperature variation

The Environment Public Authority (EPA) of Kuwait has collected surface water samples and measured the seawater temperature on a monthly basis, at 12 monitoring stations along the coastline of Kuwait, from 1983 to the present (EPA, 2008). Six of these stations are located in Kuwait Bay (Figure, 4.1). EPA measurements are not at the same specific time of the month and differ from month to month. Therefore, the data were corrected to provide values of SST data all year around.

To represent the temperature variation over the year, a curve-fitting method was used for *in situ* measurements, from 1985 to 2006 at Z6 site (Figure, 4.1). This station was selected because it is located away from local human activities. All the measured data were used in the analysis. A third order polynomial equation was used to provide SST values throughout the year.

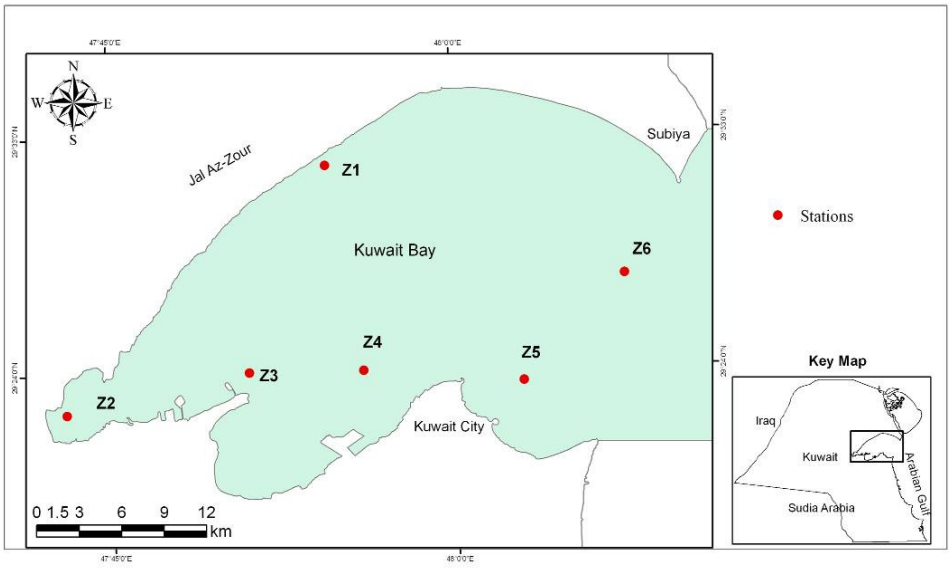

Figure 4.1: EPA monitoring stations in Kuwait Bay.

Figure 4.2 shows the SST from measured and fitted curve methods at Z6, in Kuwait Bay. The scatter and errors between the curve fitting and the EPA data are shown in Figure 4.3. The graph shows a good correlation between predicted and measured SST, where the $R^2 = 0.92$ and the standard error = 0.5 ºC. This standard

error is considered to represent the error for the other stations in Kuwait Bay used in this thesis.

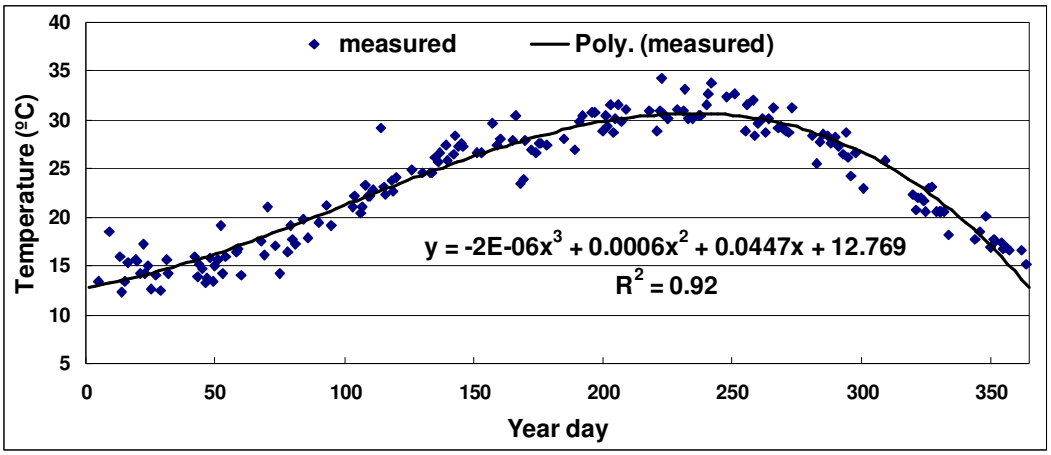

Figure 4.2: SST from the measured EPA data and the fitted curve at Z6, Kuwait Bay.

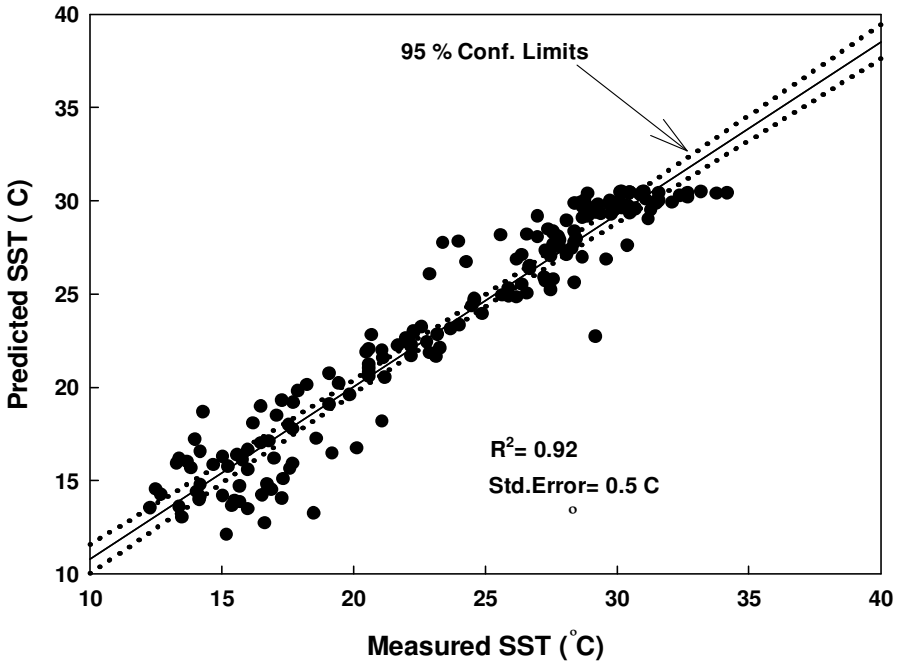

Figure 4.3: Measured and predicted SST at station Z6. The graph showed a good correlation between predicted and measured SST where the R^2= 0.92 and the standard error = 0.5 ºC.

4.2.3 Horizontal temperature distribution (sea surface temperature in the study region)

Remotely sensed data were used to show the distribution of SST in the study area. MODIS SSTs were obtained from the processed NASA Jet Propulsion

Laboratory (JPL) and the Physical Oceanography Distributed Active Archive Centre (PO.DAAC, 2009). MODIS yearly and monthly SSTs for 2006 were downloaded and used to map the distribution of the SST in the Arabian Gulf. The MODIS Aqua satellite orbits the earth approximately 14.1 times per day and covers the Arabian Gulf twice a day, once during the day and once at night. Day-time SST data were used in this study. The annual and monthly SST were derived by averaging daily coverage of the satellite (PO.DAAC, 2009). The thermal band (Band 6) of the high-resolution Landsat Enhanced Thematic Mapper Plus (ETM+, dated 29/4/2003) was processed, to obtain the SST of Kuwait Bay. This image was selected because it was the last available Landsat image covering the study area, of good quality. After May, 2003 the Landsat sensor accuracy was reduced (NASA, 2009a). Processing the Landsat image included geo-referencing and radiometric corrections. The approach followed to derive SST from satellite images has been described in Chapter 3. ArcGIS software (version 9.1) was used to produce SST layouts from the satellite images.

4.2.4 Vertical temperature variations

Temperature sensors (Miniature Temperature Loggers- SL52T) manufactured by the Signatrol Ltd Company in the United Kingdom were used to measure temperatures within the seawater, sea-bed and intertidal flat sediments of southern Kuwait Bay. The sensors included a logger, which records the temperature data and an enclosure to protect the logger (Figure 4.4). The logger has a resolution of 0.07 ºC. The accuracy of the logger clock is ± 2 minutes per month (Signatrol, 2009). The loggers were programmed to measure temperature at hourly intervals. At the end of each field measurement, the data were downloaded to a computer, through a USB interface that came with the instrument.

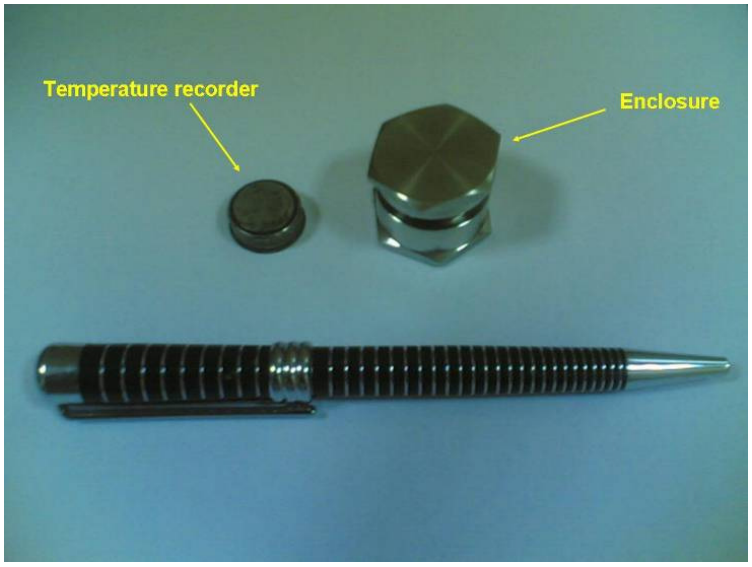

Figure 4.4: The temperature sensors used in this study; it contains a logger to record the temperature and enclosure that used to protect the logger.

Hourly temperature measurements at different depths in the sediment were carried out throughout the year at a station on the intertidal flats (Location 2) in the southern bay (29 º 20' 28.2" N, 47 º 54' 24.8" E); also at an adjacent sub-tidal station (Location 1) (29 º 21' 35.2" N, 47 º 52' 06.1" E). Figure 4.5 shows the selected locations for the measurements. The nearshore measurements were taken during winter, from 26th November to 17th December, 2007. Summertime measurements were taken continuously, from 13th June to 24th July, 2008. A professional diver inserted the probes into the sea-bed. The mean water depth at this location was 4.5 m and the bed was composed of soft mud.

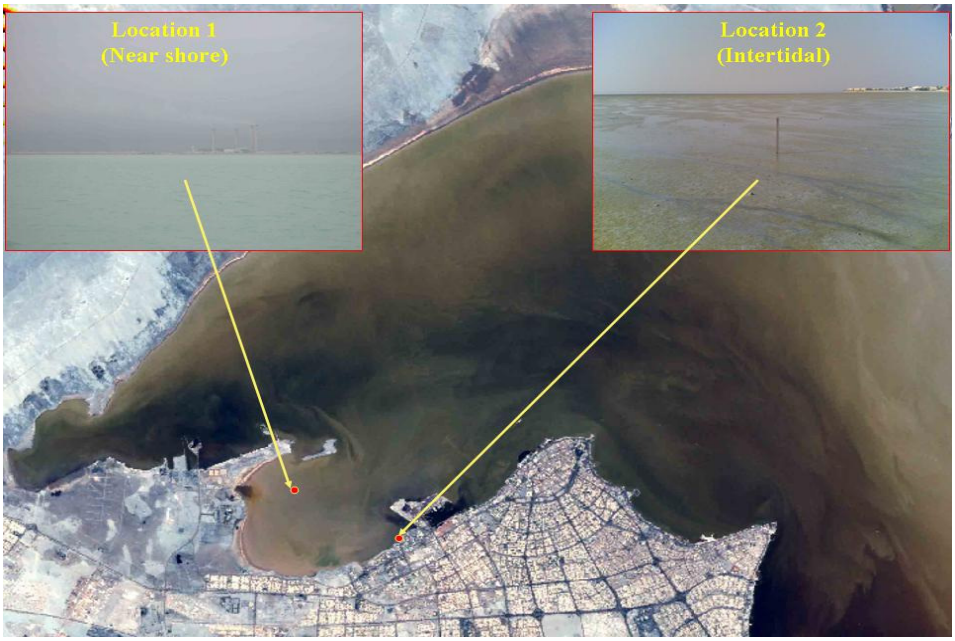

Figure 4.5: A satellite image of Kuwait Bay showing selected positions for the field measurements undertaken in this study.

Calibration of the sensor was undertaken before the field measurements, using the facilities at the Kuwait Institute for Scientific Research (KISR). The sensor was deployed in a bath for two days. The bath temperature was increased every hour by 0.5 ºC from 17 ºC to 25 ºC. The actual temperature was recorded and compared with a sensor temperature. Figure 4.6 shows the temperature calibration of the sensor. The sensor output showed a strong correlation with the control temperature ($R^2 = 0.98$); whilst the standard error was ± 0.3 ºC.

The sensors were installed in both winter and summertime at Location 1 on a 1-m long carrier, which was injected into the sea-bed using a designed probe (Figure 4.6). The sensors were located at three selected positions throughout the water column (near surface, near mid-depth (165 cm from the sea-bed), and 8 cm above the sea-bed). Three other sensors were introduced into the sea-bed, at depths of 20, 40 and 60 cm. For the summer measurements, two further probes were added, at depths of 2 cm and 10 cm. During the summer measurements, the probes were corroded which damaged some of the temperature probe covers. The temperature probes at depths of 20 and 40 were damaged and no data could be gathered from them. This could be due to chemical reactions that took place with the high temperature, where the area is

largely polluted from human activities in southern Kuwait Bay (Al-Zamel et al., 2009)

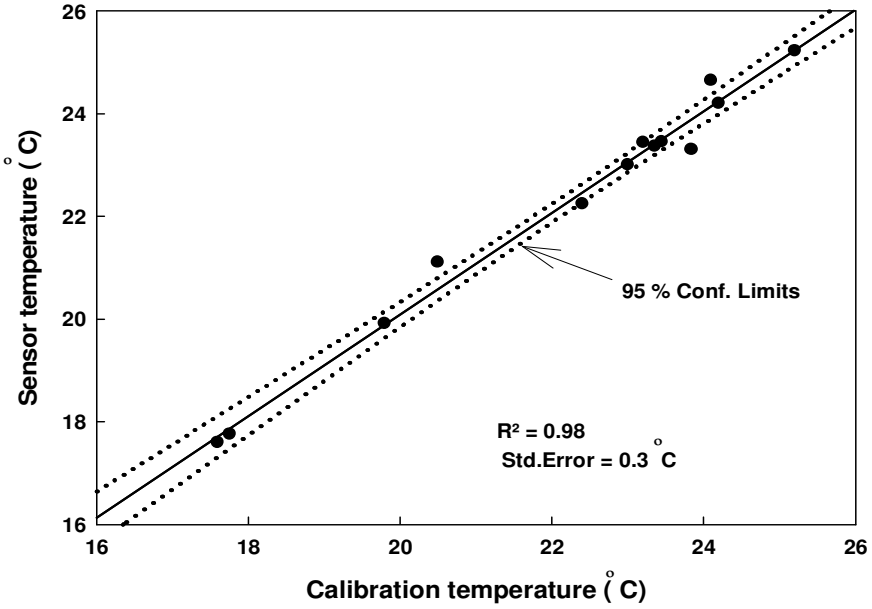

Figure 4.6: Temperature sensor calibration undertaken in a control facility at KISR. The sensors are accurate and show a linear response over the range of the calibration.

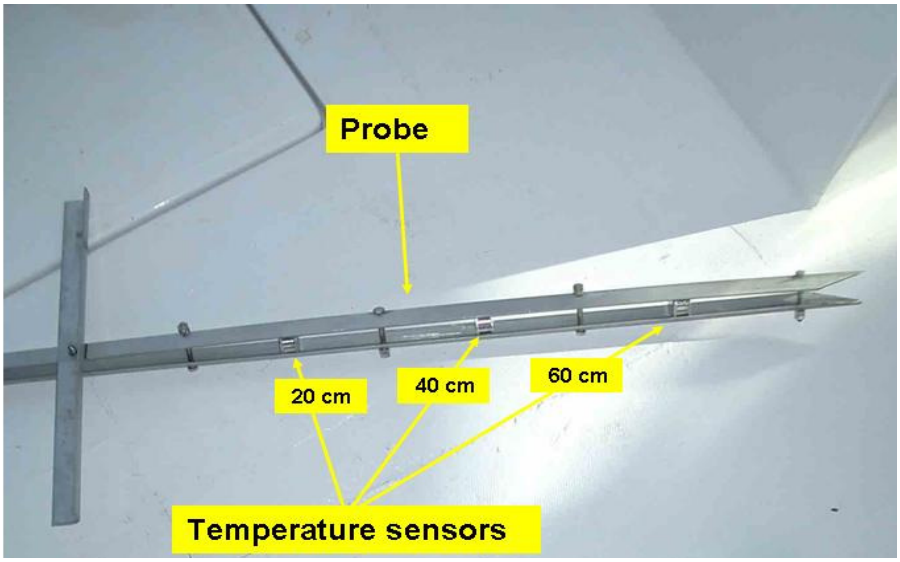

Figure 4.7: Temperature probe (carrier) designed to hold the sensors at selected levels under the sea-bed and in the intertidal flat sediments of Kuwait Bay.

The intertidal flat sediments measurements at Location 2 covered a period of approximately 1 year, from 17th December, 2007 to 28th December, 2008. The measurements began using three probes deployed at depths of 20, 40 and 60 cm

below the sea-bed. Subsequently, two more probes were added at depths of 2 and 10 cm. The water reaches the instrument at this location when the tide is 2.9 m above mean low water. Thus, the site is exposed for approximately 50% of the time, due to tidal variations.

4.2.5 Data analysis

A Fast Fourier Transform (FFT) was used to calculate the frequency components of the measured temperatures. FFT is a mathematical procedure used to extract useful information from sampled signals (Cho et al., 2005). It is used to transform a continuous time signal into the frequency domain (Subrahmanyam et al., 2009). Hourly seawater temperature measurements were used in the FFT analysis to extract the frequency components of the temperature time-series by using MATLAB software. Also, step-wise multiple regression analysis was used to determine the factors driving seawater temperature in Kuwait Bay. It is a statistical method used to understand the relationship between several independent and dependent variables (Fowler et al., 1998). This statistical approach was applied to hourly seawater temperature measurements in Kuwait Bay (as dependant variables) and several meteorological data sets (as independent variables) for winter and summer. STATISTICA software version 6.5 was used for this purpose.

4.2.6 Heat flux between the water column and seabed

The heat flux ($\frac{\Delta Q}{\Delta t}$) is defined as the heat flow per unit time per unit area (Zafiratos, 1976). Estimates of the heat flux are essential, in order to understand the heat exchange between seawater and the sea-bed and the intertidal flats. The heat flux can be calculated from the equation:

$$\frac{\Delta Q}{\Delta t} = \mathrm{KA}\frac{\Delta \mathrm{T}}{\mathrm{L}} \quad \text{..... Equation (4.1)}$$

where K is the thermal conductivity (W/m^2 ºK), A is the cross-sectional area, and $\frac{\Delta T}{L}$ is the vertical temperature gradient.

The thermal conductivity of the sediment is considered the property of a medium which transfers heat (Moqsud et al., 2008). Calculation of the thermal

conductivity requires steady state conditions, which rarely exist in nature. The thermal conductivity of sediment has been calculated experimentally in the laboratory, under steady state conditions, by Abu-Hamdeh and Reeder (2000), who provide the thermal conductivities of various types of sediment. They found that thermal conductivity ranged from 0.68 to 1.94 W/m^2 ºK for sand and from 0.36 to 0.69 W/m^2 ºK for clay. Moqsud et al., (2008) studied the thermal conductivity of the intertidal flats sediments of the Riake Sea, Japan. They found that, for moist mud, it ranged from 0.65 to 0.75 W/m^2 ºK. These values were lowest (0.40 to 0.70 W/m^2 ºK) for dry sediment. Newson and Brunning, (2004) found the thermal conductivity for deepwater offshore sediments to vary from 0.97 to 1.19 W/m^2 ºK. In this study, the thermal conductivity is assumed to be 1 W/m^2 ºK.

4.2.7 Meteorological data and tidal water level

The meteorological data (air temperature, wind speed, wind direction and solar radiation), during the campaign of field measurements were provided by the meteorological station at KISR. Hourly meteorological data were used to investigate the atmospheric factors affecting seawater temperature. The tidal level was predicted also at the time of measurements, in order to investigate the effect of the tide stage on seawater temperature. The tidal level was obtained from a tidal model called KTIDE developed by KISR. The model is based on 22 tidal constituents and was validated using field measurements of water levels in Kuwait Bay (Rakha et al., 2007).

4.3 Results

4.3.1 Long term SST

Figure 4.8 shows the long-term monthly SST in the northern Arabian Gulf, over the last 57 years, based on ERSST V3 observations as described in the methodology. Although ERSST V3 data have a low spatial resolution 2° ×2° grid, it was nevertheless used in this study to assess the long-term SST trends in the Arabian Gulf, for the period from 1950 to 2007. This was undertaken in order to understand long-term behavior of the SST in the study region. The monthly moving average shows the seasonal trends in temperature: the summer maximum reached 35 ºC (1961, 1989) and the winter minimum dropped to 16 ºC (1982, 1990, and 1991).

There was a greater year-to-year fluctuation in the winter minima, than in the summer maxima. The annual trend showed a year-to-year fluctuation. A 5-year running average eliminates the greatest part of the seasonal variability; it shows little change in mean temperature from 1950-1980 (phase 1), but there is a mean trend upwards after 1980 (phase 2) of 0.4 ºC/ decade.

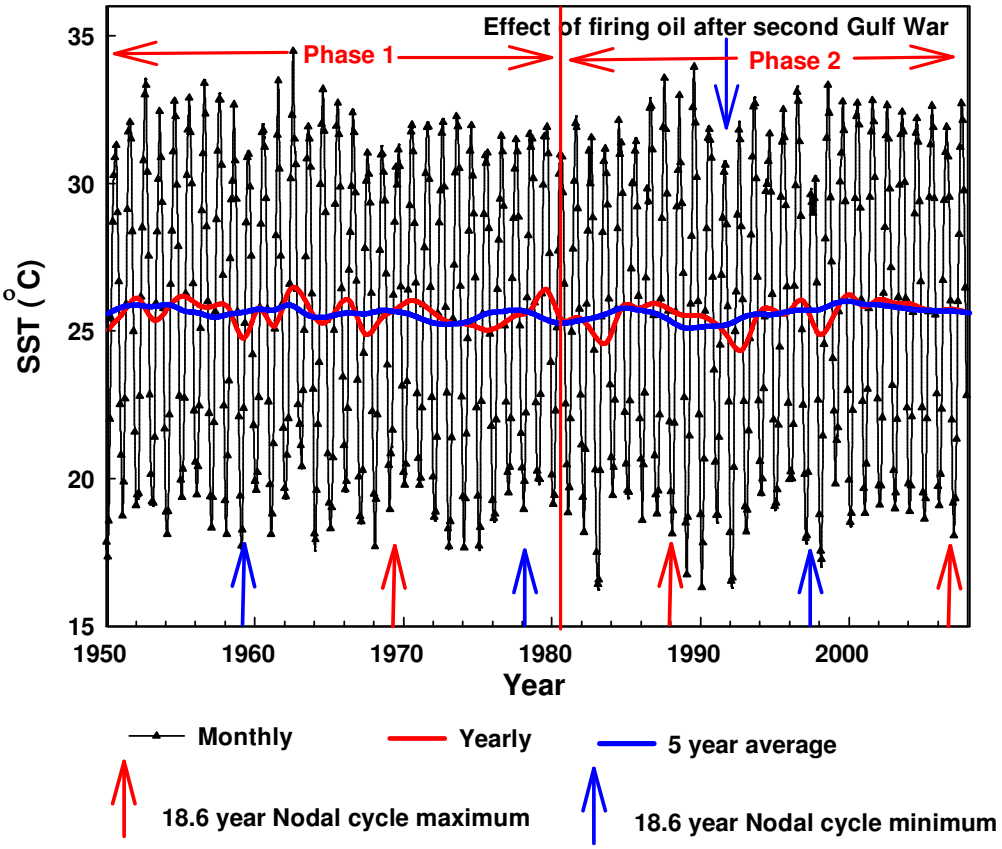

Figure 4.8: SST in the northern Arabian Gulf (1950-2007) based on ERSST V3 observations. It shows little change from 1950 to 1980 (phase 1); and an increasing trend after 1980 (phase 2). It shows a reduction in temperature in 1991 due to the effect of firing oil after the second Gulf War.

The Figure shows also a reduction in temperature during 1991 due to the effect of burning oil fields after the second Gulf War. The smoke of burning oil fields blanketed the region and blocked sun light, for several months. There are no clear trends in temperature related to the 18.6-year nodal cycle. This nodal cycle is the gravitational relationship between the sun, the earth, and the moon that generates a global 18.6-yr tide in the global ocean (Yndestad, 2008). The amplitude of this cycle had a maximum in 1987 and a minimum in 1996 (Pugh, 1996). The maxima

and the minima of the latest nodal cycles are illustrated in the figure (blue and red arrows respectively).

4.3.2. Seasonal temperature variation

Figure 4.9 shows the variation of SST in Kuwait Bay over the year, derived from the corrected average of EPA measurements at Site Z6. The data are monthly averages generated from data corrected from 1985 to 2006, as explained in the methodology. The error bars represent the standard deviation of the measurements. SST varied from 13.6 to 30.4 ºC. The greatest fluctuation was during the winter minimum, not the summer maximum. The highest fluctuations take place in December. Trends in temperature are systematic, showing a steady increase from January to August, and a steady decrease from August to December. The rate of temperature increase is less than the rate of temperature loss.

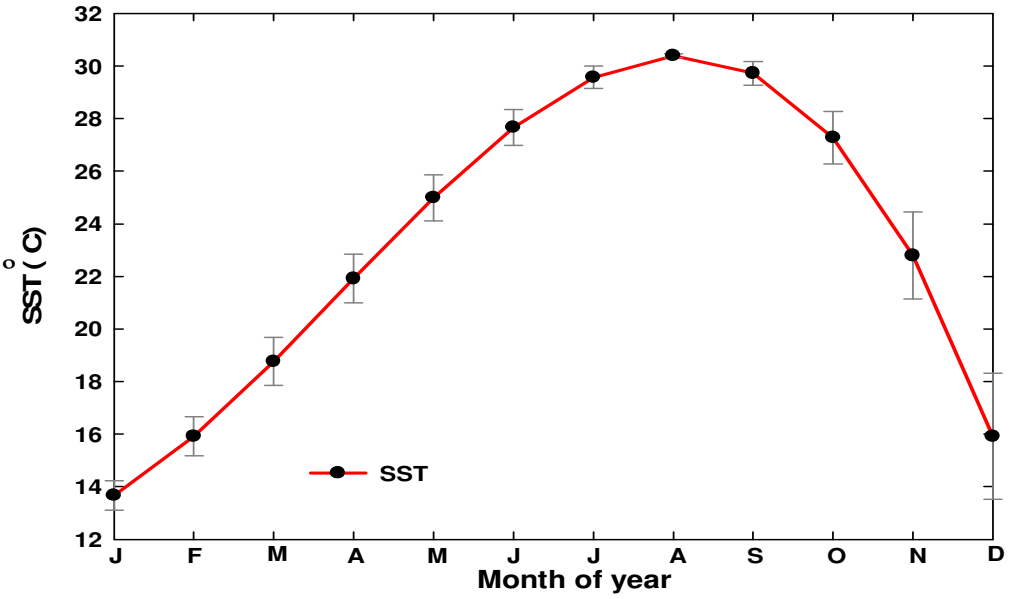

Figure 4.9: Monthly variation of SST based on EPA measurements at station Z6 in Kuwait Bay. The data are monthly averages of corrected data from 1985 to 2006. It shows the highest SST in August and lowest in January. The greatest fluctuation in temperature was during the winter minimum, and the lowest was during the summer maximum.

4.3.3 Spatial distribution of sea surface temperature (SST) in the Arabian Gulf

Figure 4.10 illustrates the day-time yearly average SST for 2006 in the Arabian Gulf, based on day-time SST, derived from daily coverage of the MODIS satellite (NASA, 2009b). As described in the methodology, annual MODIS SST is downloaded from (JPL NASA), at 4 km resolution. The SST is cooler in the north and warmer in the south. The mean temperature difference in the Gulf is about 10 ºC and appears constant across the Gulf. The yearly average horizontal gradient is 0.01 ºC/km. The cooling in the north could be due to shallow water depths; therefore, the wind has a stronger effect on the water circulation and mixing (Reynolds, 2002). The SST on the eastern side appears slightly warmer than the western side. This could be due to the upwelling that takes place on the eastern side of the Gulf (Robinson and Brink, 2006).

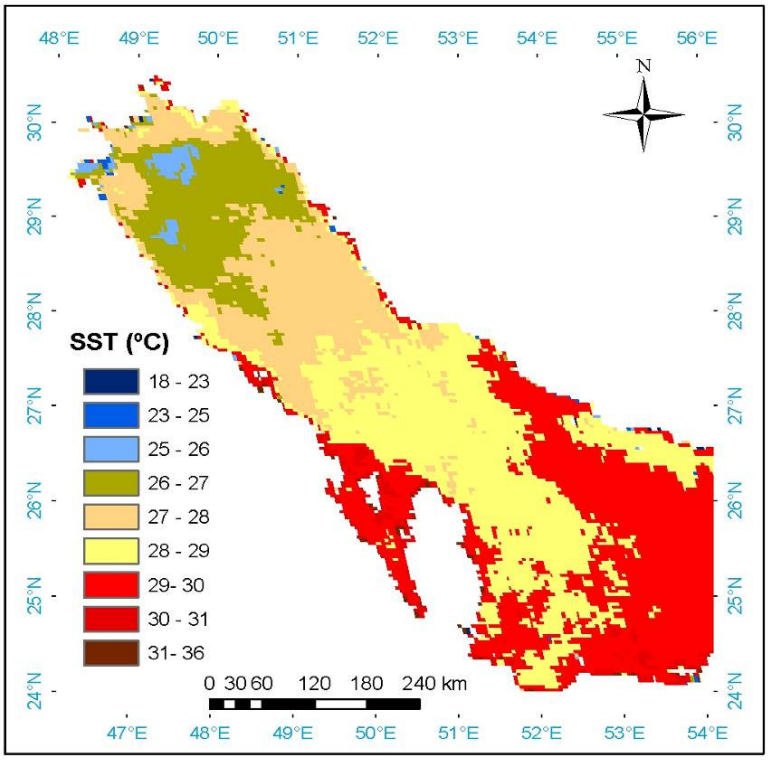

Figure 4.10: Yearly average SST in the Arabian Gulf derived from daily coverage of MODIS satellite for the year 2006. The SST is 10 ºC warmer in the south of the Gulf than in the north. Shoreline heating is about 3ºC and influences water to about 20-30 km offshore.

The minimum SST can be observed in the middle of the northern part of the Gulf. Temperature increases generally towards the coastline. This is perhaps due to

the heating effect of the local human activities which take place near the shoreline. This evidence of the local effect is clear in Figure 4.10. The heating is about 2-3 ºC within 20 to 30 km from the shoreline. In Kuwait Bay, the minimum temperature appears in the north, rather than the south of the bay.

Figure 4.11 illustrates the monthly average of the SST in the Arabian Gulf, for each month of the year. The monthly SST was derived by averaging daily coverage of the satellite orbit for the study area. The SST is consistently colder in the north. The temperature fluctuation within the northern Gulf is much higher than the temperature fluctuation in the south (18 ºC and 13 ºC, respectively). This may be again due to the shallowness of the northern Gulf. Moreover, the fluctuation in the west side of the Gulf is much higher than the fluctuation in the east side (17 ºC and 9 ºC, respectively). Once again, this could be due to the effect of the wind on water circulation and mixing (the western part of the Gulf is shallower than the eastern part). Detailed descriptions of the SST in Arabian Gulf for each month are presented below:

January: The temperature ranges from 14 ºC in the north, to 24 ºC in the south. The longitudinal gradient in temperature is 0.012 ºC/km and is sloping in the north. The eastern Gulf is 3 ºC warmer than the western Gulf. In the north part of the Gulf, the temperatures along the shoreline are lower than offshore. In the southern Gulf, the temperature along the shoreline is lower along the Arabian side. The temperature along the Iranian shoreline is higher than offshore. It is higher on the Iranian side due to the upwelling that takes place in the eastern part of the Gulf (Robinson and Brink, 2006).

February: A cooling trend is evident in the southern and central Gulf. The isothermals have migrated 100 km southwards and the longitudinal gradient in temperature is at a maximum (0.012 ºC/km). The temperature along the shoreline is lower than the offshore in the northern part of the Gulf. Also, it is lower in the western (Arabian) side of the southern part of the Gulf.

March: The temperature ranges from 16 ºC in the north, to 25 ºC in the south. The longitudinal gradient in temperature is 0.018 ºC/km. In the northern part of the Gulf, the temperature along the shoreline is lower than offshore. In the southern part of the

Gulf, the temperature along the shoreline is lower than the offshore in the Arabian side and higher along the Iranian shorelines, than offshore.

April: The temperature ranges from 19 ºC in the north, to 28 ºC in the south. The longitudinal gradient in temperature is 0.011 ºC/km. There is a lateral gradient in temperature for the western of the Gulf than is evident in earlier months. The temperature along the eastern and southwestern shorelines is higher than offshore. In contrast, the temperature along the northwestern shoreline is less than offshore.

May: The temperature ranges from 23 ºC in the north, to 32 ºC in the south. The longitudinal gradient in temperature is 0.011 ºC/km. that is, significant heating has occurred. There is a strong lateral gradient of cooling bordering the eastern side of the Gulf. The temperature along the western and southeastern shorelines is higher than offshore, whereas it is lower along the shoreline of the northeastern part of Gulf than offshore.

June: The temperature ranges from 26 ºC in the north to 35 ºC in the south. The longitudinal gradient in temperature is 0.011 ºC/km. The temperature pattern appears symmetrical about the long axes of the Gulf. This is probably due to the effect of wind blowing along the Gulf, from Iraq. Shoreline heating starts in this month, and is evident in the central Gulf.

July: The temperature ranges from 29 ºC in the north, to 35 ºC in the south. The longitudinal gradient in temperature is 0.008 ºC/km. This gradient continues to slope to the north .Coastal warming is clear in the central and southern Gulf.

August: The temperature ranges from 31 ºC in the north to 36 ºC in the south. There is a mixing of water masses (evident in the patchiness of the temperature patterns) and a very low longitudinal gradient. In the southern part of the Gulf, the temperature along the shoreline is higher than offshore on the Arabian side; it is lower along the Iranian shoreline.

September: The temperature ranges from 30.5 ºC in the north, to 35.5 ºC in the south. The longitudinal gradient in temperature has re-established and is 0.006 ºC/km. There is a mixing of water masses in the north-western part of the Gulf; this could be due to *shamal* winds. In the southern part of the Gulf, the temperature decreases towards the offshore along the Arabian side; it increases towards the offshore, on the Iranian side. The lateral gradient is dominant over the longitudinal gradient.

October: The temperature ranges from 28 ºC in the north to 34 ºC in the south. The longitudinal gradient in temperature is 0.008 ºC/km. The temperature along the shoreline is lower than offshore in the northern part of the Gulf only. The coldest water is associated with the Tigris Euphrates delta and the Shatt Al-Arab outlet.

November: The temperature ranges from 23 ºC in the north to 32 ºC in the south. The longitudinal gradient in temperature is 0.011 ºC/km. The temperature along the entire shoreline is lower than offshore.

December: The temperature ranges from 15 ºC in the north, to 30 ºC in the south. The longitudinal gradient in temperature is 0.018 ºC/km. The greatest cooling effect occurs in this month for the northern part of the Gulf. Along the Arabian side of the southern Gulf. There is a strong asymmetry in temperature across the Gulf.

The thermal band of the Landsat ETM+ sensor package (60 m resolution) was used to map the distribution of SST in Kuwait Bay. Figure 4.12 illustrates the predicted SST in Kuwait Bay, from the Landsat image obtained on 29/4/2003. The seawater temperature in the north of the bay is 3 ºC colder than it is in the south. This is considered to be due to the human activities concentrated along the southern coast (Al-Mussalam, 1999). The cooling effect is due to the dominant northwesterly winds on the waters of Kuwait Bay (at the time of this image, the wind was blowing from NW, at 10 m/s). It also could be due to the loss of heat from the water column, to the wide northern intertidal flats. This image shows also the highest temperatures near the Doha East (A) and West (B) power and desalination plants, Subia power and desalination plant (C) and Shuwaikh desalination plant (D). The thermal plumes are due to the discharge of warm water from these stations, which is typically 9 ºC above the temperature of the ambient seawater at the source. Rakha et al., (2009) used a hydrodynamic model to predict the effect of the thermal plumes from power and desalination plants in Kuwait Bay; they found daily peaks in seawater temperature occur during the ebb conditions, when the thermal plume from the station moves seawards. Plant A and B appear to be contributing heat to the water mass in western Kuwait Bay, as it is greater than 2 ºC warmer than the water mass at the mouth of the bay.

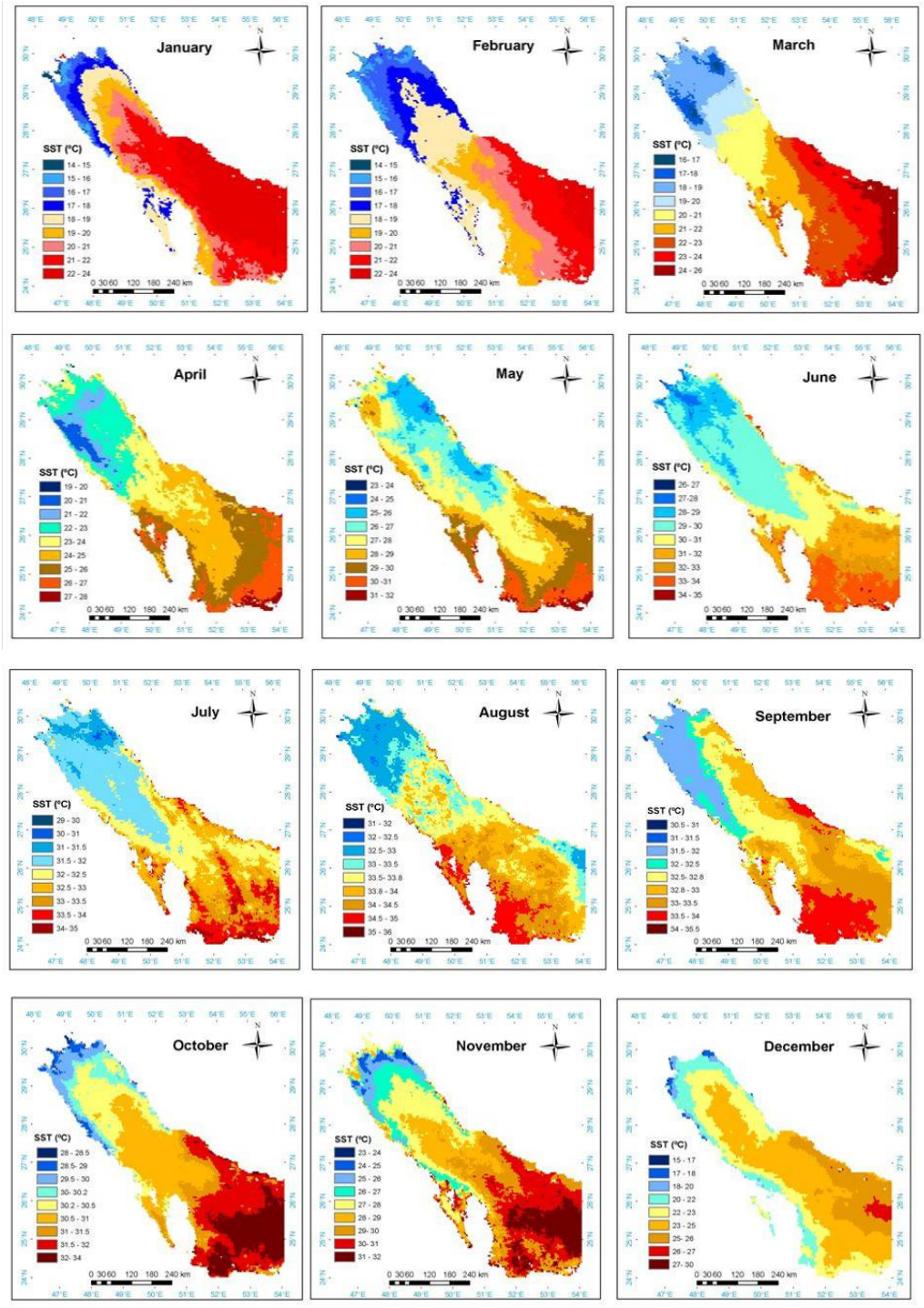

Figure 4.11: Monthly SST in the Arabian Gulf based on MODIS AQUA SST for 2006 derived by averaging daily coverage of the satellite orbit in the study area.

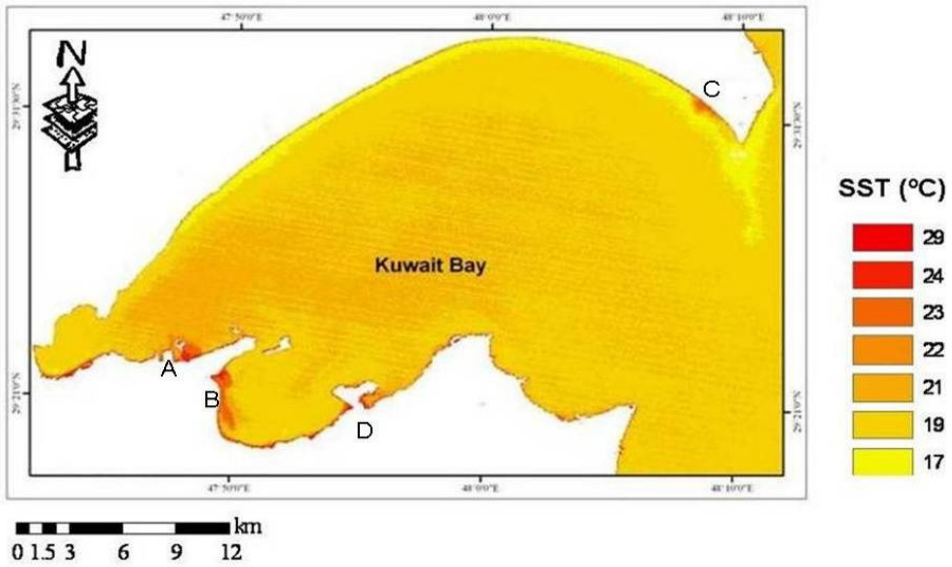

Figure 4.12: SST in Kuwait Bay from Landsat image (29th April, 2003). It shows the highest SST (red colour) near power and desalination stations at locations A, B, C and D.

4.3.4 Vertical temperature distribution in Kuwait Bay (offshore measurements)

Figure 4.13 shows the vertical temperature gradient of the near bottom waters and sub-surface, at Location 1 in Kuwait Bay, based on hourly measurements taken during both winter and summer. The Figure shows the average and standard deviation of the winter and summer measurements. The winter measurements were taken from 26th November to 17th December, 2007; the summer from 23rd June to 24th July, 2008. The temperature of the water varied in winter from 15.5 ºC to 19.5 ºC and from 27 ºC to 33 ºC in summer.

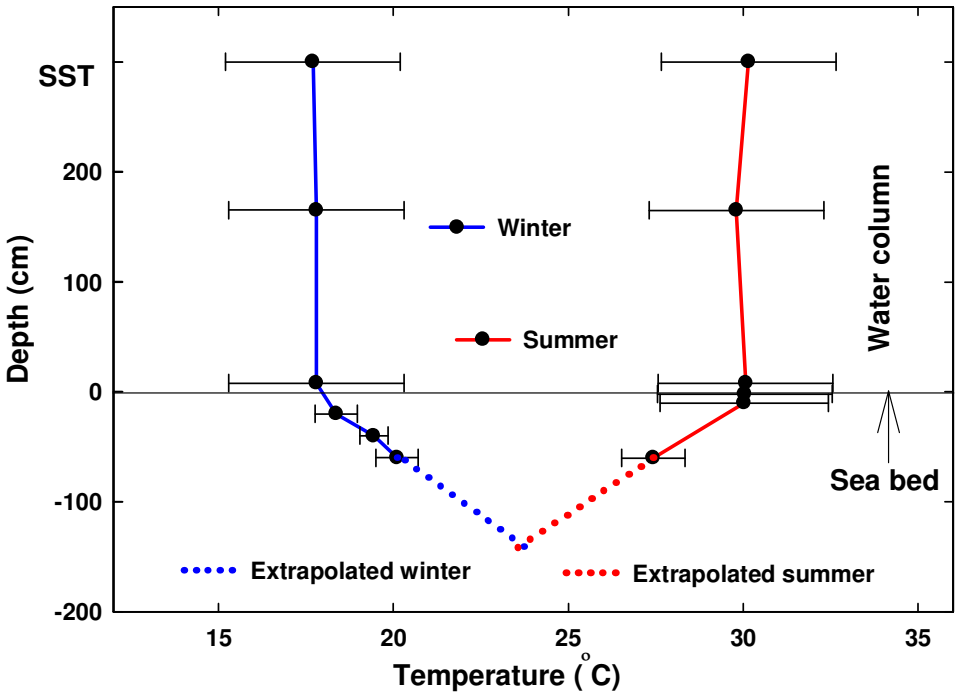

Figure 4.13: Vertical temperature measurements taken at the sub-tidal station in Kuwait Bay (location 1). Through the water column, the temperature is nearly constant. Under the seabed, the temperature increased with depth in winter and decreased with depth in summer.

The measurements showed that the temperature is nearly constant throughout the water column (Figure 4.13). The fluctuation in temperature (± 1.5 ºC) is similar for both summer and winter. Under the sea-bed, the temperature increases with depth in winter (rate= 5.5 ºC/m) and decreases with depth in summer (rate= 5.2 ºC/m). The fluctuation is much lower than in the water column (maximum± 0.2 ºC). The temperature fluctuation decreases with depth within the sea-bed sediments, for both the summer and winter periods. Based on a linear extrapolation, the depth at which no temperature change takes place is 140 cm below the seabed, where the temperature is predicted to be constant at 23.7 ºC. Interestingly, this stable temperature is the annual mean of the water temperature for the site; this showed that the sea-bed sediments temperature is controlled by the temperature of the water above it, rather than by geothermal trends.

A. Winter temperature measurements

Figure 4.14 A shows a time-series of temperature obtained from the winter measurements taken in Kuwait Bay from 27th November to 16th December, 2007 at Location 1. The water temperature is constant with depth. The temperature below the

sea-bed is higher than the temperature of the water column. This suggests heat transfer from the sea-bed to the seawater. This is associated with a geothermal gradient (Al-Temeemi and Harris, 2001) which, for this region, is 4 ºC/m. The graph shows day and night temperature fluctuations beneath the seabed. There are high temperature variations in the upper measurements, but the fluctuation decreases with depth. At a depth of 60 cm, the diurnal fluctuations are no longer evident. Figure 4.14 B shows the air temperature and wind speed for the period of the measurements. The lowest seawater temperature recorded was 15.2 ºC on 28th November at 7:00 am, where the wind speed was 4.0 m/s and the air temperature was at its lowest value, of 8.8 ºC. The highest water temperature recorded in the winter was 22.5 ºC on 7th December at 6:00 am, with a low wind speed of 3.8 m/s and a high air temperature, 22.7 ºC. This pattern illustrates that the seawater temperature is affected largely by air temperature and wind speed. The effect of air temperature is much higher than the effect of wind speed. Figure 4.14 shows the water level and solar radiation, during the measurement period. Although the tide in Kuwait Bay has a great diurnal inequality (difference in the height of the two high waters), the peaks in water temperature are always found during the middle of the day, when solar radiation and air temperature are greatest. The long-term trend shows a steeper temperature gradient beneath the sea-bed during spring tides and a lower temperature gradient under neap tides.

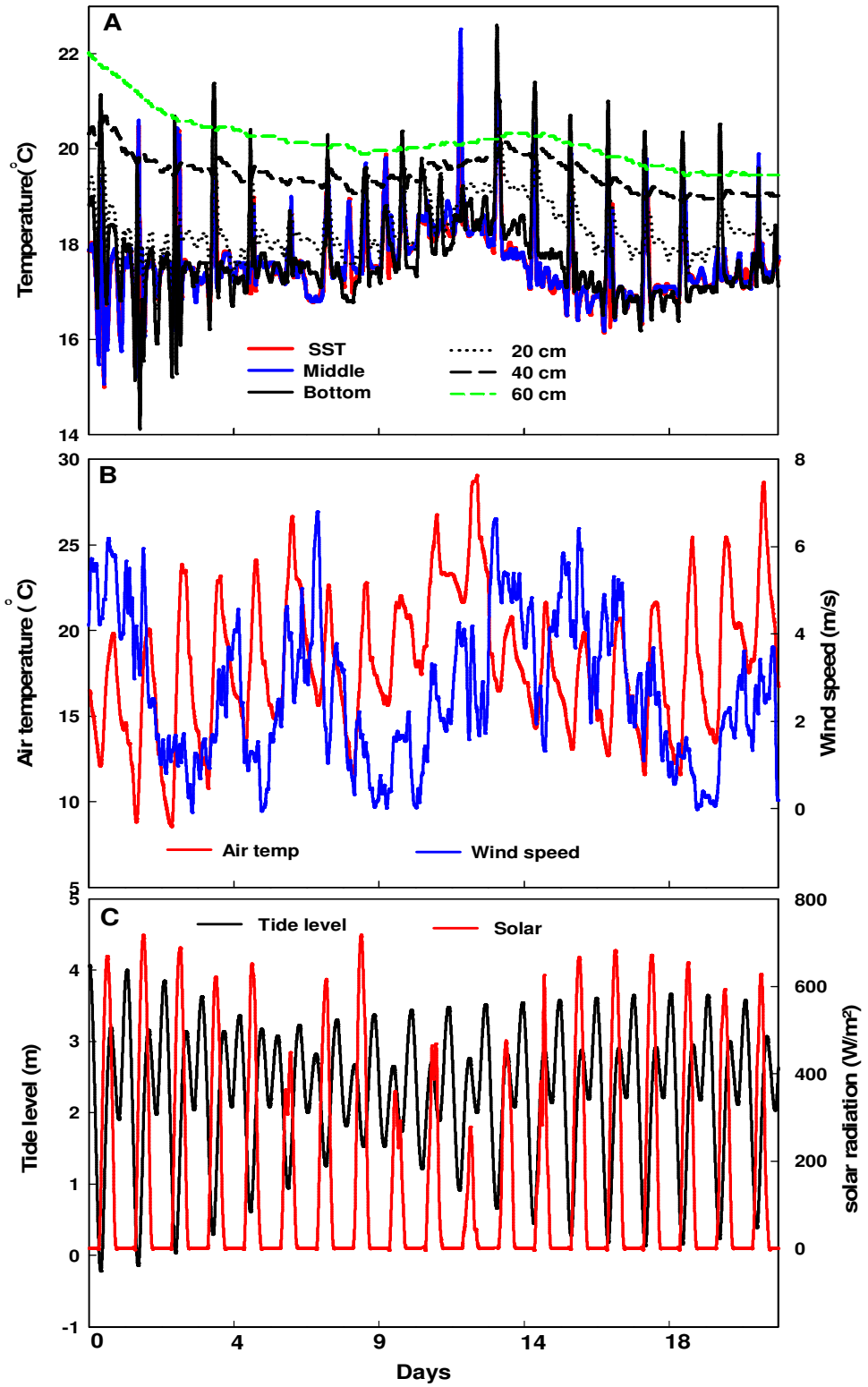

Figure 4.14: Time-series at location 1 showing (A) hourly surface, mid-water and bottom water temperatures, (B) hourly air temperature and wind speed, and (C) hourly tide and solar radiation from 27th November to 16th December, 2007.

B. Summer temperature measurements

Figure 4.15 A shows the time-series of temperatures during the summer measurements in Kuwait Bay from 14th June to 23rd July, 2008 at Location 1. The water column is well-mixed and shows strong diurnal trends which dominate the signal. The daily fluctuation is approximately 6 ºC. High temperature variations were recorded around mid-day in the water and to depths of 2 and 10 cm beneath the seabed. There were no diurnal temperature variations at depths of 60 cm. The highest seawater temperature recorded was 37.1 ºC and the lowest was 24 ºC. The temperature below the seabed is lower than the temperature of the water. This suggests heat transfer from the water to the sea-bed in summer. Figure 4.15 B shows the air temperature and wind speed during the measurements. The seawater temperature increased with increasing air temperature. When wind speed is high, the seawater temperature decreased. This illustrates that the seawater temperature is affected largely by air temperature and wind speed, similar to the results of the winter measurements. Figure 4.15 C shows the water level and solar radiation during the measurement period. Similar to the winter measurements, the peaks in the seawater temperature are always found in the middle of the day, when solar radiation and air temperature are greatest.

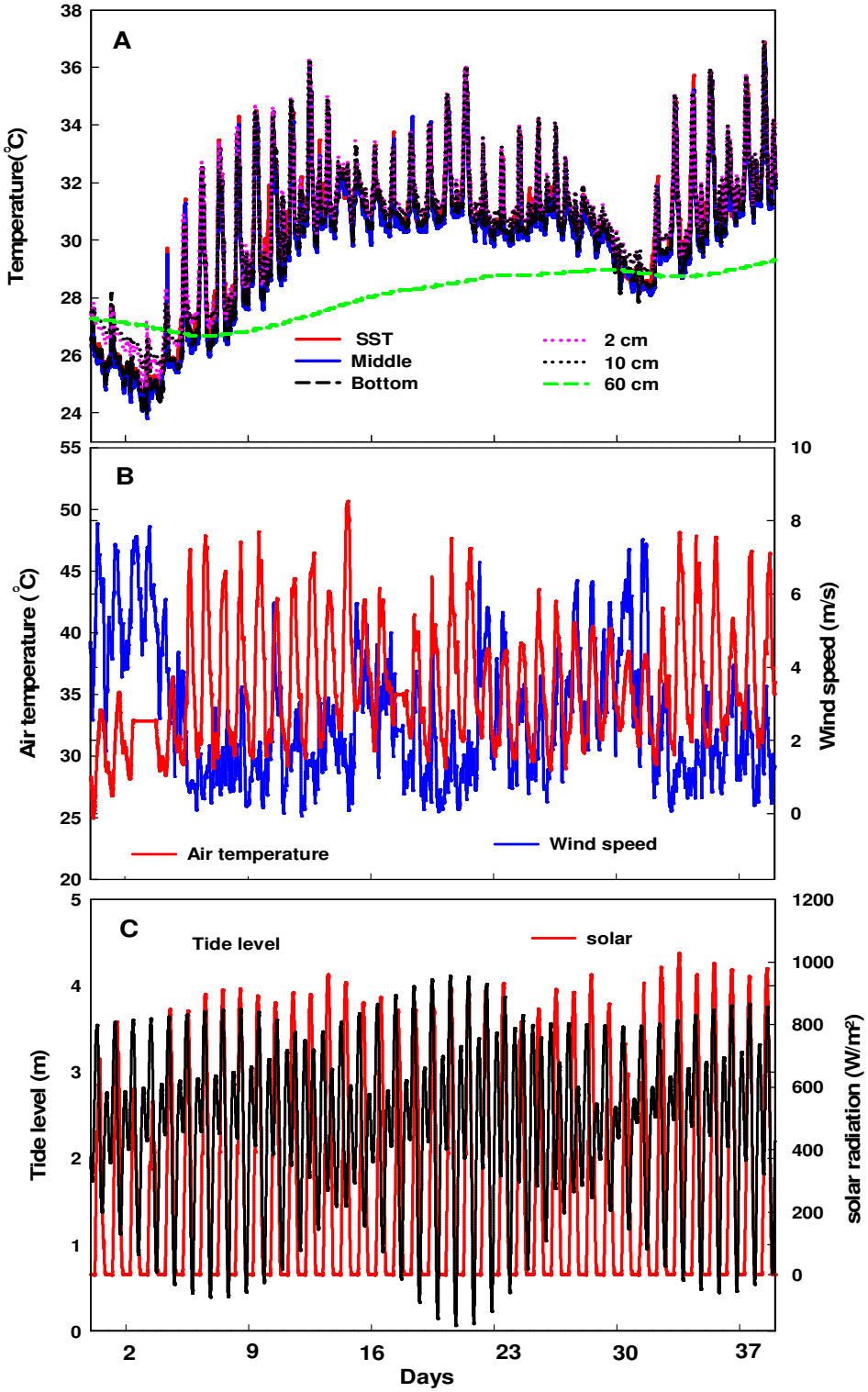

Figure 4.15: Time-series at location 1 showing (A) hourly surface, middle, and bottom water temperature, (B) hourly air temperature and wind speed, and (C) hourly tide and solar radiation from 14th June to 23rd July, 2008.

4.3.5 Vertical temperature distribution in the intertidal flat sediments

The vertical temperature gradient for the intertidal flat sediments of Kuwait Bay at Location 2 (Figure 4.3) is shown in Figure 4.16. The estimation is based on hourly measurements, taken during both summer and winter. The winter measurements were taken from 26th November to 17th December, 2007; the summer measurements were made from 23rd June to 24th July, 2008. As at location 1, the temperature increases with depth in the winter and decreases with depth in the summer. The variation (standard deviation) in temperature decreases with depth, for both summer and winter measurements, showing damping of high frequency variations. In winter, the temperature varies from 14 ºC to 17 ºC in the upper measurements (20 cm) and from 18.8 ºC to 20.4 ºC in the lower measurements (60 cm). In summer, the temperature varies from 28.5 ºC to 31.7 ºC in the upper measurements (20 cm) and from 27.2 ºC to 29.5 ºC in the lower measurements (60 cm). In winter, the intertidal flat sediments temperature increases with depth by 10 ºC/m in the upper measurements (20-40 cm) and 8.5 ºC /m in the lower measurements (40-60 cm). In summer, the intertidal flat sediments temperature decreases with depth by 4 ºC/m in the upper measurements (20-40 cm) and 4.5 ºC/m in the lower measurements (40-60 cm). The gradient in temperature is linear during both winter and summer periods. Linear extrapolation indicates that the depth at which no temperature change takes place in the intertidal flat sediments of Kuwait Bay is 1.25 m. At this depth, the temperature is constant, at 25.6 ºC. This temperature is 1.9 ºC higher than the sub-sea-bed temperature at Location 1, possibly because of direct solar heating during periods of low water.

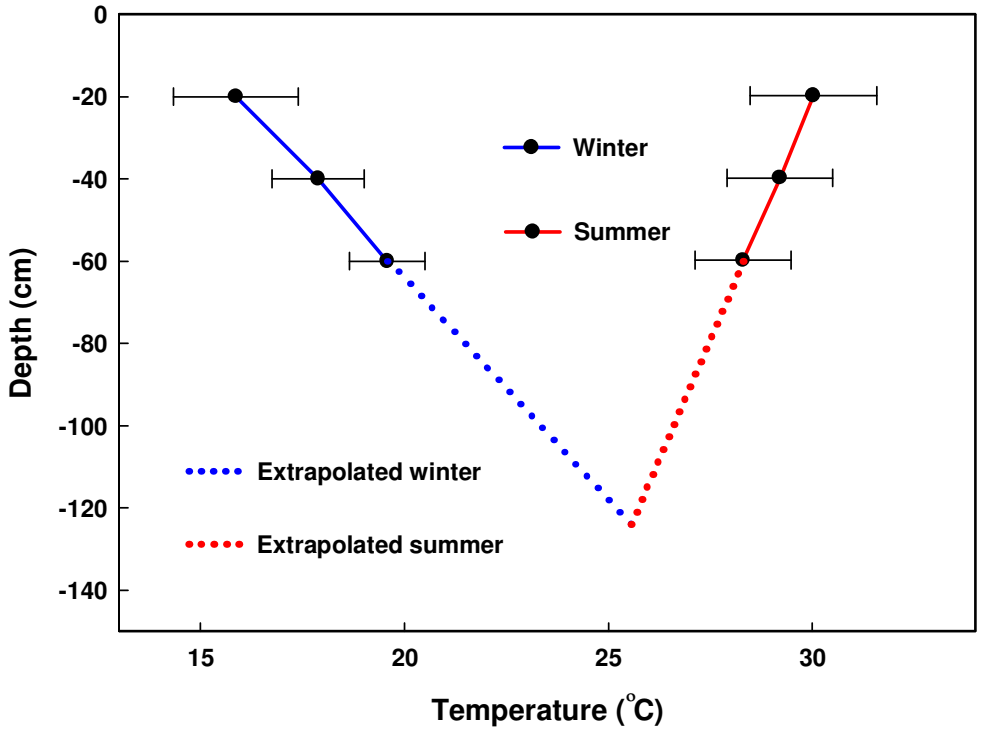

Figure 4.16: Vertical temperature distribution in intertidal flat sediments in southern Kuwait Bay at location 2. The temperature increases with depth in winter and decreases with depth in summer.

Figure 4.17 shows the time-series of hourly measurements at five depths below the intertidal flat, from 17th December 2007 to 28th December, 2008. The probes were installed at depths of 20, 40 and 60 cm. A fourth probe was added at 10 cm, from 17th March 2008. A fifth probe was added at a depth of 2 cm from the 8th April 2008. The missing data during the summer were for the period when the probes were moved to Location 1 (Figure 4.15), for the offshore measurements. The time-series shows a minimum in late January (8.5 ºC) and maximum in early September (40 ºC). The mean intertidal flat sediments temperature fluctuated, at these times, at a rate of 3 ºC/month. The subsequent autumn cooling takes place at a steady rate of 4.4 ºC/month. The greatest diurnal fluctuation in temperature takes place at shallower depths. The trend shows long-term fluctuations, which appear to respond to the neap-spring tidal cycle. The long-term variation is higher in winter, than in summer. Due to the different gradients in temperature, heat moves upwards in winter (heat source), and downwards in summer (heat sink). This indicates that the intertidal flat sediments is a source of heat to the water column in winter, but a sink for heat in the

summer. In April and October, there are no temperature gradients with depth in the intertidal flat sediments. Therefore there is no heat transfer at these times.

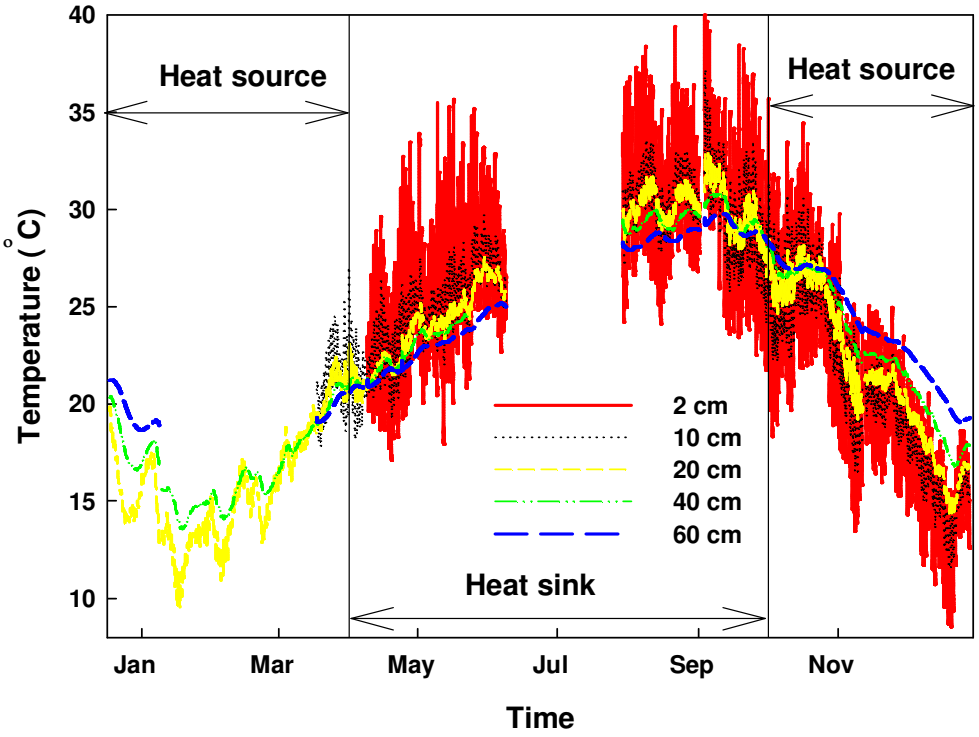

Figure 4.17: Time-series of hourly temperature records at different depths in the intertidal flat sediments of Kuwait Bay at location 2 in 2008. The greatest diurnal change takes place at the upper measurements (2 cm). Due to the different gradients in temperature, heat moves upward in winter (heat source), and downwards in summer (heat sink).

A. Winter temperature measurements at intertidal flat stations

Figure 4.18 A shows the time series of temperature during the winter measurements from the intertidal flats of southern Kuwait Bay from 17th December, 2007 to 8th January, 2008, at Location 2. The graph shows diurnal temperature fluctuations (±0.5 ºC), which are evident in the upper measurements (20 cm), but not deeper. Diurnal variations were absent at depths of 40 and 60 cm, but showed lower frequency trends; these appear to be seasonal in nature. The fluctuations in temperature appear to respond to the neap-spring tidal cycle: they are higher during neap tides. The temperature change (decrease) at 40 cm depth was 3 ºC, whilst it decreases at 60 cm depth less than 1 ºC. Figure 4.18 B shows the air temperature and wind speed during the period of measurements. Although the lowest air temperature

was 6 ºC, the lowest temperature recorded in the intertidal flat sediments was 13.9 ºC on 25th December at 02:00 am, with a relative low air temperature of 10.2 ºC and a high wind speed of 4.0 m/s. The general trend in air temperature is mimicked in the intertidal flat temperature, as are the diurnal variation. Figure 4.18 C shows the water level and solar radiation during the measurement period. The tide has a great diurnal inequality, and as explained in the methodology, the water reaches the instrument at this location at 2.9 m above Mean Low Water. Therefore, over the neap tide, the water reaches the instruments only during peak high water. The peaks in temperature are found at noon, during low tide (high exposure time).

B. Summer temperature measurements at the intertidal flat station

Figure 4.19 A shows the time-series of temperature during the summer measurements on the intertidal flat sediments of Kuwait Bay from 1st August to 22nd August, 2008 at Location 2. The graph shows large diurnal temperature fluctuations (± 5 ºC) in the upper measurements. High diurnal temperature fluctuations were also recorded at depths of 10 and 20 cm. No diurnal fluctuations were evident at depths of 40 and 60 cm. Meteorological data were not available for the summer measurements. The day-night variation was used to define the effect of solar heating, on the intertidal flat sediments temperatures. Figure 4.19 B shows the water level and day-night variation during the measurements. The fluctuations appear to respond to high and low water, also to the neap-spring tidal cycle: they are higher during neap tides. High intertidal flat temperatures were recorded during high water and low temperature recorded during low water. The peaks in intertidal flat temperature were caused by water which has been heated during the day.

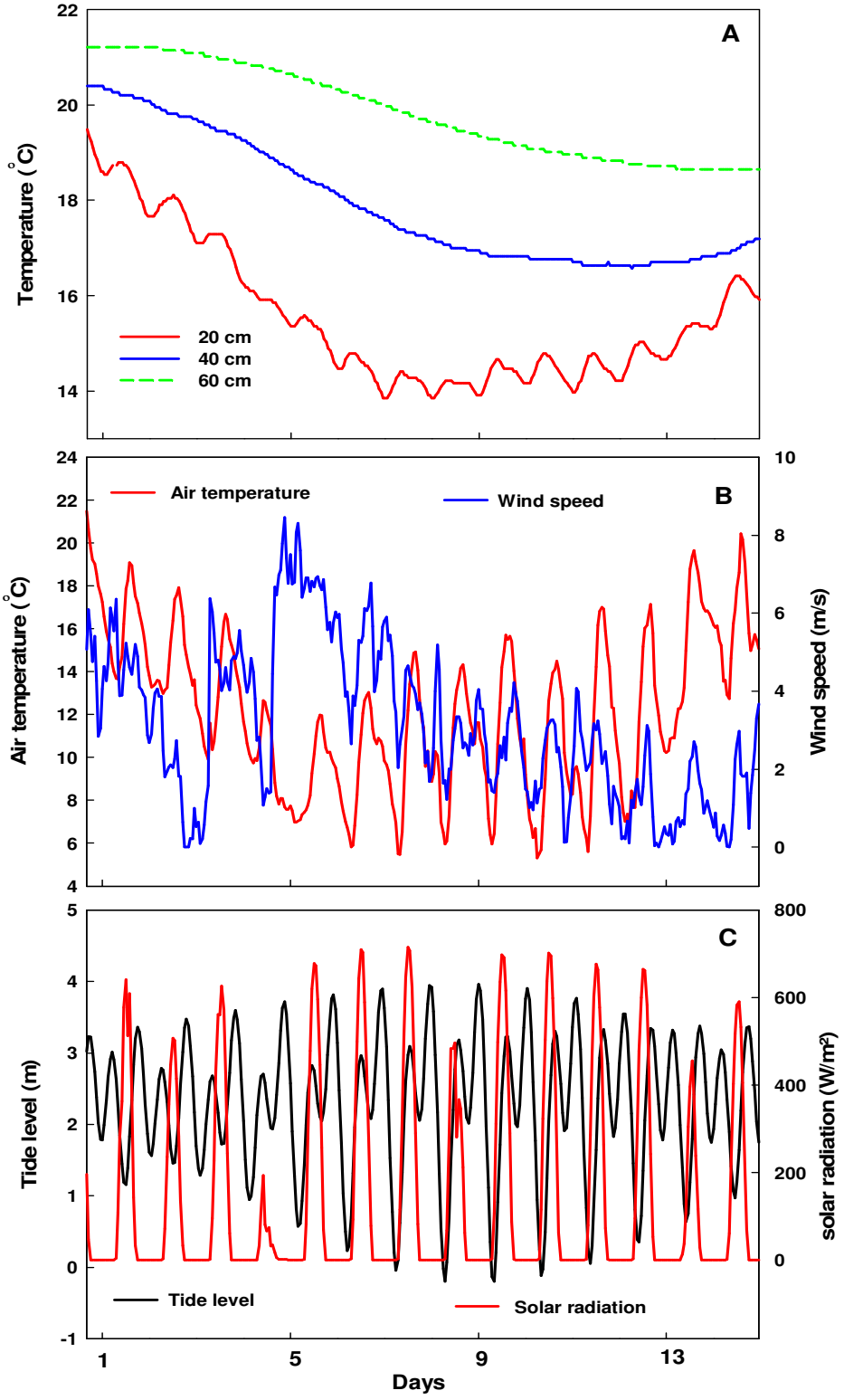

Figure 4.18: Time-series showing (A) hourly intertidal flat sediments temperatures at depths of 20, 40 and 60 cm, (B) hourly air temperature and wind speed, and (C) hourly tide and solar radiation from 17th December, 2007 to 8th January, 2008 at location 2.

Harrison and Phizacklea (1985) found that the sub-surface heat flux in the Forth Estuary, Scotland depends strongly on the time of high water. They found the effect of high water was greater, when it occurred between 0500 to 1400 GMT. Because the tide in Kuwait Bay has a large diurnal inequality, there are two peaks a day in temperature, during spring tides. Over the neap tide condition, the water reaches the instrument once a day; this suggests that large heat losses occur from the seawater to the intertidal flat sediments. This was clear in the Landsat image (Figure 4.12), where the SST in the north of the bay was 3 ºC colder than in the middle of the bay. This could be due to the wide intertidal flat in the northern part of the bay.

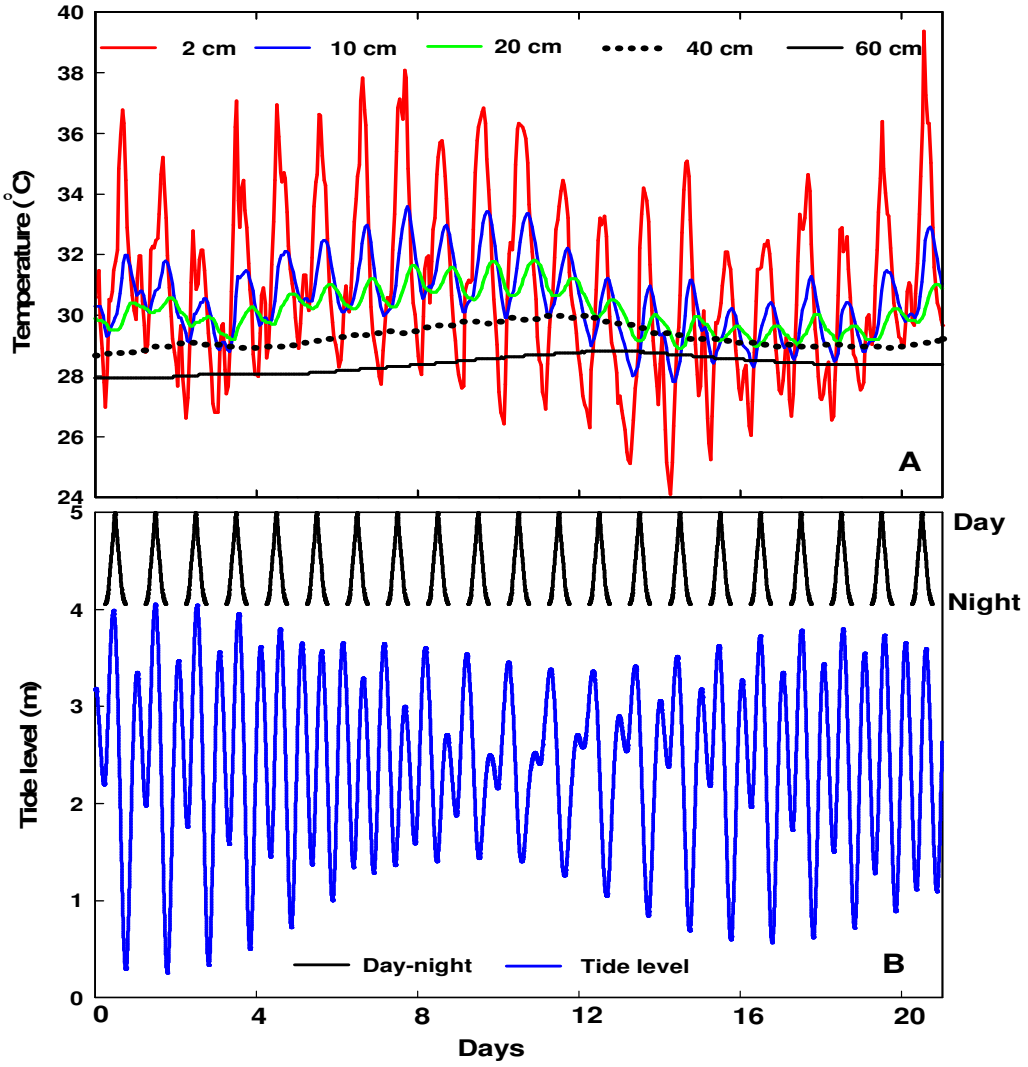

Figure 4.19: Time-series showing (A) hourly intertidal flat temperature at 2, 10, 20, 40 and 60 cm, (B) day-night variation, hourly tide and exposure index from 1st to 22nd August, 2008 at Location 2.

4.3.6 Frequency analysis of data

As explained earlier, a Fast Fourier Transform (FFT) was used to extract information about the frequencies of fluctuation in hourly seawater temperature, recorded at Location 1; this was in order to explain the periodic variability of seawater temperatures in Kuwait Bay. Figures 4.20 and 4.21 provide the FFT results of winter and summer measurements (27th November to 16th December, 2007 and 14th June, to 23rd July 2008, respectively). The energy density for both data sets shows peaks at 6.2, 8.0, 12.4 and 24 hour periods. The peak at 12.4 hours is the period of the M2 (semi-diurnal) tide. The peak at 6.2 hours is the period of M4 tide, and the peak at 24 hours is related to the solar orbit (S1). Table 4.1 illustrates the tidal constituents at Al-Shuwaikh port to the south of the bay (N 29.35 E 47.92). An 8 hour period peak appeared present in KISR station hourly air temperature measurements ; this may be related to the inequality of the day and night periods (Figure 4.22). Cho *et al.*,(2005) found similar results on a intertidal flat sediments in Korea. They found high peaks in the sediment temperatures at 24, 8 and 6 hour periods from spectral analyses. They refer the peaks at the 24 and 6 hour periods, to the day-night change and the tides, respectively. The peak at the 8 hour period was related to the unequal duration of day and night.

Table 4.1: Tidal constituents at Shuwaikh port, Kuwait Bay.

Tidal constituents	Period (hours)	Amplitude (m)
M2	12.42	0.949
S1	24	0.053
S2	12	0.34
K2	11.97	0.11
M4	6.21	0.04

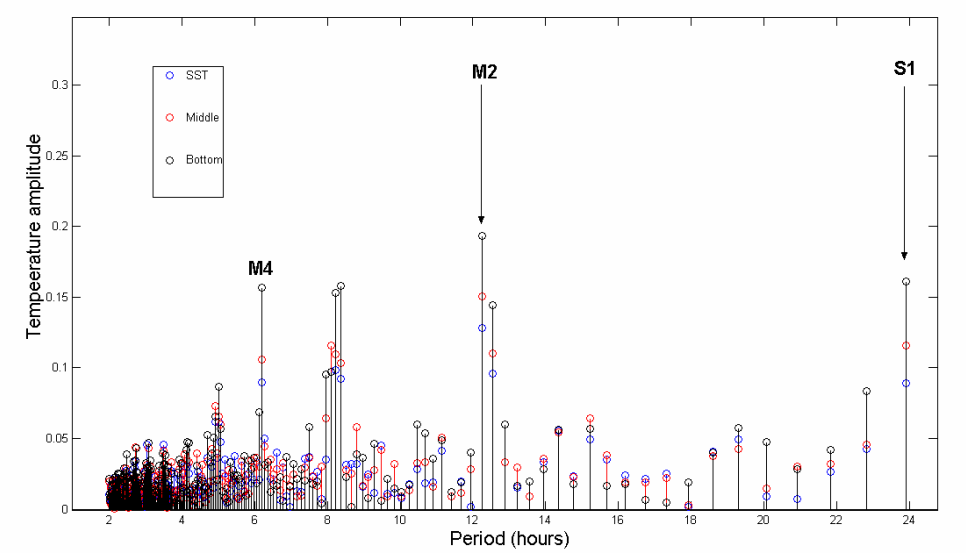

Figure 4.20: FFT for hourly temperature measurements in winter at location 1 in Kuwait Bay from 27th November to 16th December, 2007. It shows peaks at 6.2, 8.0, 12.4 and 24 hour periods. The peaks at 6.2, 12.4 and 24 hours relates to tidal constituents and day-night changes. The peaks at 8 hour period related to inequality of the day and night periods as it clear in the air temperature signal in Figure (4.22).

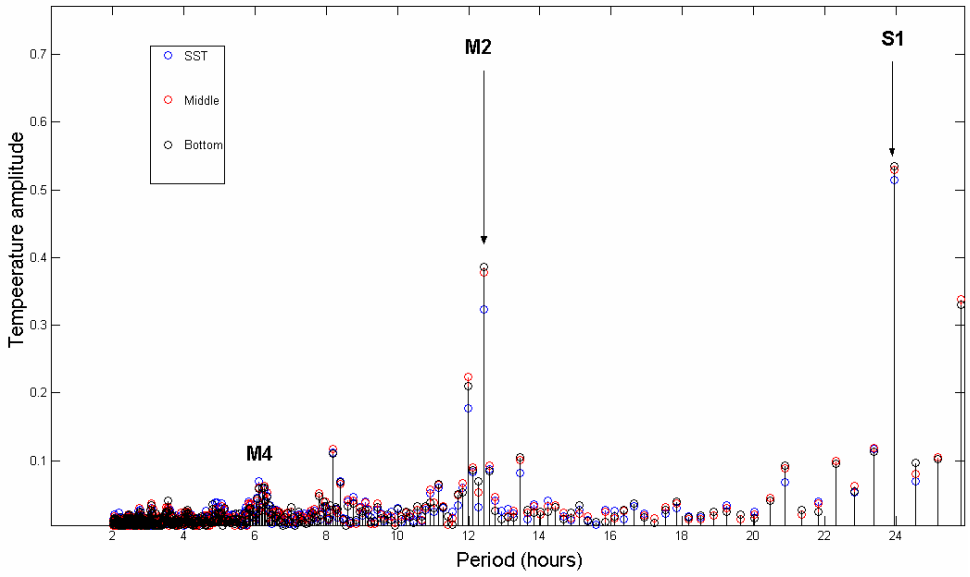

Figure 4.21: FFT for hourly temperature measurements in summer at location 1 in Kuwait Bay from 14th June, to 23rd July 2008. Again, it shows peaks at 6.2, 8.0, 12.4 and 24 hour periods similar to the winter measurements.

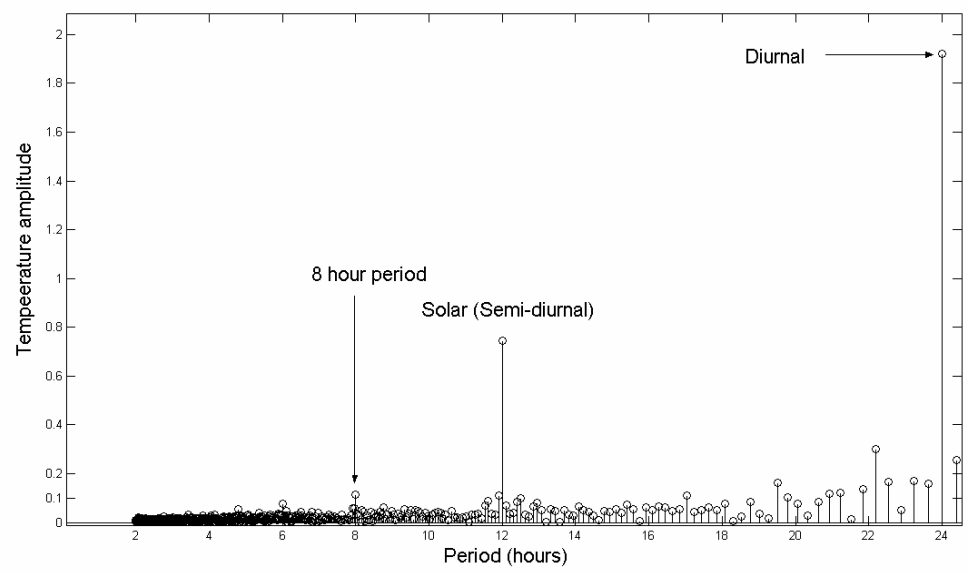

Figure 4.22: FFT for hourly air temperature at KISR station, in the southern bay. It shows peaks at 8, 12 and 24 hour periods. The peaks at 12, and 24 hours relates to day-night changes. The peaks at 8 hour period relates to inequality of the day and night conditions.

Step-wise multiple regression was used to determine the most important meteorological factors that affect seawater temperature in Kuwait Bay. This statistical approach was applied using hourly seawater temperature measurements in winter (from 26th November 2007 to 17th December, 2007), and in summer (from 13th June 2008 to 23rd July, 2008). The independent variables considered are as follows:

1. Hourly air temperature (KISR station);
2. hourly wind speed (KISR station);
3. hourly solar radiation (KISR station); and
4. tidal levels in Kuwait Bay.

In general, the results show a correlation between seawater temperature and the independent variables. A summary of the regression is given in Table 4.2 for winter, and in Table 4.3 for the summer measurements. B values represent the contribution of each variable (the independent variables) to the seawater temperature (dependant variable), and the p-level represents the level of significance. When the p-level is more than 0.05, then no relationship exists between the dependent and independent variables. Good correlations were achieved with air temperature and wind speed. As shown in Figure 4.14, the air temperature is the dominant factor. The

result of this statistical analysis shows that 43% of variance of temperature, in Kuwait Bay is explained by air temperature. Wind speed is also important and accounts for 29% of the variance in reducing the seawater temperature. This is expected, as evaporation and cooling increase with increases in wind speed. The relationship between seawater temperature and tidal range is marginal (p-levels more the 0.05). Rakha et al., (2009) showed that the flushing time of Kuwait Bay is close to three years. Thus, mixing in the Arabian Gulf has little influence on seawater temperature of Kuwait Bay.

Table 4.2: The contribution of meteorological factors influencing seawater temperature in Kuwait Bay (location 1) during winter from 27th November to 16th December, 2007. (SD is the standard deviation of the data set)

	B	SE	p-level
Air temp.	0.43	0.04	0.001
Wind speed	-0.29	0.04	0.001
Solar radiation	-0.23	0.05	0.001
Tide	-0.08	0.04	0.06

Table 4.3: The contribution of meteorological factors influencing seawater temperature in Kuwait Bay (location 1) during summer from 14th June, to 23rd July 2008.

	B	SE	p-level
Air temp.	0.09	0.04	0.004
Wind speed	-0.64	0.04	0.001
Solar radiation	0.12	0.04	0.001
Tide	-0.06	0.03	0.09

Air temperature during summer explains only 9% of the variance in seawater temperature in Kuwait Bay; this is considerably lower than the winter influence. It is suggested that evaporative processes (which increase with temperature and wind speed) are the controlling process, explaining 64% of the variance in the data. The contribution of solar radiation is greater in summer, than during the winter; this may be due to fluctuations caused by dust storms, produced by S*hamal* winds. Figure 4.23 shows a dust storm that covered Kuwait on 11th February, 2009. Figure 4.24 shows

hourly temperature measurements in the intertidal flat sediments south of Kuwait Bay from 8th to 20th February, 2009 (over the period of the dust storm).

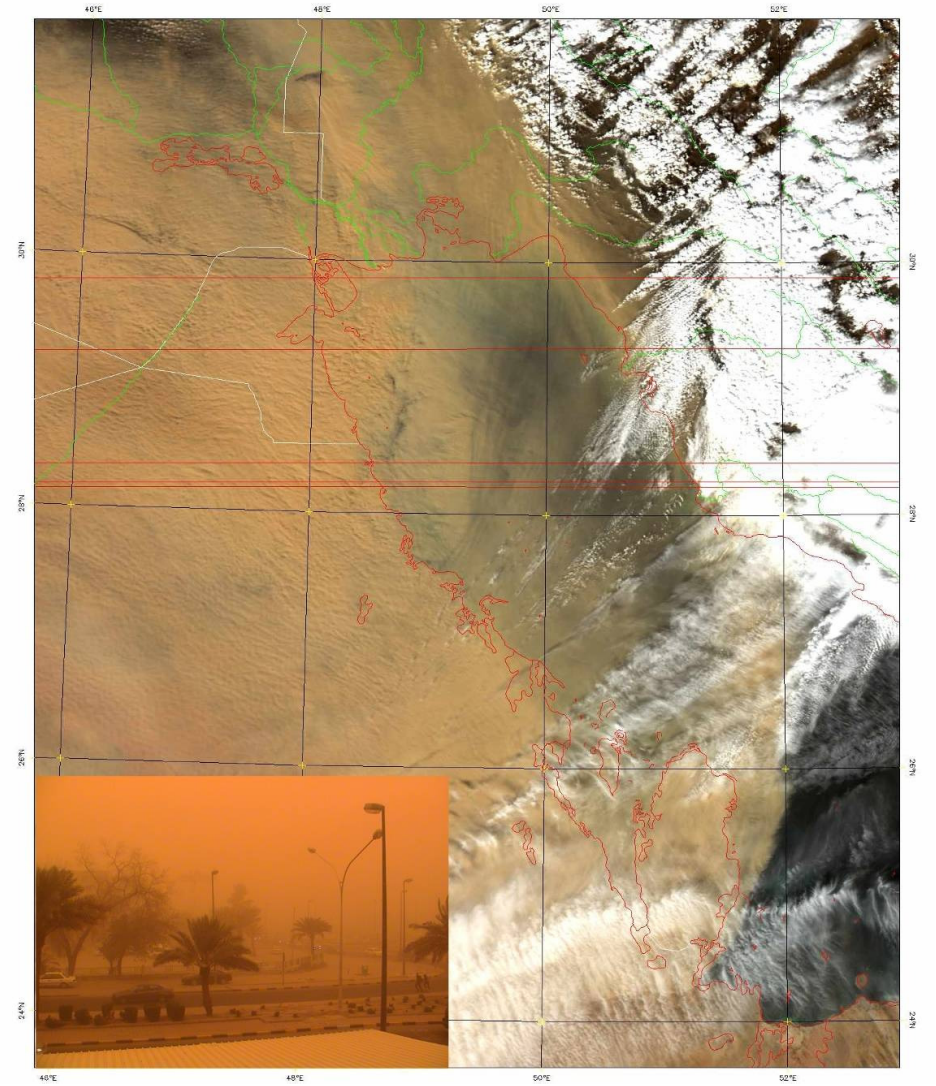

Figure 4.23: MODIS satellite image showing the heavy dust cover in the atmosphere which covered Kuwait Bay on 11th February, 2009 and a photograph taken the same day in Kuwait (Source: ROPME, Kuwait).

The Figure shows the effect of the dust suspended by the strong *shamal* wind, on the temperature of the intertidal flat sediments of Kuwait Bay; it reduced the temperature of the intertidal flat, at depth of 20 cm; by about 1.5 ºC. The dust thus has the effect of solar dimming, and reducing temperature at ground level. During the period of maximum dust cover, the diurnal fluctuation in temperature (evident in the reduction of the time-series) was greatest. This pattern shows that during such dust storms,

solar radiation is so reduced that there is no difference in solar radiation between day and night.

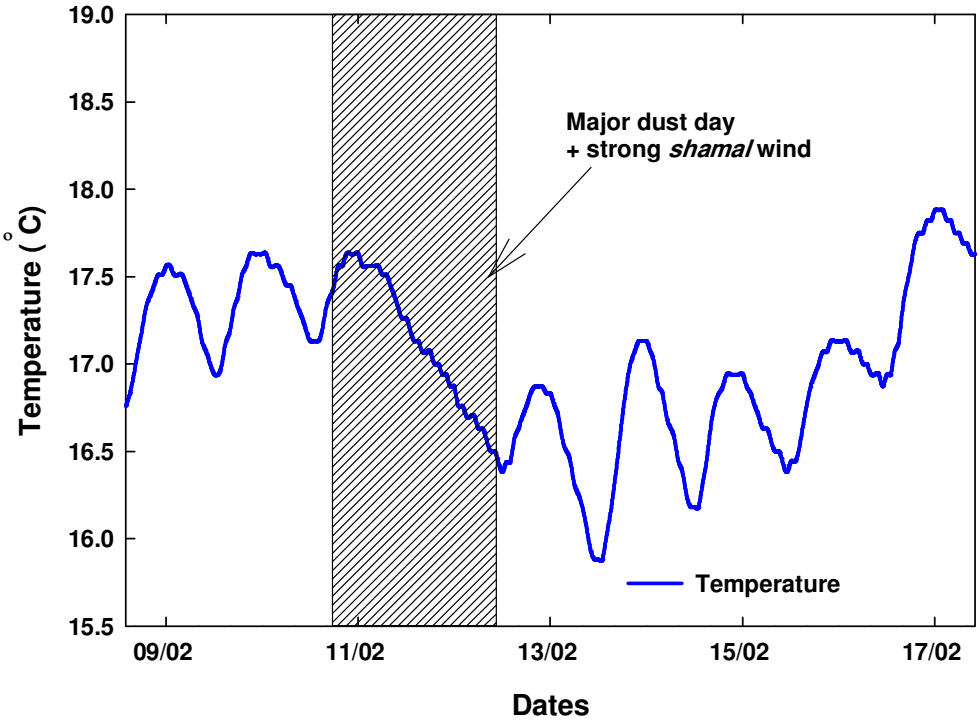

Figure 4.24: Time-series of hourly temperature measurements in the intertidal flat sediments south of Kuwait Bay at location 2 from 8th to 20th of February 2009. It shows a reduction in temperature during the major dust day and a complete attenuance of the diurnal temperature fluctuation.

4.3.7 Heat flux in the sea-bed and in the intertidal flat sediments

The field measurements were used to calculate the vertical heat flux at Locations 1 and 2. The heat flux equation (equation, 4.1) was applied for the day and night measurements, to investigate the heat transfer under different conditions of solar radiation. For the intertidal measurements, the heat flux equation was applied during low tide conditions (dry time heat flux) then during high tide conditions (wet time heat flux). Tables 4.4 and 4.5 provide the heat fluxes for the offshore measurements (Location 1), whilst Tables 4.6 and 4.7 summarise the heat fluxes for the intertidal flat (Location 2). The sign represents the direction of the flux (+'ve is a flux downwards, into the seabed). It can be seen that, during winter, the heat transfer is directed upwards into the water column. In summer, the heat transfer is directed from the water column to the seabed. The mean fluxes are - 5.39 W/m^2, for winter, and 0.28 W/m^2, for summer. This pattern corresponds to the time-series

measurements of seawater temperature that show greater losses of heat during autumn and winter, than gains in spring and summer (Figure, 4.17). The night heat flux to the water column is greater than the day heat flux for both seasons, indicating that the greatest heat losses are at night. This is apparent also in the water column measurements shown in Figure 4.17. The heat flux decreases with depth below the seabed. The heat flux is much higher on the intertidal flats than on the subtidal sea-bed, particularly during the day. The winter heat fluxes are higher than the summer values: 10.2 W/m^2 for winter and 4.2 W/m^2 in the upper measurements (20-40 cm), for summer. This is due to stronger temperature gradients between the water column and the bed, during winter. During both seasons, the heat flux from the upper measurements was higher than the heat flux from the lower measurements. The upper layer of the intertidal flats sediments are affected largely by atmospheric conditions or by water temperature during high tide (Harrison and Phizacklea, 1985; Piccolo et al., 1993). The intertidal heat flux (from the intertidal flat) during winter is 50% higher, than during summer. Once again, this is due to a greater temperature difference between the bed and the air, than between the bed and the water column.

Table 4.4: Heat flux estimates during winter for the subtidal sea-bed in Kuwait Bay (location 1) from 27th November to 16th December, 2007.

	Heat flux (W/m^2)	
Depth	20 cm-40 cm	40 cm-60 cm
Mean heat flux	-5.39	-3.32
Day time heat flux	-4.75	-3.18
Night time heat flux	-6.00	-3.48

Table 4.5: Heat flux estimates during summer for the subtidal sea-bed (location 1) from 14th June, to 23rd July 2008.

	Heat flux (W/ m^2)	
Depth	2 cm-10 cm	10 cm-60 cm
Mean heat flux	0.28	5.20
Day time heat flux	0.07	4.20
Night time heat flux	0.43	6.41

Table 4.6: Heat flux estimates for the intertidal flats during winter (location 2) from 17th December, 2007 to 8th January, 2008.

	Heat flux (W/ m^2)	
Depth	20 cm - 40 cm	40 cm -60 cm
Mean heat flux	-10.2	-8.6
Day time heat flux	-11.1	-8.5
Night time heat flux	-9.0	-8.5
Dry time heat flux	-9.9	-8.4
Wet time heat flux	-11.2	-9.0

Table 4.7: Heat flux estimates for the intertidal flats during summer (location 2) from 29th July to 31st August, 2008.

	Heat flux (W/ m^2)	
Depth	20 cm - 40 cm	40 cm -60 cm
Mean heat flux	4.2	4.6
Day time heat flux	3.1	4.6
Night time heat flux	5.2	4.6
Dry time heat flux	4.5	4.6
Wet time heat flux	3.5	4.6

The intertidal flat sediments is a strong source of heat (thermal energy) to the water of Kuwait Bay, in winter; but is a sink of heat from the bay water, in summer. The wet time heat flux of the intertidal flats in winter is much higher than the dry time heat flux. In the summer, the opposite is true.

4.4 Conclusions

The seawater temperature in the Arabian Gulf is higher in the south, than in the north. Close to the shoreline, the SST is 3 ºC warmer, due to local sources of heat. In Kuwait Bay, the SST is also higher in the south than in the north. The lower SST in the north is related to the loss of heat to the extensive intertidal flats. The highest SST is recorded near human activities; in particular, close to discharges from power and desalination plants. SST close to the power and desalination plants is 9 ºC warmer than the SST in the middle of the bay.

Vertical temperature measurements undertaken in Kuwait Bay have indicated that the seawater is well mixed throughout the year. The seawater temperature ranges from 15.2 ºC, in winter, to 37 ºC in summer. The sea-bed and intertidal flat sediments temperatures increased with burial depth in winter; and decreased with burial depth in summer. The depth where no temperature change took place was 140 cm below the seabed. At this depth, the temperature was constant (23.7 ºC). The intertidal flat sediments showed temperature gradients to a depth of 125 cm, where the temperature was constant at 25.6 ºC. Bemeath the sea-bed as well as on the intertidal flat, heat flowed upwards in winter and downwards in summer. The intertidal flat and the sea-bed sediments provided heat to the water in winter and a loss of heat from the water column in summer. The downward heat flow in winter was much greater than the upward heat flow in summer.

Kuwait Bay seawater temperature is affected largely by air temperature and wind speed. Dust storms are limiting factors that lead to reductions in the seawater temperature especially during high *Shamal* winds. Spectral analysis of the seawater temperature, in Kuwait Bay showed high peaks at frequency periods of 24, 12.4, 8 and 6.2 hours. The peaks at 24, 12.4 and 6.2 hour periods are due to the daily changes in solar radiation and the tide (S1, M2 and M4, respectively). The peak at 8 hours may be due to the unequal duration of the day and night air temperatures.

Chapter 5: Long-term drivers of seawater temperature

Abstract

The waters of Kuwait Bay, northern Arabian Gulf are well-mixed by macrotidal, semi-diurnal tides (Dames and Moore, 1983; Khalaf et al., 1982; and Reynolds, 2002). Sea Surface Temperature (SST) is thus a good proxy of water mass temperature in the bay. The factors governing SST herein have been conveniently sub-divided into global, regional, and local drivers. This chapter provides a study of long-term drivers of temperature change in the northern Arabian Gulf: that is, factors that have an influence over decadal time scales. AVHRR (NOAA) satellite data of Kuwait Bay, collected between 1985 and 2007, show that SST has steadily increased at a rate of 0.62 (± 0.01) ºC/decade. This trend is three times greater than the concurrent global average. The rate of change was greatest in the months of May and June; it was least during winter. The trends defined by the satellite data were substantiated by routine *in situ* monthly measurements of SST made in the region, they were also similar in pattern and trend to air temperature recorded at Kuwait airport. The monthly measurements of SST showed also peaks in summer temperature coincident with El Niño events in 1998 and 2003. A relatively-low summertime peak during 1991, in the aftermath of Iraqi invasion of Kuwait, is considered to be the result of atmospheric dimming brought about by dense smoke that persisted in the region for most of that year.

5.1 Introduction

Information about the drivers of climate change is important for possible future climate changes (Jacob, 2008). In this study, long term drivers of seawater temperature in Kuwait Bay have been investigated, in order to provide a better prediction of the influences of these drivers on the seawater temperature. Seawater temperature has been widely examined for long-term trends. For example, Rayner et al. (2006) found that global sea surface temperature has been increasing by 0.6 ºC over the period 1850 to 2004. Long-term trends of SST in SST the Indian Ocean increased by 0.7 ºC, over the last century. This warming has accelerated rapidly in the last three decades, to 0.14 ºC/decade (Kothawale et al., 2008). The Intergovernmental Panel of Climate Change (IPCC, 2007) stated that the global ocean warming has been 0.13 ºC/decade for the last three decades. The warming in the Northern Hemisphere has been 0.19 ºC/decade and the warming in the Southern Hemisphere has been 0.09 ºC/decade. Pearce and Feng (2007) found that SST has increased by 0.2 ºC/decade throughout the Indian Ocean, during the last 50 years. Kothawale et al. (2008) found the SST has increased in the Arabian Sea by 0.16 ºC/decade, from 1972 to 2002. Yanagi (2008) used sea water temperature measurements from 1976 to 1997 in Tokyo Bay in Japan to determine an increase of 1.5 ºC/decade in that region. Air temperature has been found also to increase by 0.2 ºC/decade world-wide, during last three decades (IPCC, 2007) whereas it has increased by 0.6 ºC /decade in some coastal cities, such as Los Angeles and Mexico City (González et al., 2005).

The NOAA Advanced Very High Resolution Radiometric (AVHRR) satellite has collected data, globally since 1981. Five thermal channels of calibrated data are available for analysis (NOAA, 2009). Thus, AVHRR is the widest used thermal infrared (IR) remote sensor for measuring SST and, in that sense, it is the most successful space platform (Robinson, 2004). Lawrence *et al.* (2004) found that the SST extracted from AVHRR data can be used to measure climate change. Khan *et al.* (2004) used AVHRR data to study the variation of SST in the Arabian Sea and Bay of Bengal. They found that SST had increased by 0.2 ºC/decade in the Arabian Sea, NW Indian Ocean (in keeping with global averages), but had increased by 0.5 - 0.6

ºC/decade along the southern coast of Oman (a rate much higher than the global average). This latter observation suggests that regional and local effects were at work on SST that was dominating global trends in temperature. It also suggests that local trends may be far in excess of the published global values. In Kuwait Bay, it is assumed that the seawater temperature is affected by a range of drivers. These drivers have a cumulative effect on seawater temperature. This increase is due to the combined effects of global, regional, and local drivers ($\Delta T = \Delta t$ (global) + Δt (regional) + Δt (local). As explained in Chapter 1, the global drivers are those drivers that influence SST everywhere. Regional drivers are the sum total effect of a number of peripheral drivers, between local and global scales. Local drivers are those sources of heat that may be detected and defined from a clearly defined adjacent source. This Chapter examines the effects of the drivers of seawater temperature in Kuwait Bay. Three stations in Kuwait Bay (Figure 5.1) were selected to measure the trend of change in the SST, based on AVHRR data from 1985 to 2007. Also, 3 stations in Arabian Gulf and 3 stations in the Arabian Sea (northern Indian Ocean) were selected to assess the trends of seawater temperature change at these stations. Since seawater is well-mixed in Kuwait Bay (Dames and Moore, 1983; Khalaf et al., 1982; and Reynolds, 2002), the satellite SST can be used as a temperature proxy for the entire water mass of the bay. In contrast, seawater is stratified in the southern Arabian Gulf (Reynolds, 1993) and in Arabian Sea (Naidu, 2006). In this study, it is assumed that the temperature structure is constant, with depth during the time period of this study.

5.2 Methodology and data analysis

Twenty three years of SST data, collected between 1985 and 2007, was acquired from the processed AVHRR Oceans Pathfinder project of NASA Jet Propulsion Laboratory (JPL), Physical Oceanography Distributed Active Archive Centre (PO.DAAC, 2009). A total of 276 SST image files for day-time, monthly mean SST at 4 km spatial resolution (4×4 km), were downloaded and analysed. The files were in a GeoTIF format (http://poet.jpl.nasa.gov/), which is suitable for input to ArcGIS. ArcGIS was used to display and define SST from AVHRR data, at 3 references stations in Kuwait Bay (29º 28' 45'' N, 47 º 56' 19'' E; 29º 28' 40'' N, 48 º 1'

33"; and 29º 27' 25" N, 48 º 7' 15") (Figure 5.1). The outer station was selected to coincide with a long-term sampling site of EPA and, hence, furnished ground truthing of satellite SST. The inner 2 stations were situated in 2 distinct water masses in the bay: a central water mass characterised by tidal exchange with the adjacent Arabian Gulf; and an inner water mass that appeared to be representative of the shallower regions of the bay. The SST values of each station are the averages of four pixels. The AVHRR satellite orbits the earth approximately 14.1 times per day and covers the Arabian Gulf twice a day: one during the day and once during the night. Monthly and yearly day-time SST data were used in this study. The monthly and yearly SST was derived, by averaging daily values from the satellite (PO.DAAC, 2009). Linear regression analysis of the monthly and yearly average of SST was used to predict the trend of SST in Kuwait Bay from 1985 to 2007.

Kuwait Environment Public Authority (EPA) collected surface water samples and measured a variety of seawater parameters, on a monthly basis at 12 monitoring stations along the coastline of Kuwait, from 1983 to the present (Figure, 4.1). EPA *in-situ* measurements at the outer station in Kuwait Bay were selected to validate the AVHRR measurements. The *in-situ* measurements obtained from 1985 to 2006 were corrected and used to define the variation in SST over the year in Kuwait Bay (Figure, 4.9). This variation was used to adjust the EPA measurements, to the middle of each month. Air temperature measurements were provided by the Meteorological Department, Kuwait airport (see Figure, 5.1) and were used also to study the change in the air temperature, for the same time period as the satellite coverage.

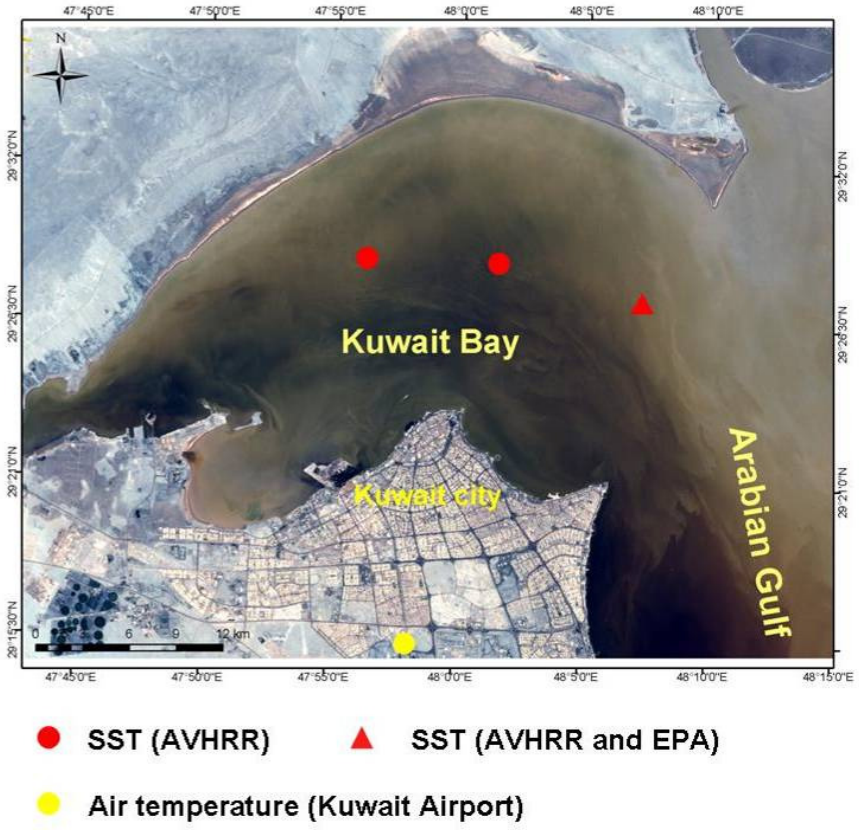

Figure 5.1: The three AVHRR stations of measurements selected in Kuwait Bay for this study. The outer station was at the same location as EPA long-term SST measurements in order to furnished ground truthing of satellite SST. The inner two stations were situated in two distinct water masses in the bay: a central water mass characterised by tidal exchange with the adjacent Arabian Gulf, and an inner water mass that appeared to be representative of the shallower regions of the bay. The figure also shows the location of long-term air temperature measurements in Kuwait airport (15 km south of the bay).

The spatial variability in AVHRR SST was examined in the first instant, in order to establish signal scatter (noise) and potential errors in spatial averaging of the data. Linear regression was used to correlate the SST extracted from AVHRR data, with SST from the field measurements (EPA) at the same location. Satellite SST values were selected to coincide in space and time, with the EPA field measurements. The time of satellite overpass was around 1400 (local time), except during the period from January 2003 to June 2005, whereas most of the EPA measurements were collected between 0700 to1000 (local time). From January 2005, EPA began to measure SST on an hourly basis at 8 buoys deployed along the coastline of Kuwait, one located in the central part of Kuwait Bay. The system is

integrated with a suite of sensors that measure and send SST remotely, on an hourly basis. The average values of hourly SST measurements in Kuwait Bay, for 2006 were used to calculate the hourly variation in SST (solar heating) for Kuwait Bay by using the average of hourly measurements over one year.

The EPA hourly data was used to adjust the EPA monthly measurements at Z6 to the time of the AVHRR overpass (14:00); and to adjust all AVHRR SST to 14:00. Forty AVHRR images were correlated against the EPA data, using least squares regression in order to examine the accuracy of the AVHRR data. The correlation was applied after adjusting the EPA measurement to the times of AVHRR overpass (as described above).

Figure 5.2 shows the location of the stations selected in the Arabian Gulf and in the Arabian Sea. The stations in the Arabian Gulf are located at least 100 km away from the shoreline and, according to the hypothesis of this study, it is assumed that they are not affected by local human activity; therefore, that these stations are influenced by regional and global drivers only. The stations in the Arabian Sea are located at least 500 km away from the shoreline. It is assumed that these stations are dominated by global drivers.

To study the regional drivers, 3 reference stations (29 º 50' 9" N, 48 º 54' 24" E; 27 º 8' 22" N, 51 º 8' 12" E; and 26 º 11' 21" N, 55º 11' 50" E) were selected in the Arabian Gulf (Figure 5.2). Each station represents the average of 4 adjacent pixels. Linear regression analysis of the average of those 3 stations was used to define the trend of SST in the Arabian Gulf (*SST*2), from 1985 to 2007. The same method was used at 3 selected stations in the Arabian Sea (northern Indian Ocean) (13 º 50' 2" N, 57 º 59' 23" E; 11 º 24' 21" N, 59 º 9' 6" E; and 13 º 24' 56" N, 61º 32' 10" E). Linear regression analysis of the average of these 3 stations in this region was used to define the trend of SST (*SST*3), from 1985 to 2007.

Thus, SST trends in Kuwait Bay (*SST*1) represent the influences of global, regional and local drivers (equation 5.1), whereas the trends in the Arabian Gulf (*SST*2) represent the influences of both global and regional drivers (Equation 5.2). Finally, SST trends in the Arabian Sea (*SST*3) represent the influences of global drivers (equation 5.3). The following equations were used to calculate the contribution of each driver, in each of these regions:

$SST1 = T_l + T_r + T_g$ ……..……Equation (5.1)

$SST2 = T_r + T_g$ ……..…...Equation (5.2)

$SST3 = T_g$ ……..…...Equation (5.3)

where:

*SST*1= SST trend in Kuwait Bay;

*SST*2= SST trend in Arabian Gulf;

*SST*3= SST trend in Arabian Sea;

T_l = trend of local drivers;

T_r = trend of regional drivers; and

T_g = trend of global drivers.

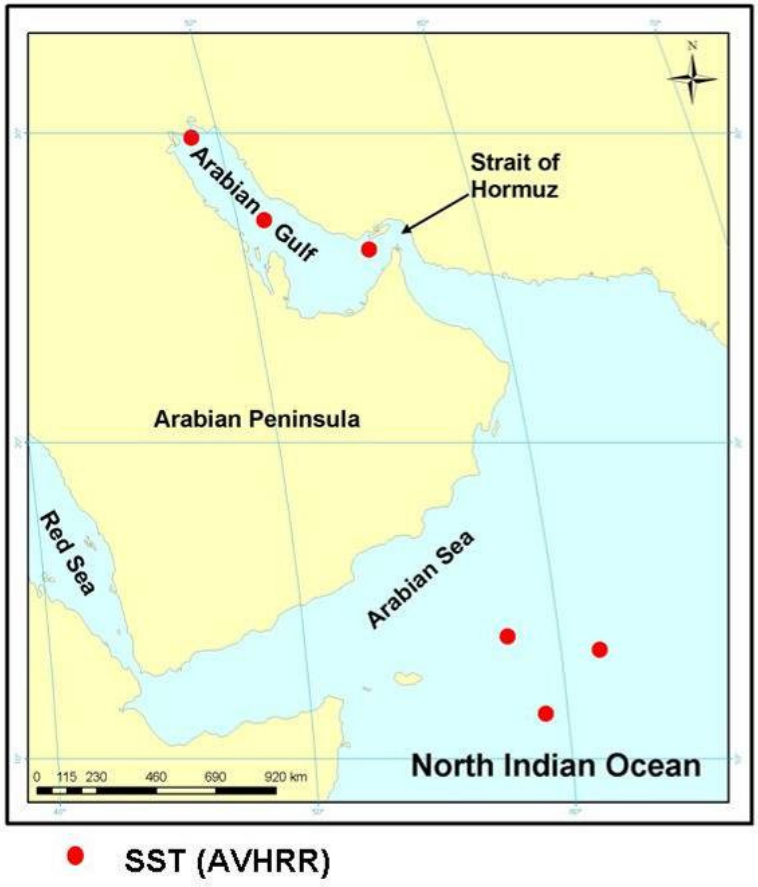

Figure 5.2: Sites of AVHRR measurements in the northern, central, and southern Arabian Gulf and three stations in the Arabian Sea. The selected stations in the Arabian Gulf are more than 100 km away from the shoreline. It is, thus assumed that they are not influenced by local human activities (local drivers), but they are influenced by global and regional drivers. The selected stations in the Arabian Sea are more than 500 km away from the shoreline. It is assumed that they are influenced by global drivers only.

5.3 Results

Figure 5.3 shows monthly mean SST obtained from the AVHRR satellite, during May, 2007. The AVHRR provides synoptic values of SST distribution, that can provide useful information on the factors influencing seawater temperature in the region. The image shows that SST varies between 22 and 33 ºC. There is a distinct difference in SST between the Red Sea and the Arabian Gulf. The SST in the Arabian Gulf is cooler than that in the Red Sea; this may be due to regional and local variation in temperature drivers. For example, high winds in the Gulf region lead to a reduction in seawater temperature, especially in the northern part of the Gulf (Reynolds, 1993). The SST is warmer in the northern Indian Ocean, than in the Arabian Gulf. Thus, heat is being transferred into the Arabian Gulf, from offshore. Figure 5.3 shows high SST (dark colour) in the Gulf of Oman (immediately outside the Strait of Hormuz). In contrast, there is a belt of low SST (yellow colour) between the Gulf of Oman and the Arabian Sea; this could be due to the upwelling that takes place in that area, as well as to the south of the Arabian Peninsula (Robinson and Brink, 2006).

The spatial variability in the AVHRR SST was compared with SST measured by EPA, in Kuwait Bay. The frequency histogram for the AVHRR SST image in the northern Arabian Gulf is shown in Figure 5.4. The data are normally distributed and show a narrow range of values (standard deviation, Std = 0.26 ºC). The example is from a sub-region of 720 km^2 (180 pixels), shown in the figure. The Gaussian, best-fit line (solid) of the measured temperature distribution is also shown. The results reveal that the data are normally distributed about the mean. The spread of the distribution is a measure of the heterogeneity in temperature at small scales; thus, it is a reflection of the uncertainty in the measurements. This uncertainty is small, compared to the spatial and temporal differences in temperature measured in this study. Thus, the mean values may be used to examine the impact of the drivers of SST over the study region.

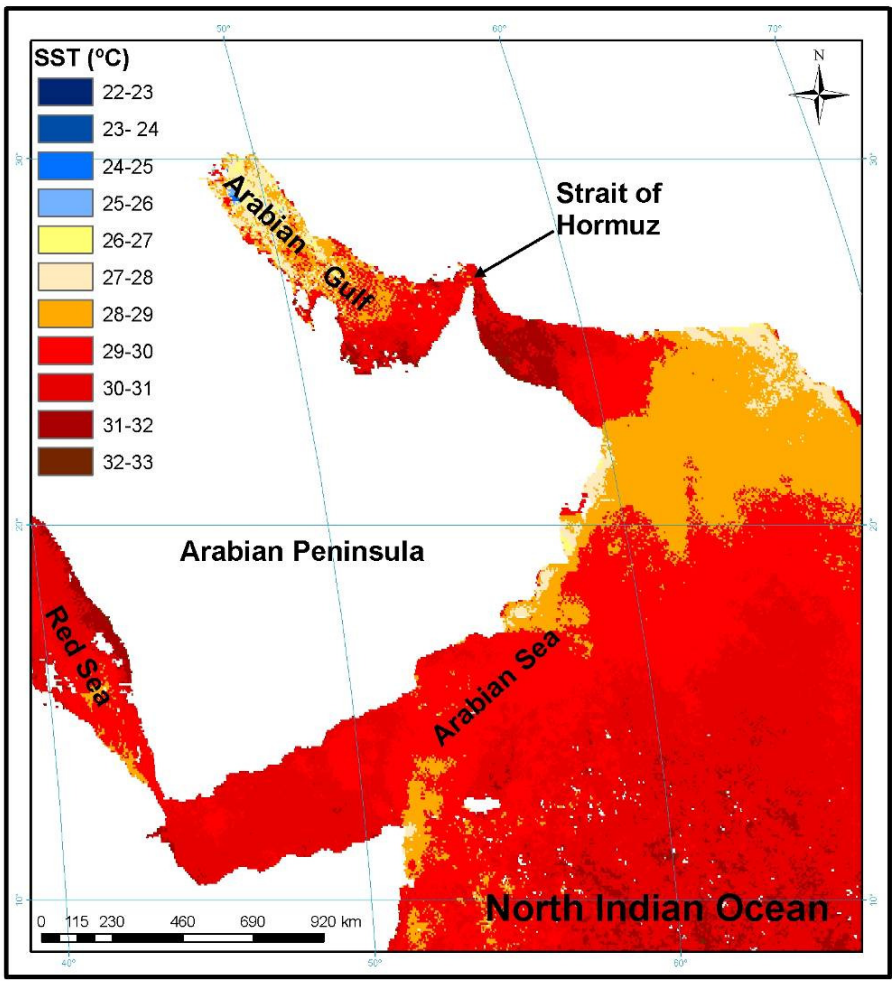

Figure 5.3: AVHRR SST in the study area for May, 2007. SST in the Arabian Sea is warmer than that in the Arabian Gulf. In the Arabian Gulf, SST is higher in the south than in the north. The figure shows high SST in the Gulf of Oman (immediately outside the strait of Hormuz) and low SST between Gulf of Oman and Arabian Sea.

Figure 5.5 shows the variation of the mean SST in Kuwait Bay throughout the day. The data are average values of hourly SST measurements made by EPA in Kuwait Bay in 2006. The variation in seawater temperature throughout the day is about ± 1.2 ºC. The graph shows the highest SST at midday (12:00) and the lowest during early morning (05:00). This variation was used to adjust EPA measurements, to the time of AVHRR overpass, in order to compare the results of AVHRR with EPA measurements.

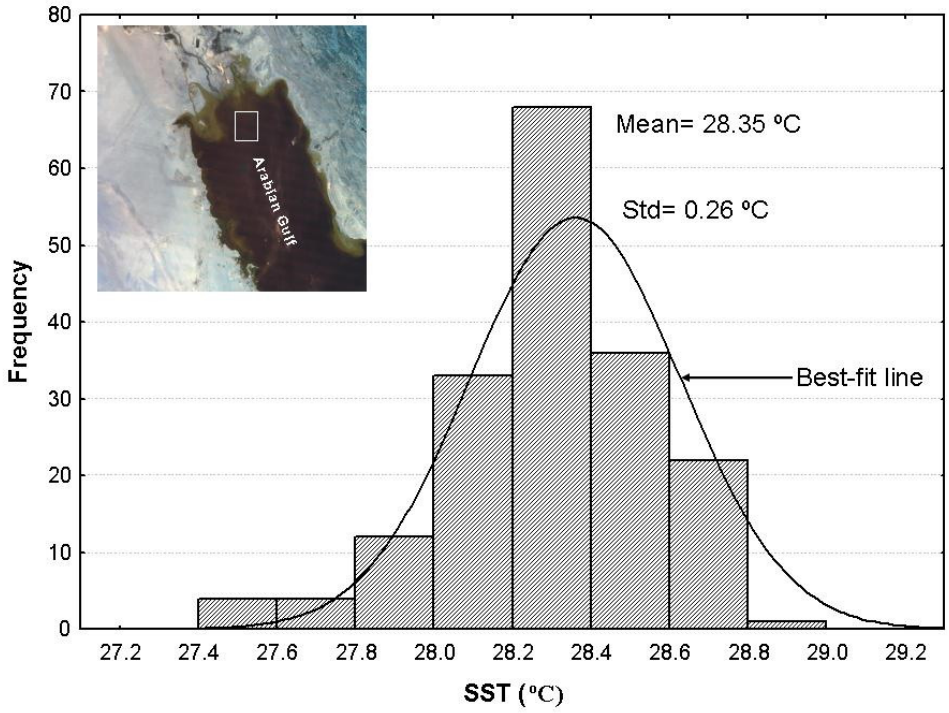

Figure 5.4: A histogram of the predicted SST from AVHRR data (180 pixels) in the northern Arabian Gulf. The graph shows that the data are normally distributed around the mean. There is a small tail of cooler temperatures that appears to be from the Shatt Al-Arab fresh water discharge.

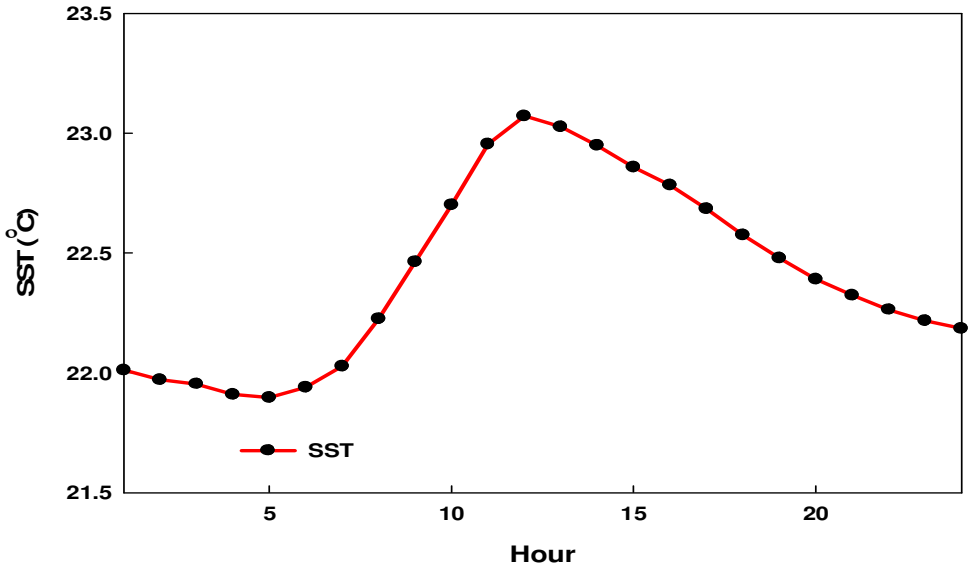

Figure 5.5: SST hourly variation in Kuwait Bay based on EPA hourly measurements. The graph shows the highest SST at 12:00 and the lowest at 05:00. It also shows that the diurnal variation in seawater temperature is about ± 1.2 °C.

A comparison between AVHRR data and EPA measurements in Kuwait Bay (see Figure, 5.1) are shown in Figure 5.6. The results indicate a strong correlation, with only a small offset between SST extracted from AVHRR and EPA measurements (r^2 = 0.99; p=0.007). The standard error was found to be 0.2 ºC (Figure, 5.6). This error includes errors in the ground measurements and errors from satellite SST. It is of the same magnitude as the spatial heterogeneity in temperature. There are no systematic errors in the temperature data over a range from 15-33 ºC. Therefore, the measurements are considered accurate over the range of temperature measured by the satellite.

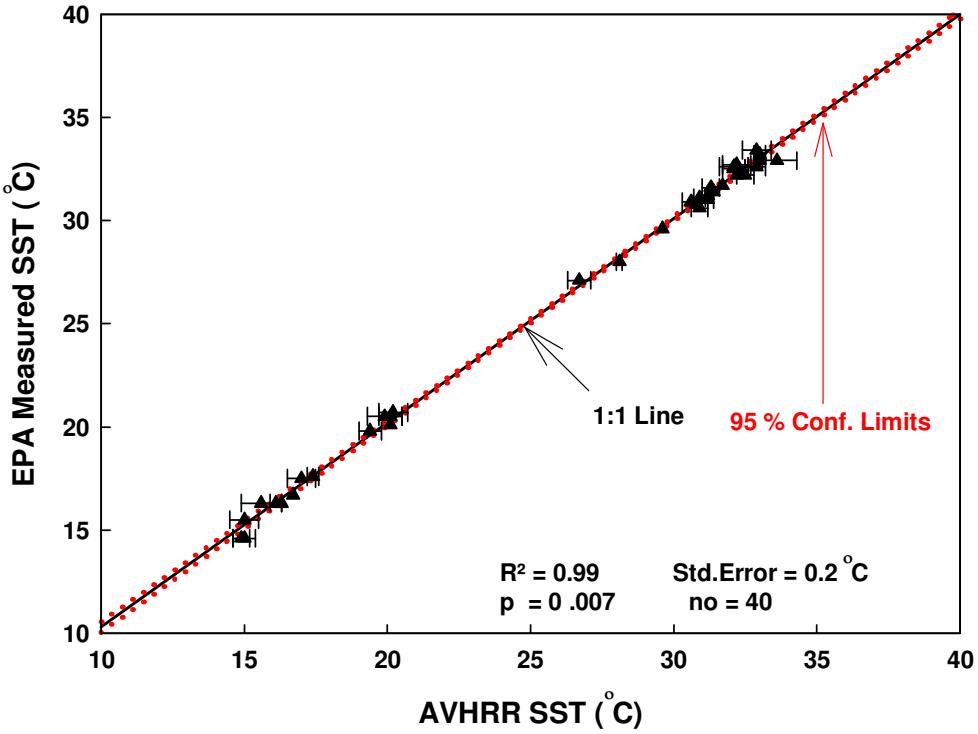

Figure 5.6: Least–squares regression between SST from the AVHRR data and EPA measurements in Kuwait Bay. The graph shows a strong correlation with little offset between AVHRR and EPA SST. The black line is represents the 1:1 line; the red dotted lines represents the 95% confidence limits.

The temperature trends in Kuwait Bay have been derived from the monthly-averaged AVHRR data and show a strong seasonal cycle with year-to-year variability (Figure 5.7). The range in temperature is 22 ºC. The highest temperature

recorded was 36.1 ºC in August, 2003 and the lowest temperature recorded was 14.2 ºC in January, 2007. The seasonal trend in the time-series is the dominant signal. Peak temperatures occur during August and minimum temperatures occur in January, each year. Changes between these extremes are rapid and systematic. Long-term trends in temperature are difficult to identify; however, yearly and 5-year smoothing removed the seasonal variation and reveal underlying longer-term trends. The annual trend (red line) shows fluctuations that are small (± 0.5 ºC) in magnitude; they appear to have a bi-annual frequency (a relatively cool year, followed by a relatively warmer year). A significant reduction in the summertime peak is evident in 1991, which is interpreted to be due to the dense smoke that covered the region from the burning of oil fields, as a result of the Iraqi invasion. In contrast, high summer peaks are evident in 1998 and 2003 due to the El Niño phenomenon. This phenomenon has been recognized as a significant large-scale (global) atmospheric event (driver), affecting weather world-wide (Giannini et al., 2001). The data provided in Figure 5.9 show that this event influences also the Arabian Gulf. Recent research in the southern part of the Arabian Gulf also found a positive SST anomaly in 1998, which led to high coral reef mortality off Dubai (Riegl, 2003). A high summer peak was recorded in 2003. It is 1 of the 5 warmest years recorded in global surface temperature (IPCC, 2007). No trend could be observed for the wintertime minima in SST.

The time-series of SST has been filtered using a 5-year smoothing average, in order to evaluate decadal trends in SST. This average is shown in Figure, 5.7 (blue line). Three trends in the time-series are evident. The first trend (between 1985 and 1992) shows falling temperatures; the second trend (from 1992 to 2004) shows a steady increase in temperature; the third trend (post 2004) shows distinct reductions in summertime peak values and the coldest winter time values recorded. This abrupt change is best seen in the yearly average trend (red line). Linear regression of the trends yields an increase in mean SST of 0.62 (± 0.01) ºC/decade. A similar trend was obtained by performing regression analysis on yearly and monthly average SST. The trends are 3 times greater than global average trends reported in the literature (IPCC, 2007). The analysis of monthly SST data shows rapid changes during May and June. The average May SST increased by 1.5 ºC/decade and the average June SST increased by 1.2 ºC/decade (see Table 5.1). This pattern shows that the duration

of the summer season is increasing almost twice as rapidly as the increase in peak summertime temperatures.

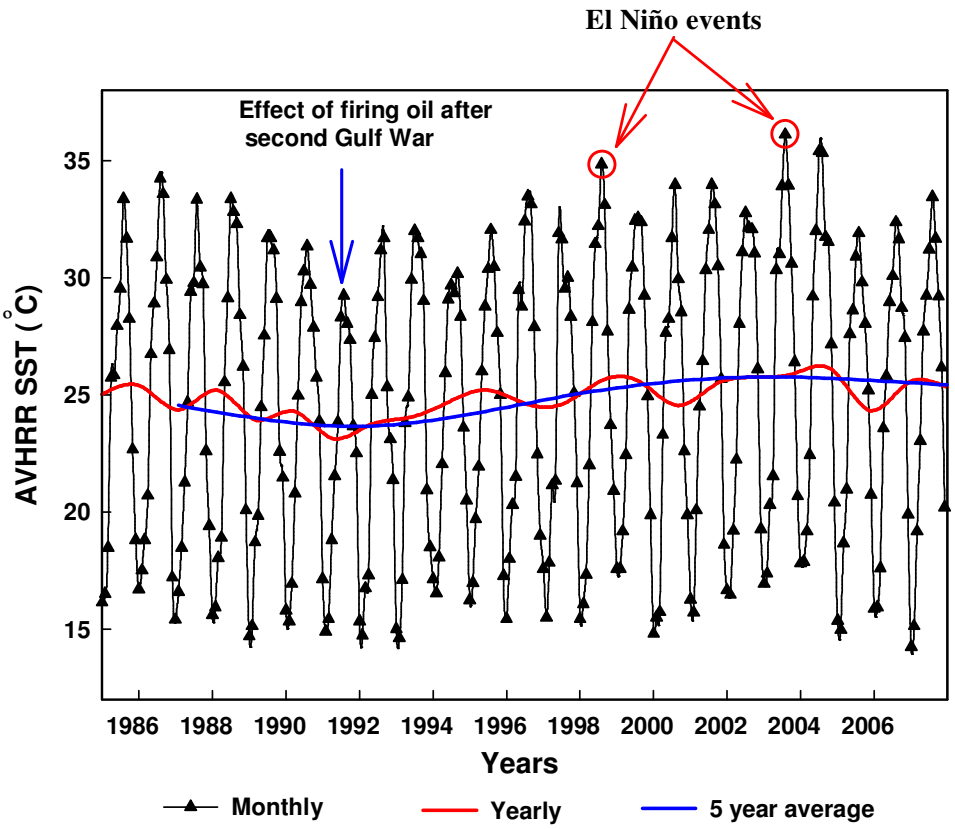

Figure 5.7: SST in Kuwait Bay from 1985 to 2007 (AVHRR data). The time-series shows three trends. The first trend shows falling in temperatures between 1986 and 1992; the second trend shows a steady increase in temperature from 1992 to 2004; and the third trend shows distinct reductions in temperature after 2004. It also shows significant reduction in 1991 due to the second Gulf War, and significant increases in 1998 and 2003 due to El Niño events.

Figure 5.8 shows a linear trend and the yearly average trend in air temperature, AVHRR SST and EPA SST. The trends show an increase in temperature over the time period. There are (3) distinct periods in the all 3 time-series. A decrease in temperature for the period from 1985 to 1992, and increase in temperature from 1992 to 2004, can be observed. The third trend shows reductions in temperature, after 2004.

Table 5.1: Trends of monthly SST change (ºC) /decade in Kuwait Bay, from 1985 through 2007, based on AVHRR data.

Month	Change/decade (ºC)	Month	Change/decade (ºC)
Jan	+ 0.0	July	+ 1.0
Feb	+ 0.1	Aug	+ 0.5
Mar	+ 0.3	Sep	+ 0.3
Apr	+ 0.7	Oct	+ 0.6
May	+ 1.5	Nov	+ 1.0
June	+ 1.2	Dec	- 0.1

The increase in SST for Kuwait Bay, based on AVHRR data was found to be 0.62 (± 0.01) ºC/decade. This is similar to the trend of air temperature of 0.64 (± 0.1)/decade, and the trend based on EPA measurements that was 0.61 (± 0.16) ºC/decade. The similarity in results between air and water temperature is noted and suggests a strong association between the two. Peaks in AVHRR SST correspond well with the peaks in air temperature. However, the EPA SST peaks do not correspond as well to those of air temperature. This may be due to local effects not present in the satellite data.

Figure (5.9) shows the monthly, yearly and five year average of SST in the Arabian Gulf based on AVHRR SST data. The results show a dominant seasonal cycle in the Arabian Gulf. The range in temperature is from 17 ºC to 35 ºC. The maxima occur during August and the minima during January. The maxima are similar to those in Kuwait Bay, but the minima are typically 2 ºC warmer due to the thermal heating provided by the warm water of the Arabian Sea (see Figure 5.4). The influences of the two strong El Niño events (in 1998 and 2003) are clear in the Arabian Gulf, as is the dimming effect of the Gulf war (1991). These effects are seen in both winter warming (El Niño) and winter cooling (Gulf War) by about 1 ºC. There are three clear periods of temperature trends. In period 1 (1985 to 1992), the temperature appeared to drop. In period 2 (1992- 2004), the temperature increased steadily, and period 3 (post 2004) shows decreases in temperature. Linear regression indicates that the SST has increased by 0.54 (± 0.01) ºC /decade in the Arabian Gulf since 1985.

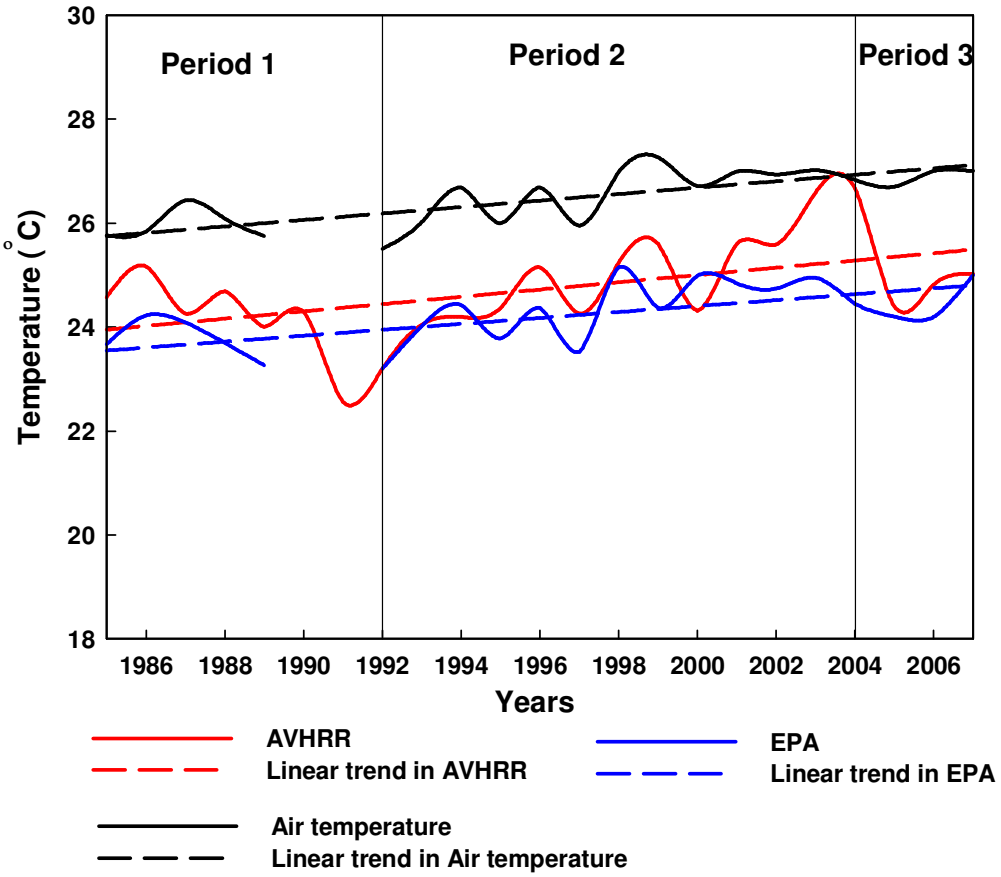

Figure 5.8: Trends of air temperature and SST extracted from AVHRR and EPA measurements in Kuwait Bay from 1985 to 2007. It shows three periods of temperature trends. In period 1 (1985 to 1992), the temperature dropped. In period 2 (1992 to 2004), the temperature increased; and in period 3 (post 2004), reductions in temperature were seen. The long-term trends show similar results between air and water temperature. Peaks in AVHRR SST correspond well with the peaks in air temperature. Peaks of EPA SST are less evident, but correspond to those of air temperature.

Figure (5.10) shows the monthly, yearly, and five-year average of SST in the Arabian Sea (northern Indian Ocean) from AVHRR data. The variation in Arabian Sea SST is largely affected by the Indian monsoon (Kothawale et al., 2008; Naidu, 2006; Prakash and Ramesh, 2007). The long-term trend shows an increase in the temperature of 0.23 (± 0.05) ºC/decade. Yearly trends in temperature are similar to those seen in the Arabian Gulf and show year-to-year fluctuations of about 1 ºC. The peaks in this trend are linked to the two dominant El Niño events. The seasonal trends in temperature are more complex than those in the Arabian Gulf or Kuwait

Bay. Two maximum are evident in any given year: the strongest one taken place during winter and corresponds to the minima in Kuwait Bay and the Arabian Gulf.

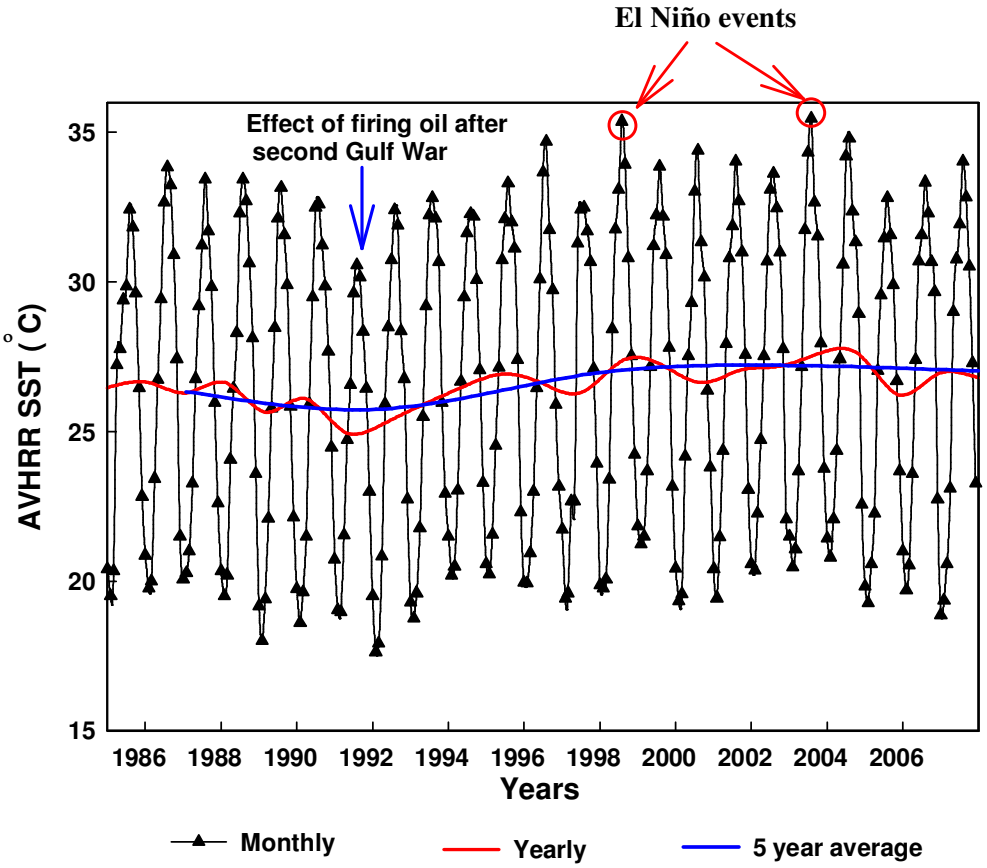

Figure 5.9: SST in the Arabian Gulf from 1985 to 2007 (AVHRR data). It shows three periods of temperature trends. Period 1 dropped in temperature from 1985 to 1992, and period 2 increased in temperature from 1992 to 2004, and period 3 decreases in temperature after 2004. The graph shows the influences of the two strong El Niño events (in 1998 and 2003), and the dimming effect of the Gulf War (1991).

The second maximum occurs during August each year and is 2-3 ºC lower than winter time maximum. Two minima are also evident each year. The lowest follows 3 months after the strongest maximum, while the warmest minimum occurs during autumn of each year. This 6-monthly cycle does not penetrate into the Arabian Gulf through the Strait of Hormuz, and indicates that exchanges across the Strait are limited. The presence of the 6-monthly cycle is due to the passage of the Indian Monsoon. Nevertheless, the longer term tends evident in Kuwait Bay and the Arabian Gulf are clear. For example, the two El Niño events are evident (which have

increased the summer peak). The effect of reduced SST due to the second Gulf War is not evident in the Arabian Sea, it is only clear in the Arabian Gulf.

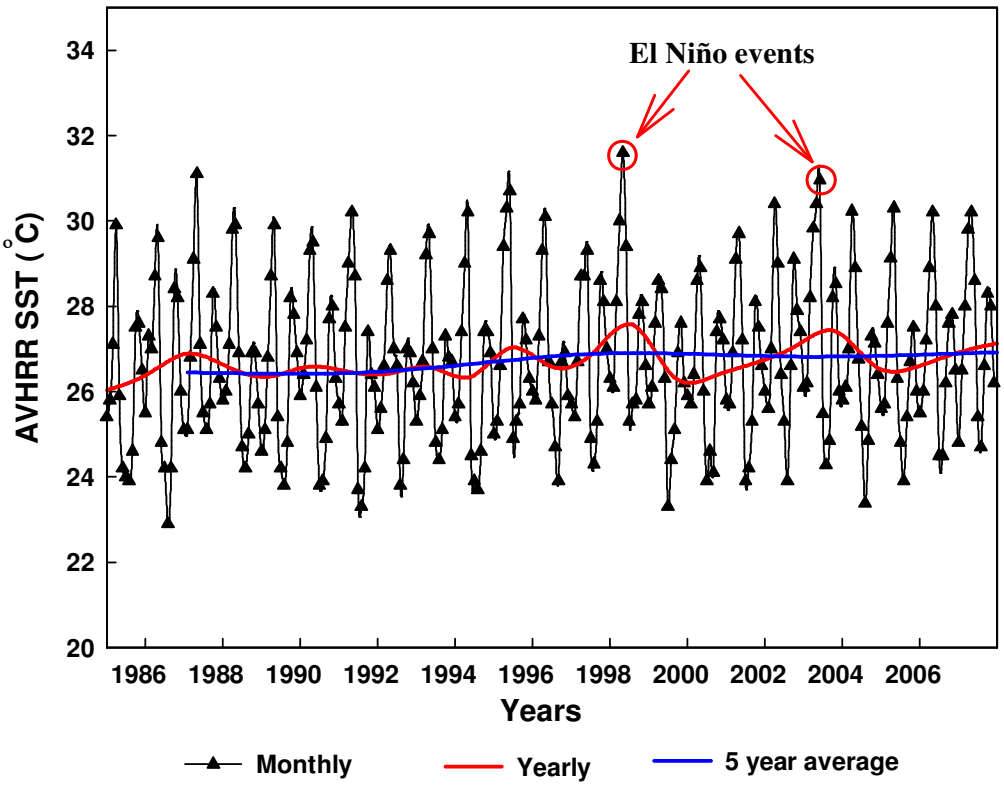

Figure 5.10: SST in the Arabian Sea from 1985 to 2007 (AVHRR data). It shows the influences of the two strong El Niño events in 1998 and 2003. The second minimum each year is due to the Monsoon winds.

5.4 Discussion

5.4.1 Long-term tends in SST

The trends of increasing SST for the three regions of interest are summarized in Table 5.2. In general, the increase of SST is highest in Kuwait Bay and least in the Arabian Sea. The difference between these regions is probably due to the different drivers of temperature in each region. Kuwait Bay shows strong influence due to the collective input of global, regional and local drivers (see equation 5.1). Based on the hypothesis of this study, the Arabian Sea is not affected by either regional or local drivers. It is considered to be affected only by global drivers (see equation 5.3). The

Arabian Gulf appears to be affected by regional and global drivers; that is, where the thermal foot print of local drivers is not evident.

Table 5.2: SST trends at the reference stations from 1985 to 2007. *SST*1 is the SST trend in Kuwait Bay, *SST*2 is the SST trend in the Arabian Gulf, and *SST*3 is the SST trend in the Arabian Sea (northern Indian Ocean).

	*SST*1	*SST*2	*SST*3
	Kuwait Bay	Arabian Gulf	Arabian Sea (north Indian Ocean)
SST (ºC/decade)	+ 0.62 (±0.01) ºC	+ 0.54 (±0.02) ºC	+ 0.23 (±0.05) ºC
Global drivers (T_g)	37%	43%	100%
Regional drivers (T_r)	50%	57%	0.0
Local drivers (T_l)	13%	0.0	0.0

5.4.2 Contribution of the global drivers by seawater temperature of Kuwait Bay

The SST trend in the Arabian Sea (northern Indian Ocean) was calculated to be 0.23 (± 0.05) ºC/decade. The assumption that the region is affected mainly by global drivers appears correct. The temperature trend is close to the trend of global SST in the northern Hemisphere reported by IPCC, 2007, which is 0.19 ºC/decade. Also, it is very close to the result of study for the Indian Ocean by Pearce and Feng (2007), who found that the SST increased by 0.2 ºC/decade over the last 50 years. Khan et al., (2004) found that SST had increased by 0.2 ºC/decade in the Arabian Sea (northern Indian Ocean). Within the context of this thesis, it is considered that the trend due to global drivers in Kuwait Bay is 0.23 (± 0.01) ºC/decade. Global warming is mainly due to an increase of greenhouse gases concentration and thermal insulation due to CO_2 in the atmosphere (Cox et al., 2000; IPCC, 2007; Jenkinson et al., 1991; Manabe and Stouffer, 1980). El Niño phenomenon has been recognized as a significant large-scale (global) atmospheric event (driver) affecting weather patterns worldwide (Giannini et al., 2001). The measurements showed that this phenomenon has impacted on Kuwait Bay as well as on the Arabian Gulf

5.4.3 Contribution of the regional drivers to seawater temperature of Kuwait Bay

The increase of SST at the Arabian Gulf stations (Figure, 5.3) was calculated to be 0.54 (± 0.02) ºC/decade. These stations are away from local anthropogenic activities and are proposed to be affected only by regional and global drivers. MODIS satellite images showed that the local heat effect in the Arabian Gulf is within 20 to 30 km from the shoreline (see Figure, 4.10). The regional influence on SST in the Arabian Gulf has been evaluated by subtracting the global trend (trend in Arabian Sea) shown in Table 5.2 (*SST*2- *SST*3). It is evident that 43% of the temperature trends in the Arabian Gulf are accounted for by global drivers; the remaining 57% is assumed to be due to regional influences (0.31 ºC/decade); while none of the signal is assumed to be due to local drivers. It is assumed that the regional drivers in the Arabian Gulf are the same as in Kuwait Bay. Therefore, this amount (0.31 ºC/decade) is considered the magnitude of regional drivers in Kuwait Bay. This result shows that the impact of regional drivers in Kuwait Bay are approximately twice that of the global drivers, and suggests that the application of IPCC predictions alone to coastal regions may not predict the true magnitude of water temperature changes.

The high contribution of regional drivers to SST in Kuwait Bay may be related to the 4 m tidal range in the region, and the resulting circulation and mixing of seawater with the Arabian Gulf. The Gulf is a dynamic water body with both vertical and lateral tidal mixing and strong residual circulation (Swift and Bower, 2003). This circulation will have impacts on Kuwait Bay through controls on stratification and residence times of the bay. Weather patterns including air temperature, wind speed, wind direction and relative humidity can also be considered as regional drivers as there is a high correlation between air temperature recorded at Kuwait airport and SST in the northern Gulf despite being separated by 100 km. Regional weather patterns, for example the dominant northwesterly wind (*Shamal*) influences may reduce SST due to the evaporation of seawater. The high evaporation leads to increases in salinity and density in the surface layer of the waters in Arabian Gulf which enhance mixing (Robinson and Brink, 2006). Fresh-water discharge from the Euphrates and Tigris rivers through Shatt Al-Arab could directly influences

Kuwait Bay by reducing summertime temperature. Finally, dust storms coming from the desert have significant effects on seawater temperature through atmospheric dimming that reduces sunlight passing through the atmosphere (Al-Ghadban and El-Sammak, 2005).

5.4.4 Contribution of the local drivers to seawater temperature of Kuwait Bay

The sites in the Arabian Gulf are influenced only by global and regional drivers of temperature change, therefore, any difference observed between these sites and Kuwait Bay may be considered to be the result of local drivers. Thus, to evaluate the contribution of local drives to seawater temperature in Kuwait Bay, the trend of SST in the Arabian Gulf (0.54 ºC/ decade) was subtracted from that determined for Kuwait Bay shown in Table 5.2 (*SST*1- *SST*2). The results indicated that the SST increased in Kuwait Bay by 0.08 ºC/decade more than in the Arabian Gulf. This increase represents 13% of the observed total temperature trend. An evaluation of the contributions to the temperature changes in Kuwait Bay shows that 37% of the observed change is due to global drivers (0.23 ºC/decade), and 50% (0.31ºC/decade) is due to regional drivers (see Table 5.2). The influence of local and regional drivers over global trends is even more pronounced than in the Kuwait Bay. Though global warming due to climate changes is important to the coastal SST, local and regional drivers dominate trends in Kuwait Bay.

Local drivers of SST are largely related to human activities along the coastline of Kuwait Bay. In this region, the extensive intertidal mudflats have been influenced by dredging and landfill of urban and industrial developments (Al-Ghadban and El-Sammak, 2005; Al Bakri and Kittaneh, 1998; Khan, 2006). Furthermore, there are four power and three desalination plants distributed around Kuwait Bay. Such plants have direct impacts on the marine ecosystem of Kuwait Bay in terms of increasing the water salinity and water temperature (Saeed et al., 1999). Al-Rashidi et al., (2007) studied the human impact on SST in Kuwait Bay and concluded that there is a high correlation between human activities in the coastal zone and the increase of sea surface temperature. They found high SST near the power and desalination plants due to thermal discharges from these plants.

5.5 Conclusions

The evaluation of long-term drivers of seawater temperature in Kuwait Bay has been evaluated using data from three sources: air temperature from Kuwait airport; monthly seawater temperature measurements carried out by the Kuwait EPA, and AVHRR SST images. The measurements span the period from 1985 to 2007. The main conclusions of this study are:

(1) Seawater temperature has increased in Kuwait Bay by 0.62 (± 0.01) ºC/decade in the last two decades;

(2) temperature trends in Kuwait Bay have been affected by drivers, conveniently sub-divided into global (which contributes 37% of the change), regional (which contributes 50% of the change) and local (which contributes 13% of the change);

(3) the distribution of SST from AVHRR is Gaussian and exhibits a spread of ±0.26 ºC. This spread is considered to be the spatial scatter in data due to random processes;

(4) the error of AVHRR SST, calibrated against EPA measurements, is ±0.2 ºC. This error is the same order as the spatial scatter in temperature;

(5) the seasonal pattern of temperature dominates the SST signal in Kuwait Bay, Arabian Gulf and Arabian Sea, though the influences of El Niño events and the Gulf War are evident in the records;

(6) the influence of the seasonal monsoon is evident in the Arabian Sea, but is not evident in the Arabian Gulf and Kuwait Bay;

(7) although, the majority of the increase in seawater temperature in Kuwait Bay is driven by global and regional drivers, mitigation could be undertaken by controlling the local drivers (local human activities).

6. Chapter 6: Regional drivers of seawater temperature in Kuwait Bay and the northern Arabian Gulf

Abstract

Regional drivers could be a significant contributor to the rapid increase in seawater temperature of Kuwait Bay. The regional drivers considered are: the fresh water discharge mainly from the Shatt Al-Arab; weather patterns; and dust storms.

AVHRR SST images from 1985 to 2007, recorded in the northern Arabian Gulf, were used to understand and investigate the drivers of SST on a regional scale. Data on fresh water discharge from the Euphrates after 1994 were not available; therefore, salinity data, measured by Kuwait EPA during 1983-1994, were correlated with fresh water discharge data in order to predict the discharge after 1994. Statistical analyses showed that the regional drivers were contributing to 52% in the signal of seawater temperature trend in Kuwait Bay. This contribution is close to that derived in chapter 5 (50%) by subtraction of the Global and local drivers. The greatest influence was from the air temperature. *Shamal* winds play a major role in mixing the water masses in the northern Arabian Gulf as well as in Kuwait Bay. Reducing fresh water discharge from the Shatt Al-Arab has contributed to increasing seawater temperature in Kuwait Bay. Dust storms reduce the seawater temperature in the bay by reducing the sunlight reaching the sea surface. Dust frequency has markedly increased in the region over the last few years as a result of decreasing rainfall and desertification. Wars have also impacted seawater temperature. Seawater temperature decreased as a result of a smoke cover during the second Gulf War in 1991. The first Gulf War took place in 1981. Dust storms increased in frequency after the US invasion of Iraq in 2003 (the third Gulf War). The US vehicles and tanks crossing the desert of Iraq may have removed the top layer of sand and increased desertification, with the result that underlying dust is now more easily suspended by wind.

6.1 Introduction

The northern Arabian Gulf is characterized by well mixed temperature profiles in winter and stratification in summer (Mubarak and Kubryakov, 2000; Reynolds, 1993). Fresh water is discharged from the Euphrates, Tigris, and Karun rivers in to northern Gulf through the Shatt Al-Arab delta (Al-Yamani et al., 2007). The mean flow of the Shatt Al-Arab is 1,456 m^3 /s (Reynolds, 1993). The northern Arabian Gulf and Kuwait Bay are largely influenced by the fresh water discharged from Shatt Al-Arab waterway (Al-Yamani, 2008; Mubarak and Kubryakov, 2000). The cool air from Turkey enters the northern part of the Arabian Gulf through the Tigris-Euphrates valley. This brings to the region the well-known phenomenon, the *shamal* (Arabic for north) wind. In summer, the *shamal* winds are manifest as hot dry dust storms, particularly during July and August (Reynolds, 2002; Robinson and Brink, 2006). In the last few years, the frequency of dust storms has increased to occupy 25% of the year in Kuwait (Alsharhan, 2009). Thus, it appears that regional events are important and active in the study region.

In the previous chapter, AVHRR SST was used to study the drivers of the seawater temperature in the northern Arabian Gulf and Kuwait Bay. It was found that the SST in the Arabian Gulf has increased by 0.54 ºC/decade. About 57 % of the signal was attributed to regional drivers. These drivers are the sum total of the effects of a number of peripheral drivers. In Kuwait Bay, the regional drivers include weather patterns, discharge from the Euphrates and Tigris rivers, and dust storms, in addition to water exchanges at the Strait of Hormuz and the circulation in the Arabian Gulf. A selected station in the northern Arabian Gulf was chosen to evaluate the drivers of SST on the regional scale (Figure, 6.1). The selected station is 100 km away from the shoreline. This location was chosen since it is far from local human activities and is thus assumed to be affected only by the regional and global drivers. Regional drivers are those drivers that may be considered to influence the Gulf region as whole. Therefore, the regional drivers affecting this station are those which also affect Kuwait Bay. In this chapter AVHRR SST from the station in the northern Arabian Gulf from 1985 to 2007 (Figure, 6.1), together with meteorological data recorded in Kuwait airport (Figure, 5.1), were used to study and investigate the

regional drivers of seawater temperature at this station. The ultimate aim of this chapter is to investigate the related influences of regional drivers of seawater temperature in Kuwait Bay.

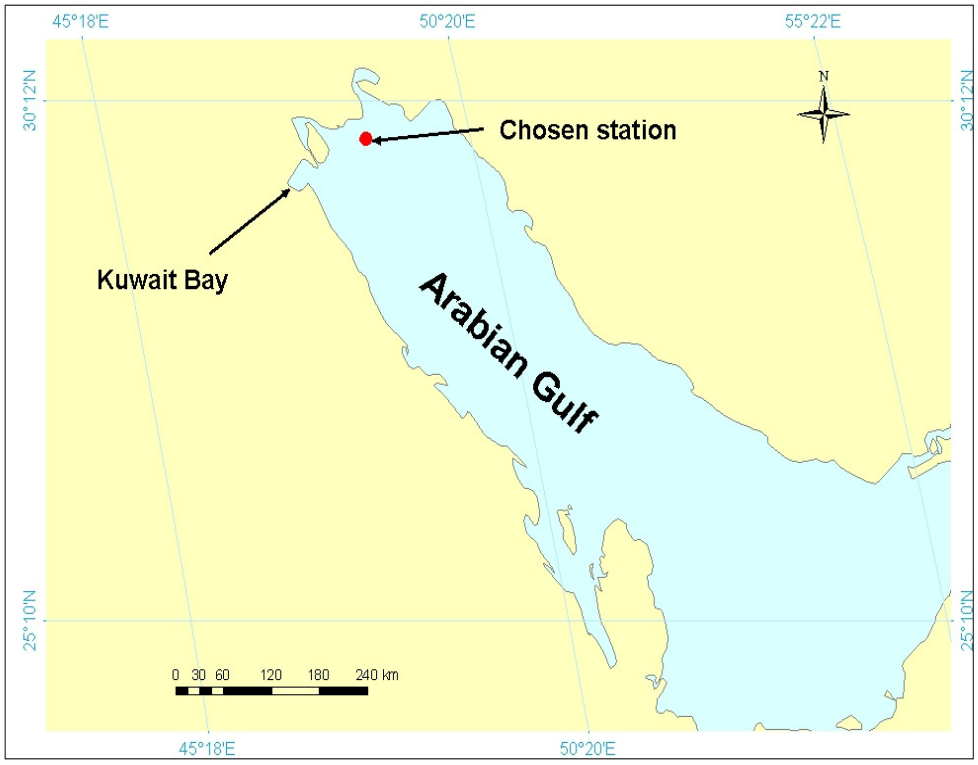

Figure 6.1: The selected station chosen to study the regional drivers of SST in Kuwait Bay and the Arabian Gulf. The station is 100 km away from the populated shorelines, and it's not affected by local human activities.

6.2 Data and methodology

Twenty-three years of SST data, collected between 1985 and 2007 in the northern Arabian Gulf (29 ° 50' 9" N, 48 ° 54' 24" E) (Figure, 6.1), were acquired from the processed AVHRR Oceans Pathfinder project of NASA Jet Propulsion Laboratory (JPL), Physical Oceanography Distributed Active Archive Centre (PO.DAAC, 2009). A total of 276 SST image files for day-time, monthly mean SST at 4 km spatial resolution (4×4 km) were downloaded and analysed. In this study, the meteorological data (air temperature, wind speed, and relative humidity) for the same time period were provided by the Meteorological Department in Kuwait

airport. Frequency of dust storms collected yearly from 1985 to 2007 in Al-Shuwaikh station, south of Kuwait Bay was provided by Kuwait Institute for Scientific Research (KISR). Unfortunately, recent measurements of fresh water discharge from Shatt Al-Arab are not available. Altinbilek (2004) provided the hydrologic records of the annual flow for the Euphrates River from 1946 to 1994. In this study, the salinity data (EPA measurements in Kuwait Bay) from 1983 to 1994 were correlated with the fresh water discharge data (Altinbilek, 2004) in order to predict the discharge after 1994.

A step-wise multiple regression analysis was used in order to investigate the effect of the regional drivers in the SST north of the Arabian Gulf and in Kuwait Bay. This statistical approach was applied using the annual SST data from the AVHRR satellite in the north Arabian Gulf from 1985 to 2007 as the dependant variable. The independent variables were:

1. annual average air temperature (recorded at Kuwait airport);
2. annual average wind speed (recorded at Kuwait airport);
3. annual average relative humidity (recorded at Kuwait airport);
4. annual average fresh water discharge from the Euphrates River (predicted)
5. annual dust storm frequency collected by KISR, south of Kuwait Bay.

6.3 Results and interpretation

Salinity data in Kuwait Bay was compared to the available freshwater discharges of the Euphrates and Tigris rivers between 1983 and 1994 in order to predict the fresh water discharge after 1994. Figure 6.2 shows the correlation between the freshwater discharge from the Euphrates river and the salinity in Kuwait Bay. Figure 6.3, shows the calculated and measured fresh water discharge from the Euphrates River as an indicator of the inflow of Shatt Al-Arab waterway into the Arabian Gulf. Fresh water discharge is different from year to year. Highest discharge was recorded in 1998 and the lowest was in 2002. The long-term time-series showed a decrease in the fresh water discharge from Shatt Al-Arab to the Arabian Gulf for the time period considered.

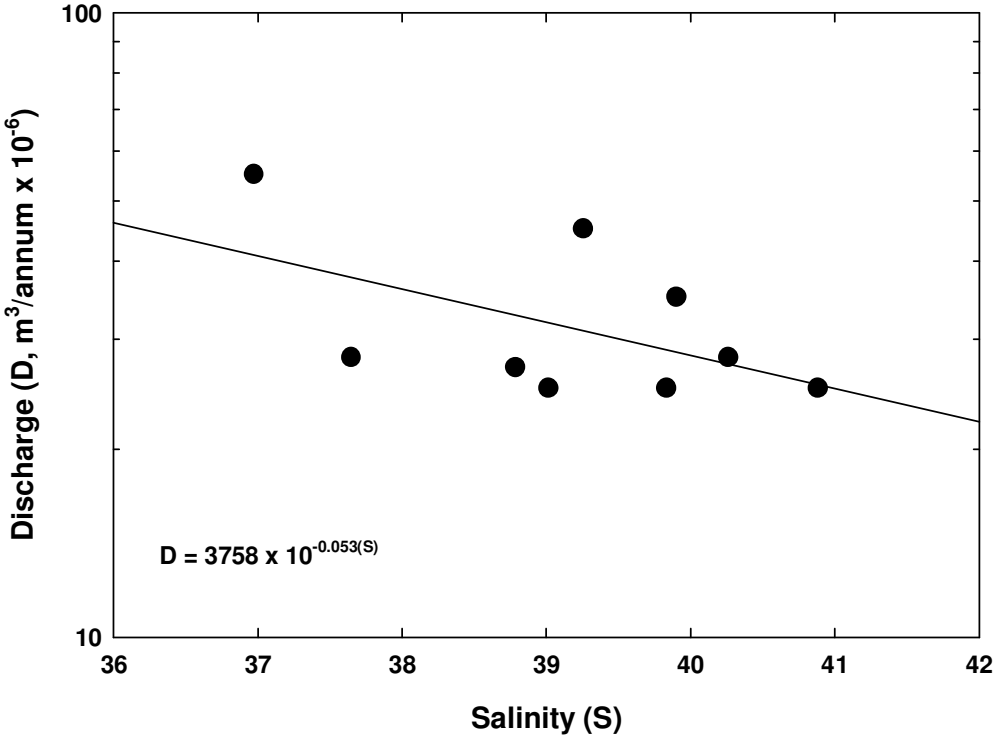

Figure 6.2: Correlation between the salinity in Kuwait Bay and the discharge from the Euphrates to the Arabian Gulf from 1983 to 1994. This correlation was used to predict the freshwater discharge after 1994.

Figure (6.4A) shows the yearly SST and air temperature in the northern Arabian Gulf from 1985 to 2007. The lowest SST was in 1991, which resulted from the smoke which covered the region as a result of the Iraqi invasion, during which time the oil fields were set alight. This smoke resulted in a reduction of the temperature in the region in 1991 (Husain, 1997). In Kuwait and in the northern Saudi Arabia, the drop in air temperature was up to 10 ºC. 250 from south of Kuwait, the temperature reduction was 5-8 ºC and 1-2 ºC beyond 750 km (Khordagui and Alajmi, 1993).

The highest SST was recorded in 2004. This year was described globally as one of the five warmest years ever recorded (IPCC, 2007). Figure (6. 4B) shows the time-series of the predicted discharge and the frequency of dust storms that covered the region in the time period of this study. The trends in data are complicated and do not always correspond to the seawater temperature trends.

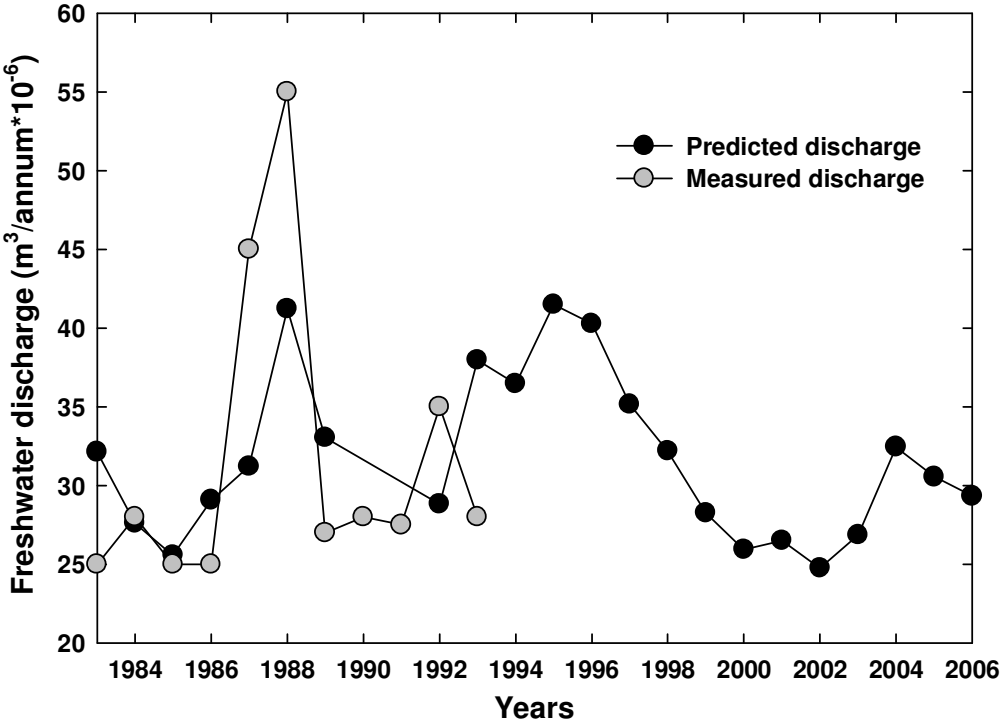

Figure 6.3: Predicted freshwater discharge from the Euphrates river from 1983 to 2007. Freshwater discharge data from 1983 to 1994 was correlated with measured salinity in Kuwait Bay to predict the discharge after 1994.

The high seawater temperature in 2003 corresponds to the low fresh water discharge from Shatt Al-Arab rivers due to the restoration of the marsh land in the south of Iraq (UNEP, 2006). Also, the dust storm frequency was low in 2003; this could be another factor contributing to the increase in SST in that year. Figure (6.4C) shows the time-series of relative humidity and wind speed for the studied time period. Again, the trends are complicated and do not always correspond with the seawater temperature trends. A high SST in 1999 corresponds with low wind speed for that year. Relative humidity shows no obvious relationship with SST in Kuwait Bay.

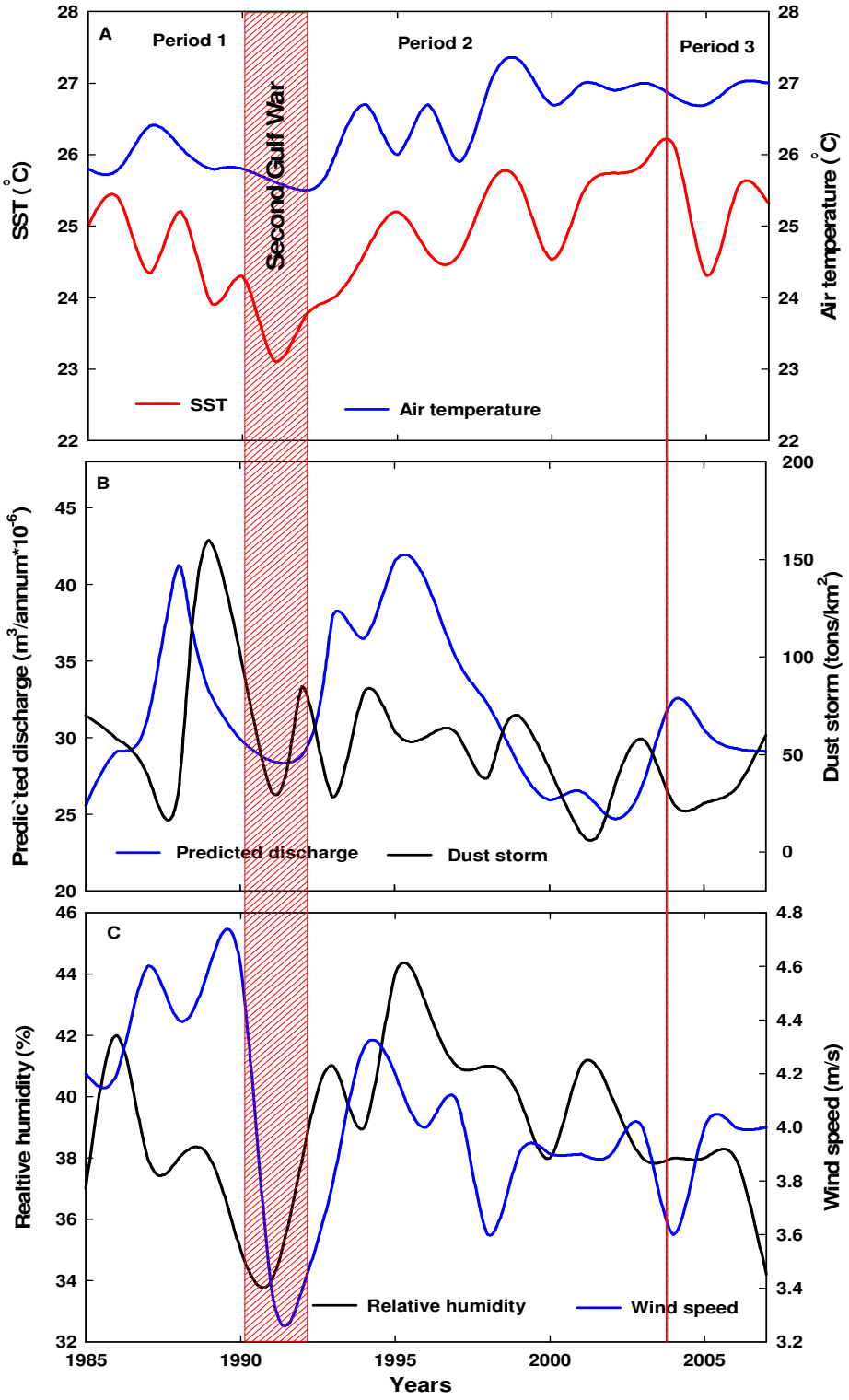

Figure 6.4: Yearly average: (A) SST in the northern Arabian Gulf and air temperature; (B) predicted freshwater discharge and dust storm frequency; and (C) relative humidity and wind speed.

The statistical analysis (step-wise multiple regression) indicated that the SST (dependant variable) has been affected by regional drivers (independent variables). These drivers explain 52% (R^2= 0.52) of the variance and are significant in their contribution (p-level= 0.02) to the northern Arabian Gulf. This result is close to the calculated influence of regional drivers of the seawater temperature in Kuwait Bay discussed in Chapter 5 (50% of the signal). Table (6.1) illustrates the contribution of each regional driver to the SST. The B value represents the contribution of each variable (the independent variables) to seawater temperature (the dependant variable), and the p-level represents the level of significance. When the p-level exceeds 0.05, then no significant relationship exists between the dependant and independent variables. The Table illustrates that air temperature is the only variable that could be significantly influencing SST in the Arabian Gulf (B value= 0.63; p-level = 0.003). The Table shows the contribution of the other drivers for completion. Although, the statistical analysis shows no relationship with the other parameters (p-levels greater than 0.05), (for the entire duration) the time-series shows that there is some correspondence between seawater temperature trend and the trend of these factors in some years. This could be caused by using yearly averaged data which may mask some of the exiting trends.

Table 6.1: The contributions of regional drivers to SST trend in the northern Arabian Gulf. B represents the contribution of each variable to seawater temperature. SE is the standard error of B. P-level is the level of significance.

	B	SE	p-level
Air temperature	0.63	0.18	0.003
Relative humidity	0.24	0.17	0.18
Wind speed	-0.14	0.19	0.45
Predicted fresh water discharge	-0.07	0.18	0.72
Dust storm	-0.06	0.19	0.73

6.4 Discussion

6.4.1 The influence of air temperature on seawater temperature

The result of this study show a strong correlation between SST in the northern Arabian Gulf and air temperature measured at Kuwait airport. Figure (6.4)

shows the time-series of SST and air temperature between 1985 and 2007. Three periods are clear in both air and seawater temperature trends: period 1 from 1985 to 1992 (prior to the Gulf war) shows a general cooling; period 2 from 1992 to 2004 (after the Gulf war) shows a general warming. Period 3, after 2004 shows a drop in temperature. These trends are complicated by fluctuations on a frequency of 2 years; i.e. a relatively warm year is followed by a relatively cold year. The relatively warm SST does not always correspond to relatively warm air temperatures. The results of the statistical analysis show that the long-term SST in the northern Arabian Gulf is largely driven by ambient mean air temperature (Table 6.1). Thus, air temperature is considered as an important regional driver for the seawater temperature in Kuwait Bay.

6.4.2 The influence of fresh water discharge on seawater temperature

The water temperature in Shatt Al-Arab ranges from 9.1 ºC in winter to 27 ºC in summer (Alhassan, 1987). The water temperature in the northern Arabia Gulf is ranges from 15 ºC in winter to 35 ºC in summer (Al-Yamani et al., 2004; Mubarak and Kubryakov, 2000; Reynolds, 2002). Thus, the water temperature from the Shatt Al-Arab is a source of cooling to the northern Arabian Gulf as well as to Kuwait Bay. While there is a trend of increasing SST in the region, there has been a decrease in the fresh water discharge from the Shatt Al-Arab into the Northern Arabian Gulf. Also, the long-term trend shows a correspondence between yearly SST and yearly freshwater discharge. The increase in SST in 2003 corresponded with low freshwater discharge due to marshland restoration in the south of Iraq.

The fresh water discharge from the Euphrates has been affected by the south-eastern Anatolia Development project (GAP) in Turkey (Al-Yamani et al., 2007). A total of 22 dams and 19 power plants were constructed on the Euphrates and Tigris river which impound 122×10^9 m^3 of water, covering an area of 3,000 km^2. These projects have led to a reduction in the flow from the Shatt Al-Arab by 80% (El-Fadel et al., 2002). In addition, the discharge from these rivers into the Arabian Gulf has been affected by restoration of the marshlands in the south of Iraq (see Figure 6.5). The marshes dried after the construction of the third river in the 1990s. The third river is a man-made river diverting the water from the Euphrates river to channel called Shatt Al-Basra (Figure, 6.5). The United Nations Environment Programme

(UNEP) initiated the flooding of the original marshlands in April, 2003 (UNEP, 2006). This initiative has significantly reduced the discharge of fresh water into the Arabian Gulf. This effect is likely to continue for many years into the future, thus compounding the impact of climate change in the region.

6.4.3 The influence of dust storms on seawater temperature

Aerosol dust has the effect of solar dimming that reduces seawater temperature (Kaufman et al., 2005). Figure (4.24) shows drops in temperature over the Intertidal flats south of Kuwait Bay during periods of dust storms in the region. Thus, dust storms contribute to reducing seawater temperature in the region (see Figure 6.4). Recently, the increase in the incidence of dust storms in Kuwait has been exceptional. This dust originates from the north; from Iraq in particular (Khalaf et al., 1985). The frequency of dust storms in Kuwait has increased over the last few years to occupy 25% of the year (Alsharhan, 2009). Decreasing rainfall and increasing desertification is the main reason for the increasing frequency of occurrence (Harrison et al., 2001). The GAP project in Turkey contributes to increasing dust storms in the region by reducing the flooding of Euphrates and Tigris rivers. The reduced floods from these rivers caused thousands of acres of agricultural land to dry resulting in increased desertification (Al-Haddad, 2009). The Gulf War also contributed to an increase in dust storms in the region. The movements of tanks and vehicles of the US army across the desert from Kuwait to Iraq in the 2003 invasion removed the top layer of sand and contribute to the desertification process (Tharp, 2009). Thus provided a source of dust to the region that is easily suspended by winds.

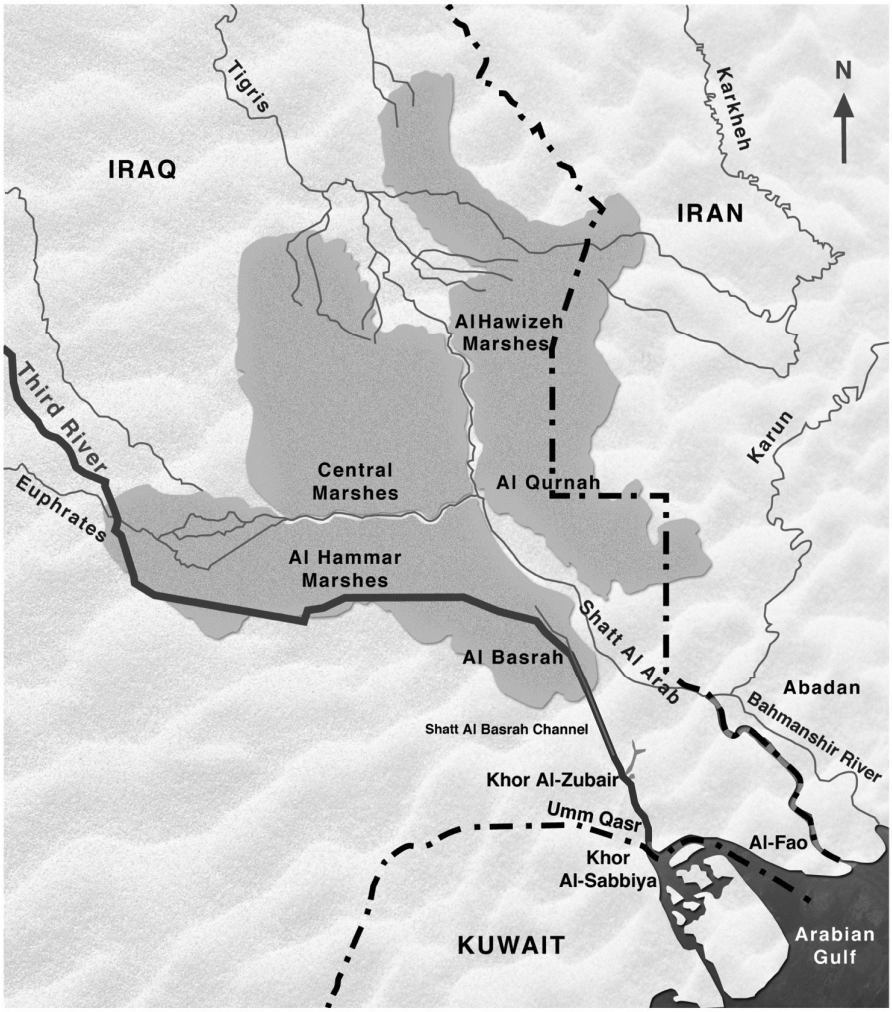

Figure 6.5: The Shatt Al-Arab, Euphrates, Tigris, and third rivers. The figure shows the marshlands in the south of Iraq that are subject to flooding under UNEP recent initiative (Adapted after Al-Yamani et al., 2007)

6.4.4 The influence of circulation patterns in the Gulf to the seawater temperature

Seawater temperature in the region is influenced by circulation and mixing. Mixing of the water column in the Arabian Gulf is driven by tides, winds, waves, and evaporation (Lardner et al., 1993; Robinson and Brink, 2006). The tidal range in the northern Arabian Gulf is 3 m in range, and 4 m in the northern Kuwait Bay (see Figure, 2.3). In the northern Arabian Gulf, tide is important in mixing of water masses, and also in horizontal mixing at scales of 10 km (Reynolds, 2002). The

dominant north-westerly wind (*Shamal*) may reduce SST due to evaporation of seawater and mixing of water masses. According to Robinson and Brink (2006) the general circulation in the Arabian Gulf is from the south to the north along the Iranian coast and from north to south along the Arabian coast (see Figure, 2.3). MODIS satellite images showed that the south side of the Gulf is warmer than the North part (see Figures, 4.10 and 4.11). Thus, the warmer water is moving from south of the Gulf to the north and colder water is moving from north to south. The circulation of the northern Arabian Gulf is counter-clockwise and is dominated by wind (Reynolds, 2002). This circulation drives the freshwater flow from Shatt Al-Arab into Kuwait Bay and then along the Kuwait coast. Thus the seawater temperature in Kuwait Bay will be influenced by the quantity of freshwater discharge from the Shatt Al-Arab.

6.5 Conclusions

Analysis has been carried out of the regional drivers of seawater temperature in Kuwait Bay. It is clear from this analysis that regional drivers have a much larger effect on seawater temperature than global drivers have, and that the trends that define periods 1, 2, and 3 are the result of variations in temperature input at regional scales. The following are the major points of conclusion of this chapter:

(1) Regional drivers contributed 52% of the observed trends of seawater temperature in Kuwait Bay. The greatest influence was air temperature;

(2) reduced freshwater discharges from the Shatt Al-Arab into the Arabian Gulf has increased seawater temperature in northern Gulf as well as in Kuwait Bay. Reduction of fresh water discharge from the Shatt Al-Arab was due to man-made projects in Turkey and restoration of the marshlands in the south of Iraq;

(3) recent increases in dust frequency over the region obstructs sunlight and thus reduces seawater temperature. The increasing occurrence of dust storms is caused by reduced rainfall and an increase in desertification in the region;

(4) wars have an impact on seawater temperature in the region. Firing oil wells after Iraq invasion to Kuwait in 1991 (second Gulf War) reduced SST in the northern Arabian Gulf and Kuwait Bay. Military operations in the desert due

to US invasion of Iraq in 2003 (the third Gulf War) removed the top layer of sand and reduced desert vegetation thus increasing dust frequency; and

(5) *Shamal* winds are important in reducing seawater temperature through evaporation and mixing of water masses. The counter-clockwise circulation in the northern part of the Gulf influences seawater temperature in Kuwait Bay by bringing fresh water flow from Shatt Al-Arab along the Kuwait coast.

Chapter 7: Evaluation of local drivers of seawater temperature in Kuwait Bay

Abstract

Rabid urbanisation in Kuwait has been concentrated locally along the coastal zone during the last three decades. This is especially true along the southern part of Kuwait Bay where impacts on the marine environment are evident (Al Bakri and Kittaneh, 1998). The main impacts are related to the discharge of treated and untreated sewage; aquaculture; power generation; desalination of marine water; land filling and dredging activities; and construction of marinas (Al-Mussalam, 1999; Al Bakri, 1996). This chapter attempts to quantify the thermal effect of these local drivers and provides an estimation of their effect on seawater temperature in Kuwait Bay.

The processed thermal band (band 6) of high resolution satellite images (Landsat) indicates that the seawater temperature in southern of Kuwait Bay is higher than in the north. The heat transfer to the northern intertidal flats reduces seawater temperature in the north of the bay. High seawater temperatures were recorded near the human activities. The difference between the SST in the middle of the bay and SST near the sites of human activities was 3.4 ºC in 1985. This increased to 6 ºC in 2002. This impact is mainly due to the thermal discharge from power and desalination plants.

7.1 Introduction

Recent urban development has taken place along the coast line of Kuwait, especially along the southern coast of Kuwait Bay. Currently, the population of Kuwait is about 3 million; 1.5 million reside along the southern side of Kuwait Bay (Ministry of Planning, 2005). Rapid urbanization impacted the marine ecosystems in the bay (Al-Rashidi et al., 2007; Al Bakri and Kittaneh, 1998). The main impacts are related to the discharge of treated and untreated sewage; aquaculture; oil navigation routes; desalination of marine water; oil refinery plants near the shoreline; land filling and dredging activities along the coast line; and construction of marinas, resorts, and tourism facilities (Al-Mussalam, 1999; Al-Zaidan et al., 2003; Al Bakri, 1996). There are a number of desalination and power plants distributed around the bay (Figure 7.1). Such plants have direct impacts on the marine ecosystem of the bay in terms of increasing seawater temperature (Al Bakri and Kittaneh, 1998; Saeed et al., 1999).

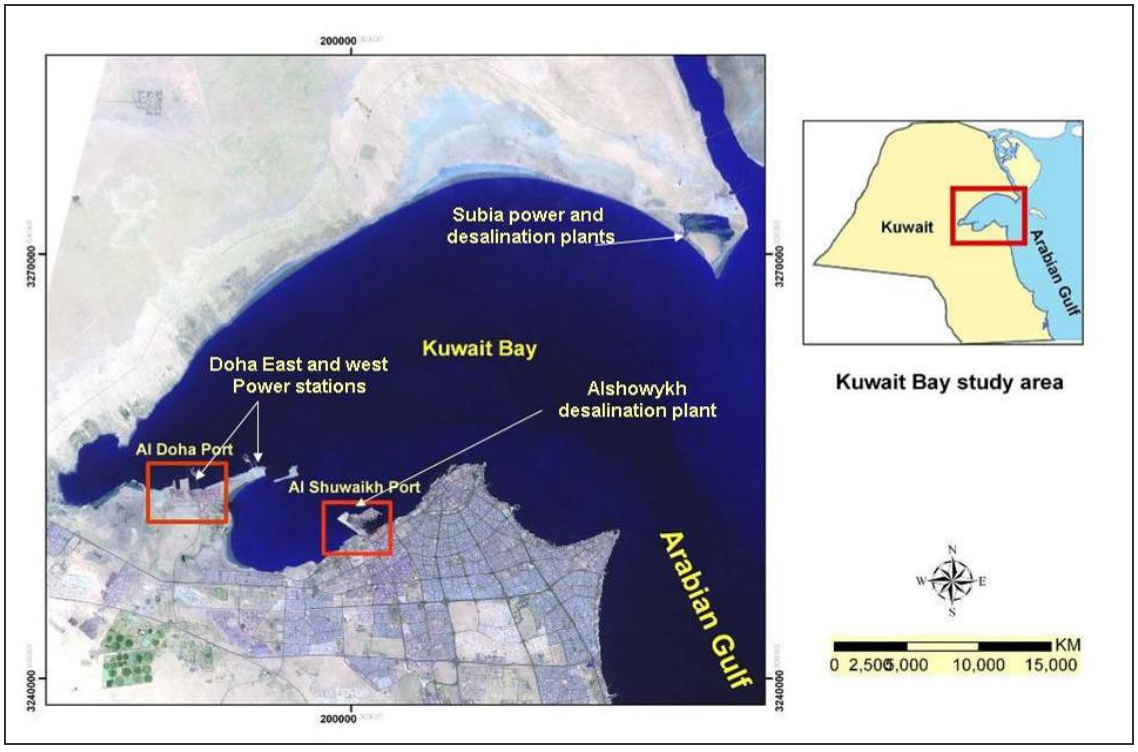

Figure 7.1: Landsat image showing the location of power and desalination plants in Kuwait Bay. It also shows the location of the urban areas, and sewage outfalls.

Landsat sensors play an important role in monitoring temperature changes in the dynamic environment of coastal zones (Nelson et al., 2003). The thermal infrared channel can be used to study changes in the sea surface temperature (SST), which could be related to thermal pollution (Ahn et al., 2006; Fisher and Mustard, 2004). Landsat (TM) images are appropriate for inland surface water body assessments, due to their low cost, high temporal coverage (every 16 days) and good spatial resolution (Álvarez-Robles et al., 2006). The Landsat TM sensors measure radiation in seven bands of the electromagnetic spectrum with a spectral resolution of 30 m, except band 6 which measures emitted thermal infrared radiation with a spatial resolution of 120 m.

As it explained in Chapter 1, the local drivers are those sources of heat that may be detected and defined from a clearly defined adjacent source, and which may be traced without interruption from that source. In Kuwait Bay, local drivers of seawater temperature rise are largely anthropogenic and are found along the coastline. The purpose of this chapter is to define the local contributors of heat to seawater temperature in Kuwait Bay, and quantify the magnitude and distribution of the contributors. From this analysis, the relative contribution of local drivers of temperature change will be evaluated against regional and global drivers in the bay. This analysis will be undertaken using the Landsat Thematic Mapper (TM). The thermal band of Landsat images are used to detect the sources and magnitude of thermal discharge along the coastal line of Kuwait Bay. A thermal box model is used to investigate the contribution of the thermal discharge from power and desalination stations to the seawater temperature in Kuwait Bay.

7.2 Methodology

The Landsat Thematic Mapper (TM) has been covering the study area since 1985, whereas Landsat Enhanced Thematic Mapper Plus (ETM+) covers it since 2001. Almost 20 years of satellite coverage is thus available. After May, 2003 however, the ETM+ sensor accuracy was reduced (NASA, 2009a). In this study, Landsat images from a given month of the year (June) with no cloud cover and no dust cover were selected. Eight images were obtained based on these criteria. The images were used to investigate the source and magnitude of the thermal plumes in

the study area. Table (7.1) summarises the Landsat images (TM and ETM+) used and the tidal conditions during the satellite overpasses. The meteorological data were provided by Kuwait airport station located 15 km south of the bay.

All images were taken at a tidal level between full and half tide. None of the selected images was taken at low tide condition. Figure 7.2 shows the tide level at the time of the Landsat images. These data were obtained from the KTIDE program developed by KISR. The tides in Kuwait Bay are semidiurnal and range from 4 m during spring tides to 0.5 m during neap tides (Al-Yamani et al., 2004; Rakha et al., 2007).

Table 7.1: Landsat images used in this study and the associated tidal and meteorological conditions during satellite overpass.

	Date of Landsat image	Time (local)	Range of tide (m)	Stage of tide	Air Temperature (°C)	Wind Speed (m/s)	Wind Direction	Relative humidity (%)
1	22/06/1985	09:46	2.3	Flood	36.0	11.3	NNE	7
2	09/06/1986	09:40	2.7	Flood	36.4	2.1	NNE	27
3	12/06/1987	09:40	3.6	Ebb	36.5	9.3	NNE	10
4	09/06/1989	09:50	2.2	slack	34.0	5.1	N	6
5	12/06/1990	09:46	2.3	Flood	42.2	7.2	NNE	-
6	10/06/1998	09:54	2.9	Flood	43.0	6.2	NNW	8
7	10/06/2001	09:50	2.2	Flood	37.2	5.0	NNW	11
8	13/06/2002	09:50	2.5	Flood	41.1	4.3	NNW	10

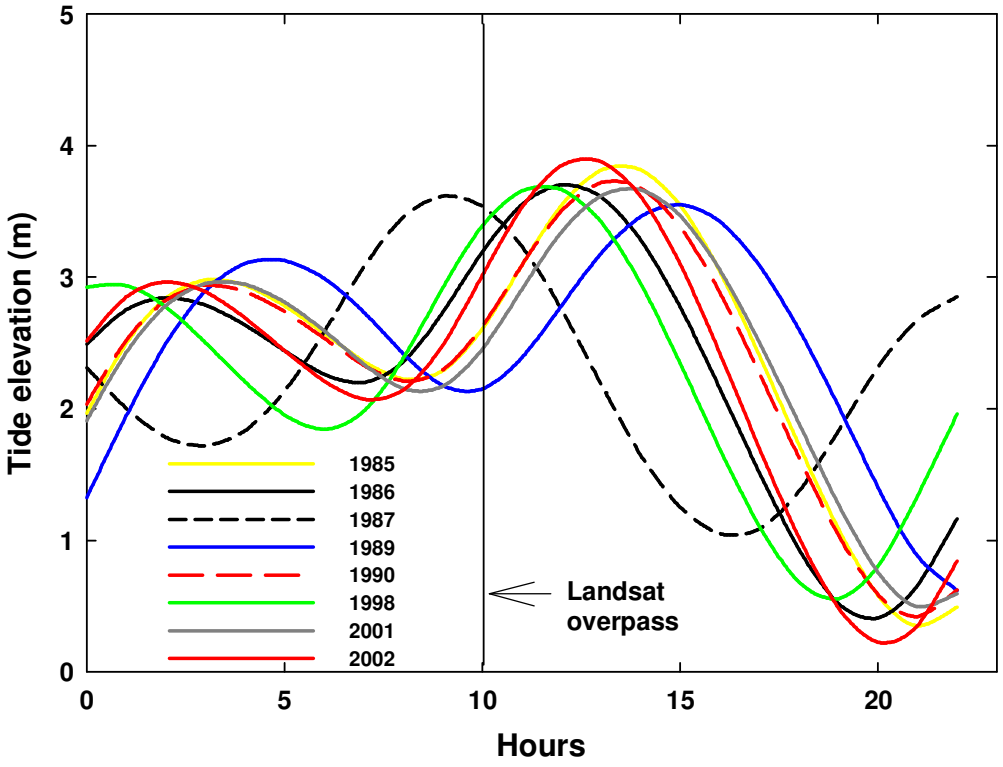

Figure 7.2: Tide level at the time of Landsat overpass over Kuwait Bay for the selected images cited in Table 7.1.

Advanced Very High Resolution Radiometer (AVHRR) SST was acquired from the processed AVHRR Oceans Pathfinder project of NASA Jet Propulsion Laboratory (JPL), Physical Oceanography Distributed Active Archive Centre (PO.DAAC, 2009). The data from Landsat SST was correlated against the AVHRR SST in Kuwait Bay in order to check the accuracy of Landsat SST. EPA measurements taken in Kuwait Bay were also included in the analysis and used to calibrate the Landsat SST. The quantity of electrical energy produced from the power stations in Kuwait Bay, and the quantity of fresh water produced from desalination plants were obtained from the Ministry of Energy in Kuwait. The monthly produced energy and water were correlated with monthly SST in Kuwait Bay in order to investigate the relationship between thermal discharge from power and desalination plants and seawater temperature of Kuwait Bay.

7.2.1 Image processing techniques to predict sea surface temperature

The Landsat data were processed through a number of sequential steps before producing the final SST images. These steps include georeferencing, radiometric correction, and applying the SST equation to the radiometrically corrected image. The standard approach to predict SST from satellite images (Han and Jordan, 2005; Kloiber et al., 2002; Thomas et al., 2002) was adapted herein. Each of these processing steps are described in detail below. Figure (7.3) illustrates the analysis procedure used to produce the corrected SST data from raw Landsat files.

A. Geometric correction of satellite imagery

Landsat images were first geometrically corrected using ERDAS Imagine software. The correction was carried out on the image of 22nd June, 1985 based on 14 Ground Control Points (GCPs) in the region extracted from the topographic base map (scale 1:50,000). The base map has a UTM coordinate system with a spheroid on WGS 84 and a datum on WGS 84 (zone 39). The geo-referenced image of 22nd June, 1985 was used later as a master image for the geometric correction of the other images, using the image-to-image technique. The root mean square error of the geo-referenced image calculated by the ERDAS Imagine software was less than 0.5 pixels.

B. The production of water-only images

A mask to remove reflectance from land features was created using ERDAS imagine software. To create the water-only mask, the unsupervised classification method (10 classes) was run on the geometrically corrected images for the entire land and marine sectors. This classification method is recommended to be used when the characteristics of the region are less unknown before classification (NASA, 2009a). Subsequently, the classified images were re-coded to produce two classes, one for seawater and the other for land. The water class was assigned a value of 1 whereas the other class was assigned a value of zero. Finally, the subset functions of ERDAS imagine software was used to produce the water-only image of the study area for each image.

D. The radiometric correction for atmospheric effects

The absolute reflectance of the ground target in a multi temporal imagery is affected by atmospheric conditions, solar angle, solar view angle and sensor

characteristics (Olthof et al., 2005). Therefore, radiometric correction is used to remove these effects in order to extract the absolute surface reflectance (Chen et al., 2005; Vicente-Serrano et al., 2008).

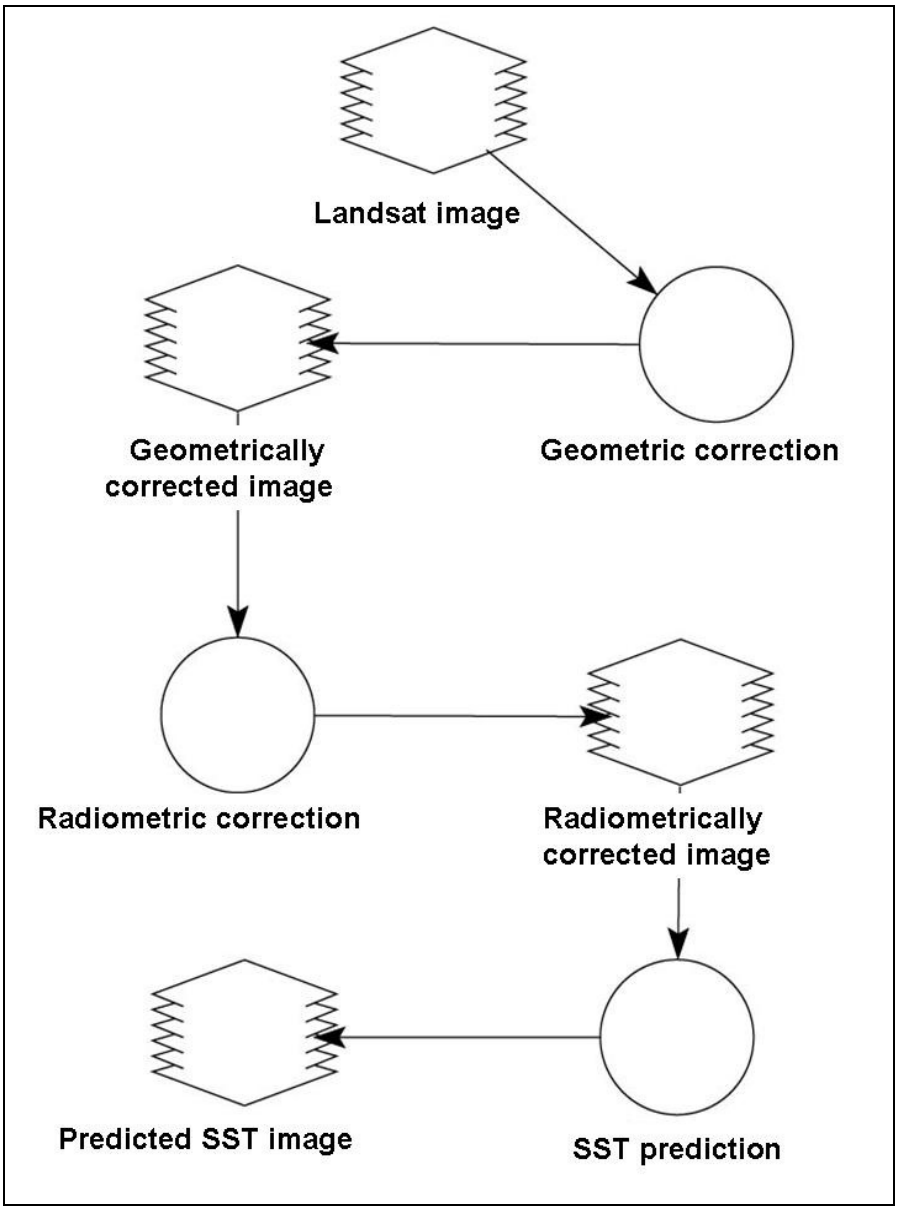

Figure 7.3: The sequences of analysis used to derive predicted SST from Landsat row data files.

In this study, a radiometric correction was applied to different Landsat images to convert the digital number (DN) values of image pixels into -at sensor- radiance, in order to derive absolute values of ground reflectance. The spatial modeler of ERDAS Imagine software was used to carry out the radiometric

correction of different images. The following equation, which has been approved by NASA, is used to carry out the radiometric correction:

$$L_\lambda = (\frac{L_{\max} - L_{\min}}{QCAL_{\max} - QCAL_{\min}}) * (DN - CAL_{\min}) + L_{\min}$$ ……. Equation (7.1)

where:

L_λ = radiance (W/m^2 * stranding * µm);

DN = digital number of each pixel (0-255);

L_{max} and L_{min} = calibration constants;

$QCAL_{max}$ and $QCAL_{min}$ = the highest and lowest range of values for rescaled gain radiance in DN.

The above mentioned parameters and coefficients came from the header files of images and the published documents from NASA (NASA, 2009a).

E. The prediction of sea surface temperature (SST)

The spatial modeler of ERDAS Imagine software was used to produce the SST for different images. The Landsat TM sensor has a spatial resolution of 120 x 120 m whereas the Landsat ETM+ has a 60 x 60 m resolution for the thermal infrared band (band 6). The other bands of TM and ETM+ sensors (bands 1, 2, 3, 4, 5 and 7) have 30 x 30 m resolution, while the panchromatic band of ETM+ sensor has a 15 x 15 m resolution. The spectral resolution of band 6 is 10.45 -12.42 m (for Landsat TM) and 10.31 – 12.36 m (for Landsat ETM+). SST from the transferred radiance data was calculated using the following equation which has been approved by NASA (2009a):

$$T_R = \frac{K_2}{Ln(\frac{K_1}{L_\lambda} + 1)}$$ …….. Equation (7.2)

where:

T_R = radiance temperature in degrees Kelvin;

K_1 = calibration constant;

K_2 = calibration constant; and

L_λ = spectral radiance for the pixel.

The above mentioned parameters and coefficients came from the header files of images data files and published documents from NASA (NASA, 2009a).

7.2.2 The evaluation of coastal thermal plumes

The input of heat at the shoreline is based on Δt measured between the peak plume temperature and the adjacent water mass in the middle of Kuwait Bay. Therefore, in each image the average value of 120 pixels in the middle of the bay was assumed to be an unaffected background temperature. This was subtracted from the average value of 120 pixels in the thermal plume. The monthly SST of AVHRR satellite was correlated with monthly electricity and water production from the power and desalination plants in the bay, in order to investigate the effect of the thermal discharge from power and desalination plants,

Tables 4.2 and 4.3 show that the seawater temperature in Kuwait Bay has been influenced by heat flux from the atmosphere (air temperature, wind speed, solar radiation) and tidal exchange with the Arabian Gulf. Tables 4.4 and 4.5 showed that the sea-bed is a source of heat to the water column in winter. During summer the opposite is true. Figure (4.12) shows high SST near the power and desalination plants in the bay. The thermal plumes are due to the discharge of warm water from these stations, which is typically 9 ºC above the temperature of the ambient seawater at the source.

Figure 7.4 illustrates the schematically heat exchange between Kuwait Bay and the surrounding area. In order to find the influence of thermal discharge from power and desalination plants to the seawater temperature of Kuwait Bay, a relative thermal box model was constructed. This box model was provided by Kuwait Institute for Scientific Research (KISR). The box model does not include heat exchange with the atmosphere nor the heat exchange with the seabed. In this study, it was assumed that the water temperature at the Bay entrance is the same as the ambient temperature; it was also assumed that there is no change in the meteorological conditions.

The heat budget in Kuwait Bay can be represented by the following equation:

$$\frac{dH}{dt} = \frac{d}{dt}\left(\rho c_p \mathrm{V}_{KB}\, \mathrm{T}_{KB}\right) = \frac{dH_{pp}}{dt} + \frac{dH_{Gulf}}{dt} \qquad \text{..... Equation (7.3)}$$

where H is the heat balance, t is the time; ρ is the water density; c_ρ is the specific heat of water; V_{KB} is the water volume for Kuwait Bay; $\mathrm{T_{KB}}$ is the water temperature in

Kuwait Bay; H_{pp} is the total heat transfer from power and desalinations plants; H_{Gulf} is the heat transfer from the Arabian Gulf (due to tidal exchanges). The above equation can be written as:

$$\rho C_p \, A_b \, \frac{\Delta (hT_{KB})}{\Delta t} = \rho C_p \sum_{J=1}^{N_{pp}} Q_{pp_j} \, (T_{K.B} + \Delta T_{PP_J}) + \rho C_p \, \frac{\Delta (Q_{tide} \, T_t)}{\Delta t} \quad \text{..... Equation (7.4)}$$

where A_b is the area of the bay; $\Delta T_{PP_J J}$ is the temperature rise at the outfall of a power plant J ; Q_{PP_J} is the discharge of water from the power plant J; Q_{tide} is the discharge of seawater at the bay entrance due to tides; T_t is the temperature of water at the tidal boundary; and h is the water depth at time t. T_t is equated with the ambient Northern Gulf water temperature; T_o for flood conditions and is the same as the temperature of the bay; T_{KB} for ebb conditions. The discharge of seawater due to the tides can be written as:

$$Q_{tide} = A_b \frac{dh}{dt} \quad \text{..... Equation (7.5)}$$

where $h = h_0 + h_t$; h_0 is the average depth at lowest tide (5 m for Kuwait Bay); h_t is the tidal water level above the lowest level of water.

Equation (7.4) was solved using an explicit time marching finite difference scheme. This relative heat budget box model was then applied to Kuwait Bay during winter and summer.

7.3 Results and interpretation

7.3.1 The accuracy of Landsat SST

The spatial variability in the predicted SST from LANDSAT was examined in order to establish thermal scatter and potential errors in spatial averaging of the data. A sub-region of 400 km (1112 pixels) was examined as a frequency histogram of corrected temperature. The results obtained for the sub-region are shown in Figure 7.5. The Gaussian, best-fit line of the measured temperature distribution is also shown. The results show that the data are normally distributed around the mean. The scatter is ± 1.2 ℃. The normal distribution indicates that the sub-region used to interpret temperature trends in Kuwait Bay is representative of the entire population

of data. The scatter is a measure of local variability that is not explained in the averaged data.

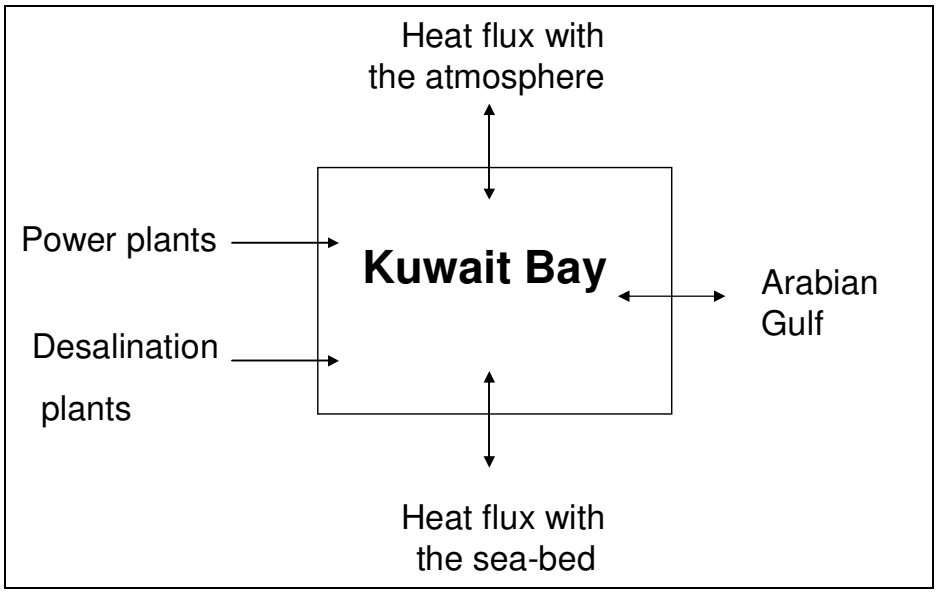

Figure 7.4: A schematic diagram of a heat box model for Kuwait Bay. The figure illustrates the heat exchange between Kuwait Bay and the surrounded area. In this study, a relative heat box model is constructed without including the heat exchange with the atmosphere and the seabed.

LANDSAT SST values were chosen to coincide in space and time with the EPA field measurements and the AVHRR SST. The time of LANDSAT overpass was around 1000 (local time) whereas, the time of AVHRR overpass was around 14:00 (local time), and most of the EPA measurements were taken between 0700 to 10:00 (local time). It is known that solar heating influences SST over the diurnal cycle (Figure, 5.5). As a result, the EPA SST and AVHRR SST have been adjusted to the time of LANDSAT overpass (10:00) based on EPA hourly measurements. This adjusted SST is correlated with LANDSAT SST in Figures 7.6 and 7.7. A 1:1 correlation was found with field measurements ($r^2 = 0.96$; $p<0.05$, Std = 0.4 ºC) and also with AVHRR ($r^2 = 0.99$; $p<0.01$, STD = 0.2 ºC).

.

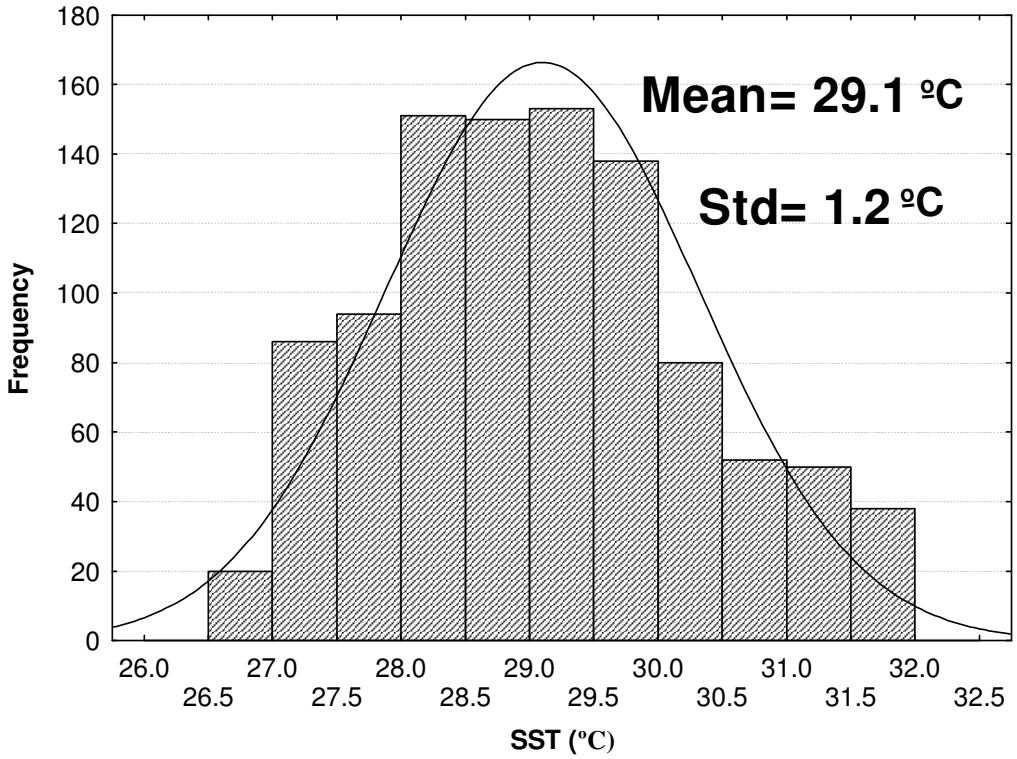

Figure 7.5: Histogram of the predicted SST from a Landsat image (1112 pixels) of Kuwait Bay. The graph shows that the data are normally distributed around the mean.

7.3.2 Predicted SST from Landsat images

A map of corrected SST was generated for each of the eight Landsat images cited in Table 7.1. These maps are illustrated in Figure 7.8 and Figure 7.9. The SST ranges from 22 to 36 ºC. Panels A to H are the processed images files in time sequence from 22nd June, 1985 to 13th June, 2002. Although the absolute temperature varied in the images (where the highest was in 1985 and lowest in 1989), the pattern is generally the same. The main difference between the warmest year (1985) and the coldest year (1989) is mainly due to the effects of the regional drivers that operate in the northern Arabian Gulf. Figure 6.4 shows that SST in 1989 in the northern Arabian Gulf is lower than in 1985 due to high dust storm frequency and high fresh water discharge from the Shatt Al-Arab.

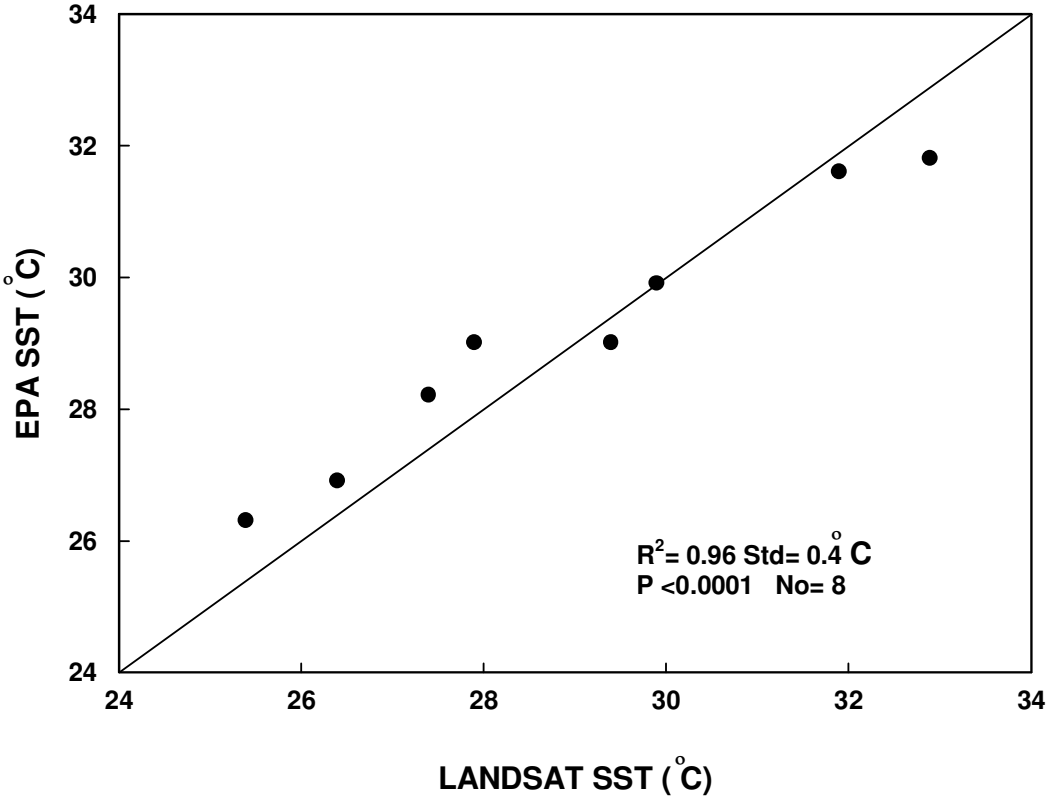

Figure 7.6: Correlation between predicted SST from LANDSAT images and measured SST (EPA measurements) in Kuwait Bay (after correction of EPA SST to 10:00).

The general pattern show inner warm water masses and outer colder water masses for all images. A strip of relatively cool water is evident in all images fringing the northern part of the bay. This fringe is approx 3 km wide and widens from west to east. This fringe of cool water is considered to result from heat losses to the outer intertidal flats of the region. Upwelling has been discounted as the cause as the water in this region is well-mixed. Furthermore, the image taken during 1989, shows relative warming in this region (when the intertidal flats are a source of heat). The water mass in the central bay shows a constant temperature diagnostic of well-mixed, homogeneous water mass. Differences in temperature are within the scatter of the data shown in Figure 7.7 and appear to describe large eddies within the water mass. The warmest regions are found to be in the southern part of the bay. The cool fringe evident in 1985 is not evident in subsequent images, where it has been replaced with relatively warmer plumes that expanded in area and intensity through

till 2002. The SST south of the bay is higher than SST north of the bay. High SST was recorded close to human activities especially close to the sources of thermal discharge from power and desalination plants. Figure 7.1 shows the location of the power and desalinations stations. Figure 2.9 illustrates the sewage and storm water discharges into the bay. Landsat images show high SST close to urban areas where the sewage outlets exist.

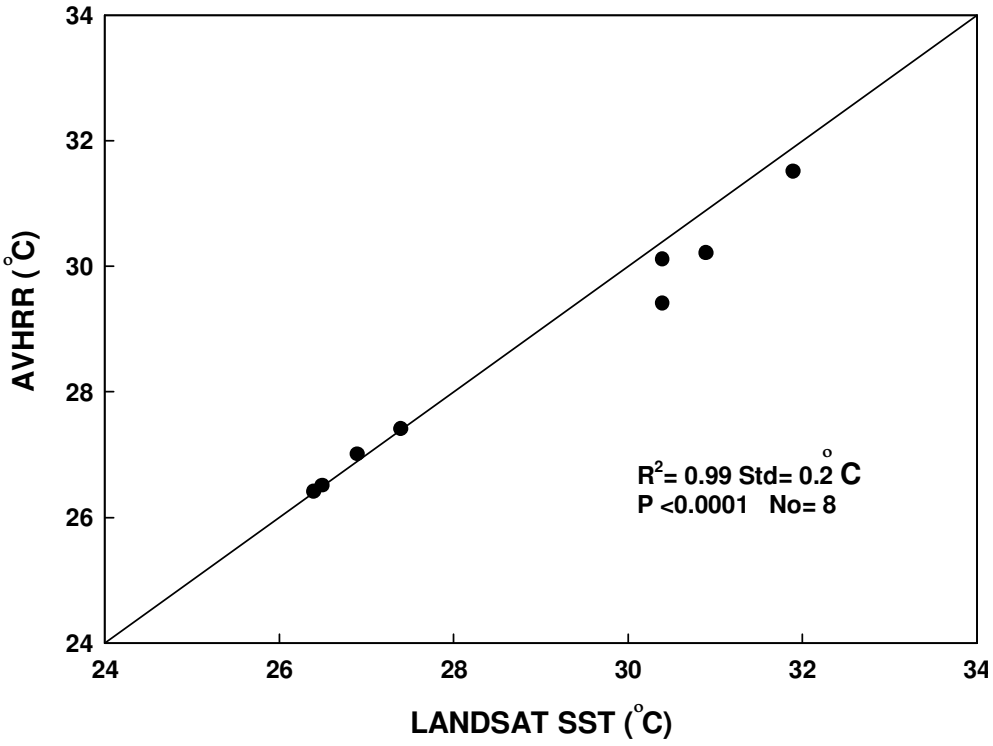

Figure 7.7: Correlation between predicted SST from LANDSAT images and SST from AVHRR in Kuwait Bay (after the correction of AVHRR SST to 10:00).

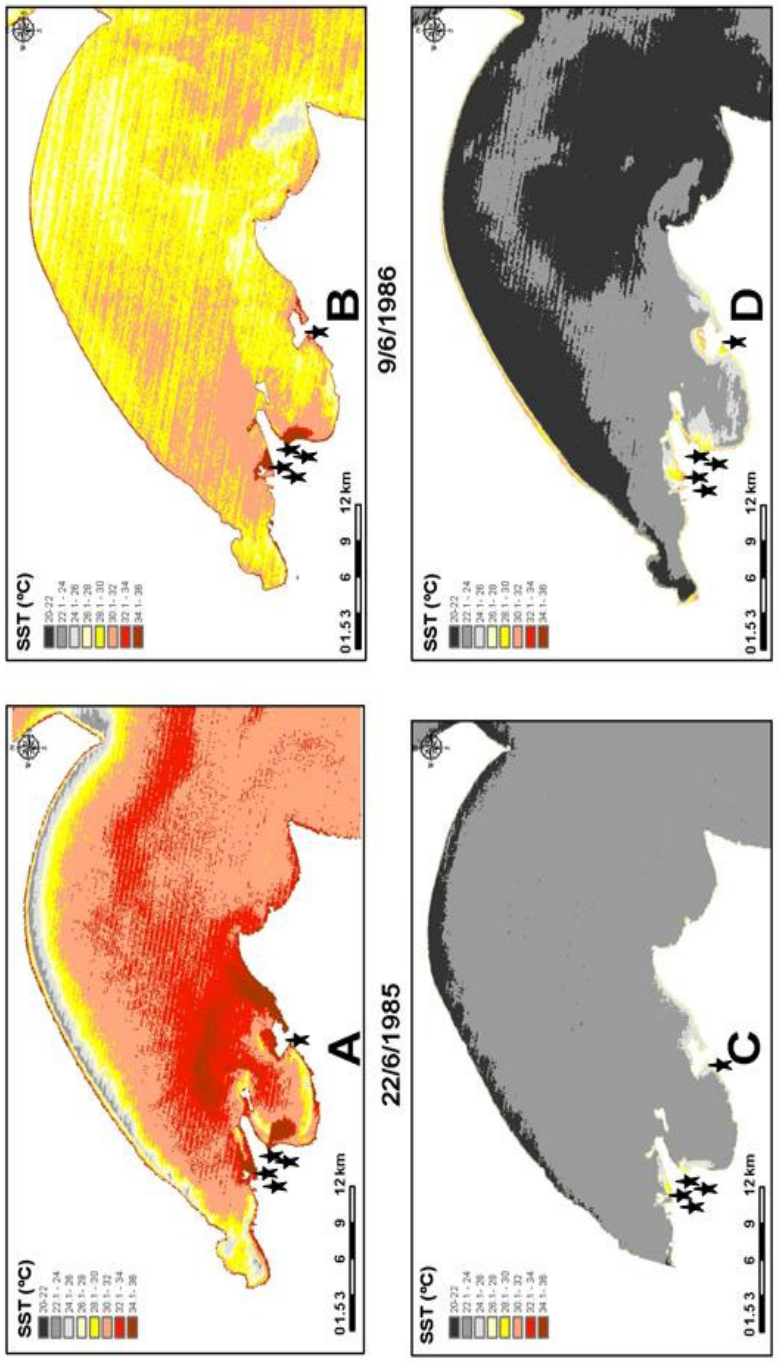

Figure 7.8: Predicted SST in Kuwait Bay. Panels A to D are the processed images files in time sequence from 22nd June, 1985 to 9th June, 1989. The stars show the location of power and desalination plants. The general pattern is similar for all images showing inner warm water masses and outer colder water masses. SST in the north of the bay is lower than in the south. SST close to the power and desalination stations are high due to the thermal plumes from these stations.

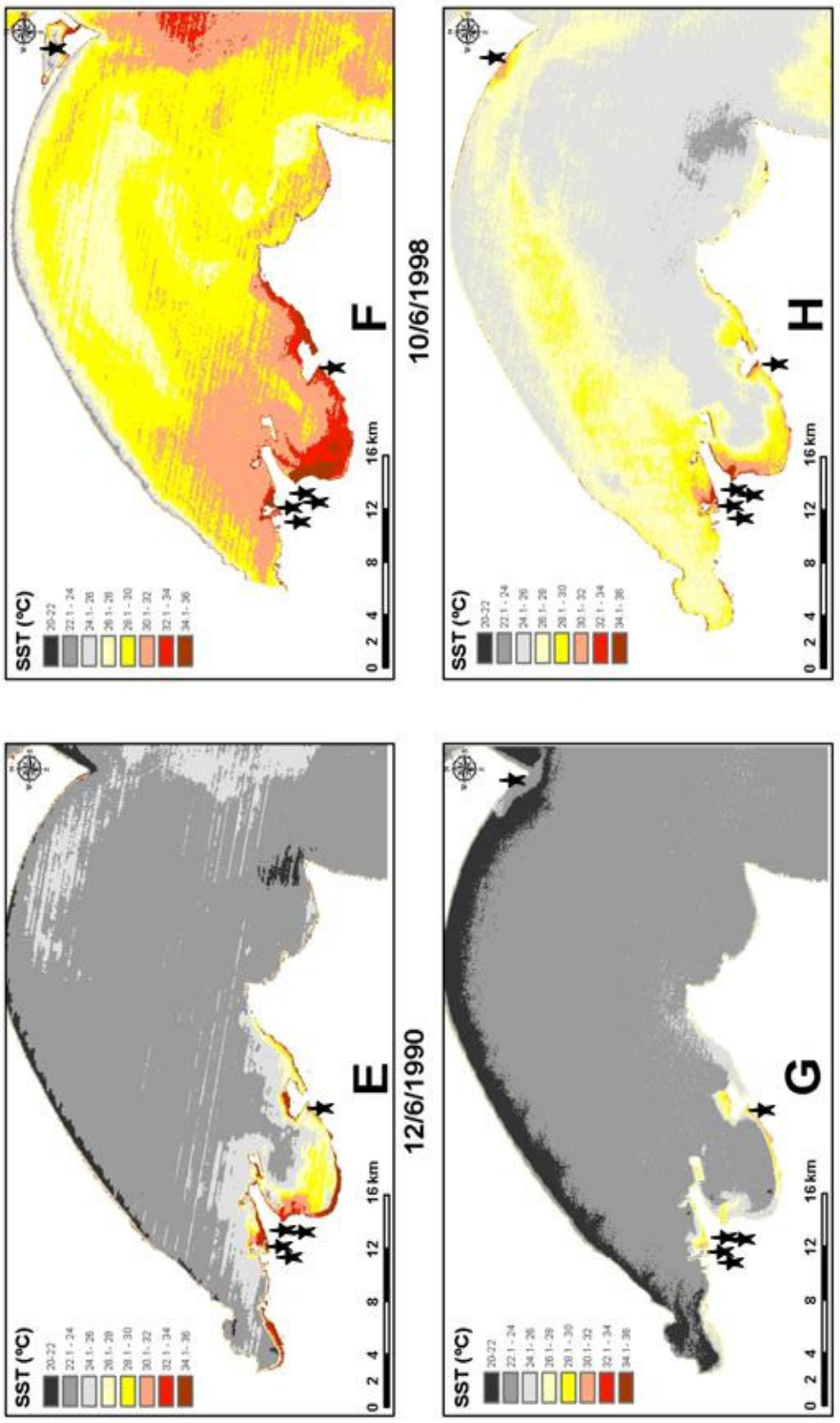

Figure 7.9: Predicted SST in Kuwait Bay. Panels E to H are the processed images files in time sequence from 12th June, 1990 to 13th June, 2002.

.

The Landsat image of 2002 shows a peak in high SST along the northeastern shore of the bay near Subia power station (Figure 7.1) which is interpreted to be the thermal plume from the station. Figure (7.9) shows the thermal discharge from this station. The images before 1998 show no plume because the power station was built after 1997.

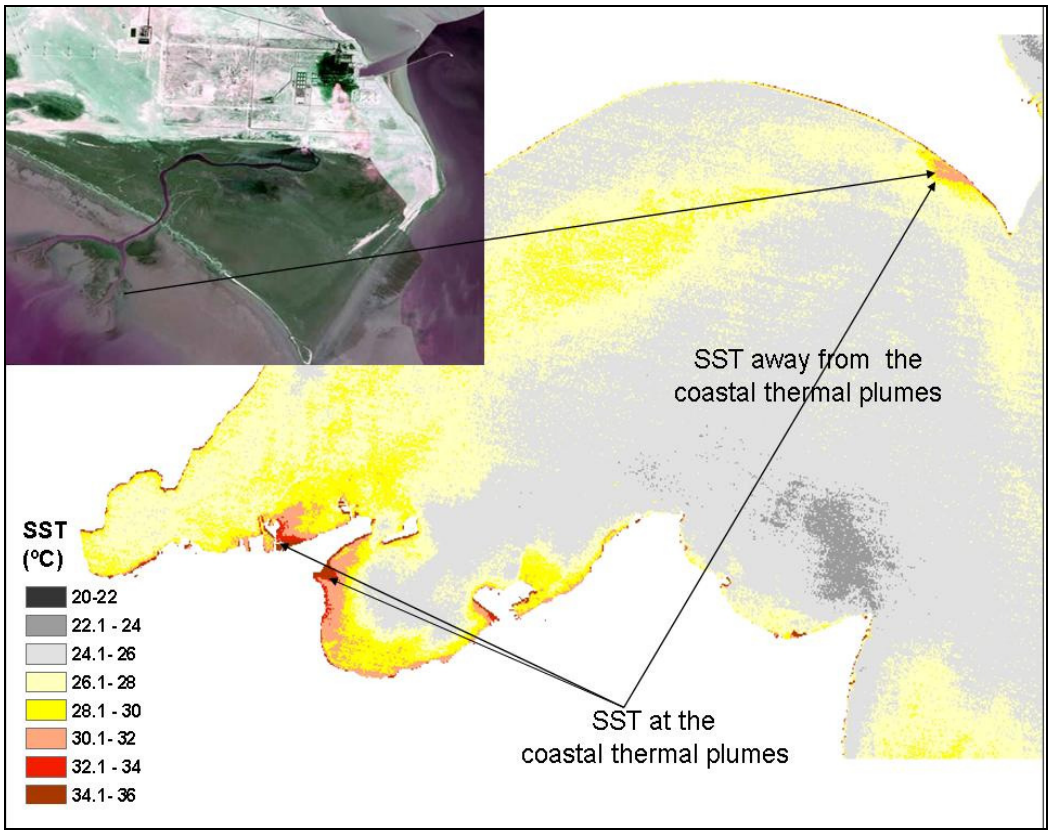

Figure 7.10: Sites selected to measure SST away from thermal discharge and close to the power and desalination stations. The top left image shows the thermal discharge from Subia power station in the northern part of the bay.

Figure 7.10 shows the increase in the SST (Δt) over ambient seawater in Kuwait Bay. Δt is the difference in SST between coastal thermal plumes and SST in the central bay (see Figure, 7.9). It appears that Δt has almost doubled over the time interval covered. Thought that the increased in Δt with time is due to an increase in local activities which have caused increases in power and fresh water production. It is clear that theses plumes are manifestations of local effects of human activities (local drivers) in increasing the SST. The human impact on SST in Kuwait Bay was

thus 3.4 ºC in 1985, and increased to 6 ºC in 2002. According to the data provided by the Doha East power station, SST in the plume from the station in 2008 was about 9 ºC above ambient.

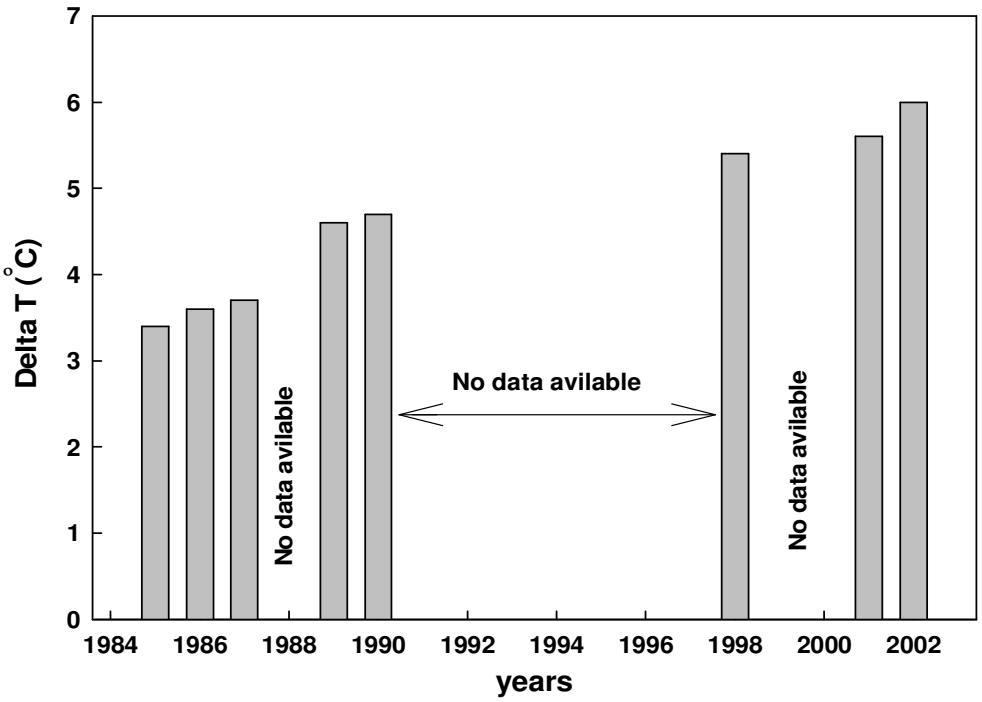

Figure 7.11: The difference in SST between coastal thermal plumes and SST in central Kuwait Bay (shown in Figure 7.9).

7.3.3 Influence of power and fresh water production on seawater temperature of Kuwait Bay

Landsat images show that the thermal plumes from power and desalination station have led to an increase in the SST near these stations. However, it is not clear to what extend these sources of heat affect the entire bay. In order to evaluate this influence, monthly SST in Kuwait Bay determined from the AVHRR satellite was correlated with monthly electricity and water production from the power and desalination plants in order to investigate the relationships with SST in Kuwait Bay. Figure 7.11 shows a scatter plot between SST in Kuwait Bay and electricity production from 2000 to 2007. Figure 7.12 shows the scatter plot between the SST and water production in Kuwait Bay from 2000 to 2007. Both graphs show positive correlations between SST with electricity and water production. The scatter plots show that seawater temperature has increased in Kuwait Bay in parallel with the

increase in electricity and power production. This however can partly be explained by the fact that during the summer the electricity and water consumption is higher in Kuwait.

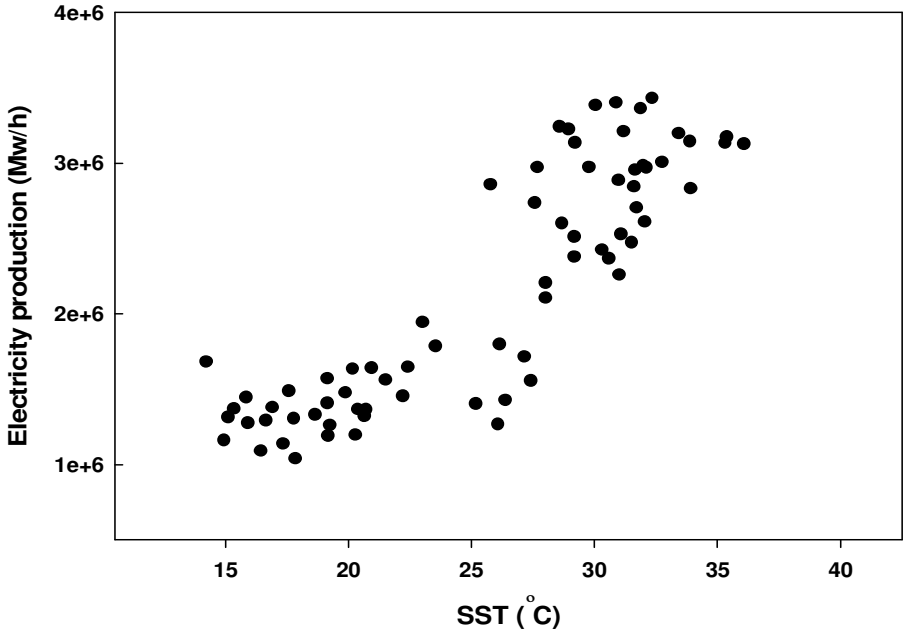

Figure 7.12: A scatter plot of monthly SST and monthly electricity production in Kuwait Bay from 2002 to 2007.

The heat box model described earlier was used to study further the impact of the power and desalination plants on seawater temperature in Kuwait Bay. The temperature input to Kuwait Bay was restricted to the thermal plumes. The temperature losses from the bay were through exchanges (horizontal advection) with the northern Arabian Gulf. The initial ambient temperature in Kuwait Bay is assumed to be 18 ºC for winter and 30 ºC for summer. The system is assumed to be closed, other than to the effects of the power plants and horizontal advection. Waters advected out of the bay are returned at the initial temperature. That is, the water lost from Kuwait Bay on ebb tides are assumed to be completely replaced by new seawater from the northern Arabia Gulf. Figure 7.13 (A) shows the tide levels in Kuwait Bay during January 2007 and Figure (7.13 B) shows the tidal prism entering the bay, Q_{tide} used in the box model. Figure 7.13 (C) shows the results of applying the heat box model for Kuwait Bay. Thus the water temperature at the Bay entrance is the same as the ambient temperature. The fluctuations in temperature result from the tidal fluctuations in Kuwait Bay as during spring tides the tidal prism entering the

bay is higher and advection is greatest; this leads to a decrease in temperature. By contrast, during neap tides, the temperature increase is greater as the cooler water mass is lower, as is advection. The average increase in temperature over a period of 600 hours was found to be about 0.4 ºC. On neap tides, the diurnal fluctuation in temperature is larger (0.1 ºC), than on spring tides (0.06 ºC). Figure 7.14 (A, B and C) shows similar results for the summer. The mean increase in temperature was found to be about 0.6º C.

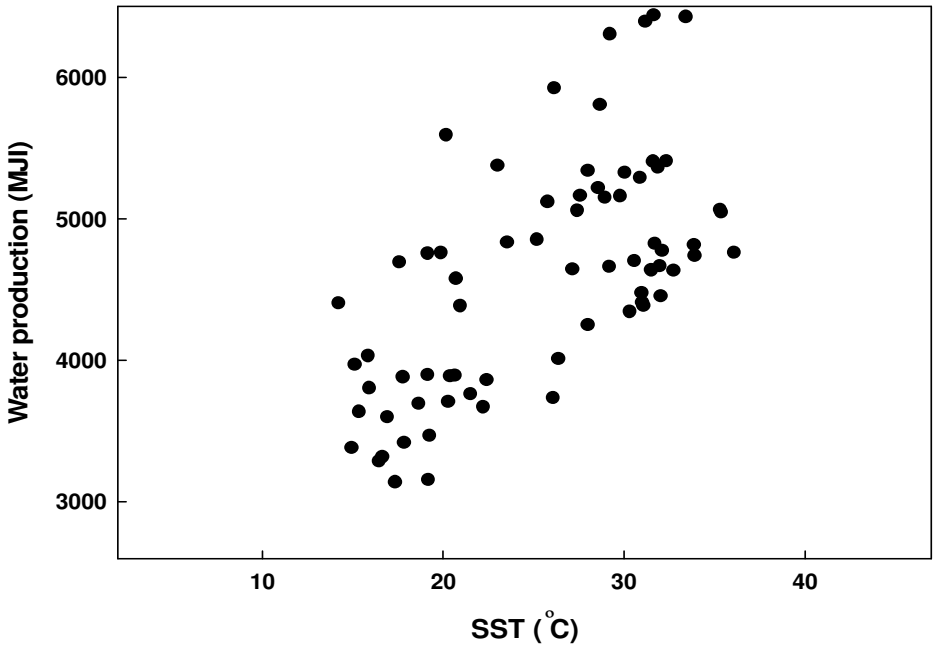

Figure 7.13: A scatter plot of monthly SST and monthly water production in Kuwait Bay from 2002 to 2007.

The temperature trends in June are remarkably similar to those predicted in January since a relative temperature model is used. Thus the main difference is due to the larger discharge from the power and desalination plants during summer. The warmest values occur over neap tides and (relatively) cooler water is evident over spring tides. On neap tides, the thermal contribution is larger than heat losses due to horizontal mixing and advection to the northern Arabian Gulf, and so the mean seawater temperature in Kuwait Bay increases. Over spring tides, the opposite is true, and there is a reduction in mean seawater temperature. These results show that indeed the average contribution of the power and desalination plants to the entire bay seawater temperature is small but significant.

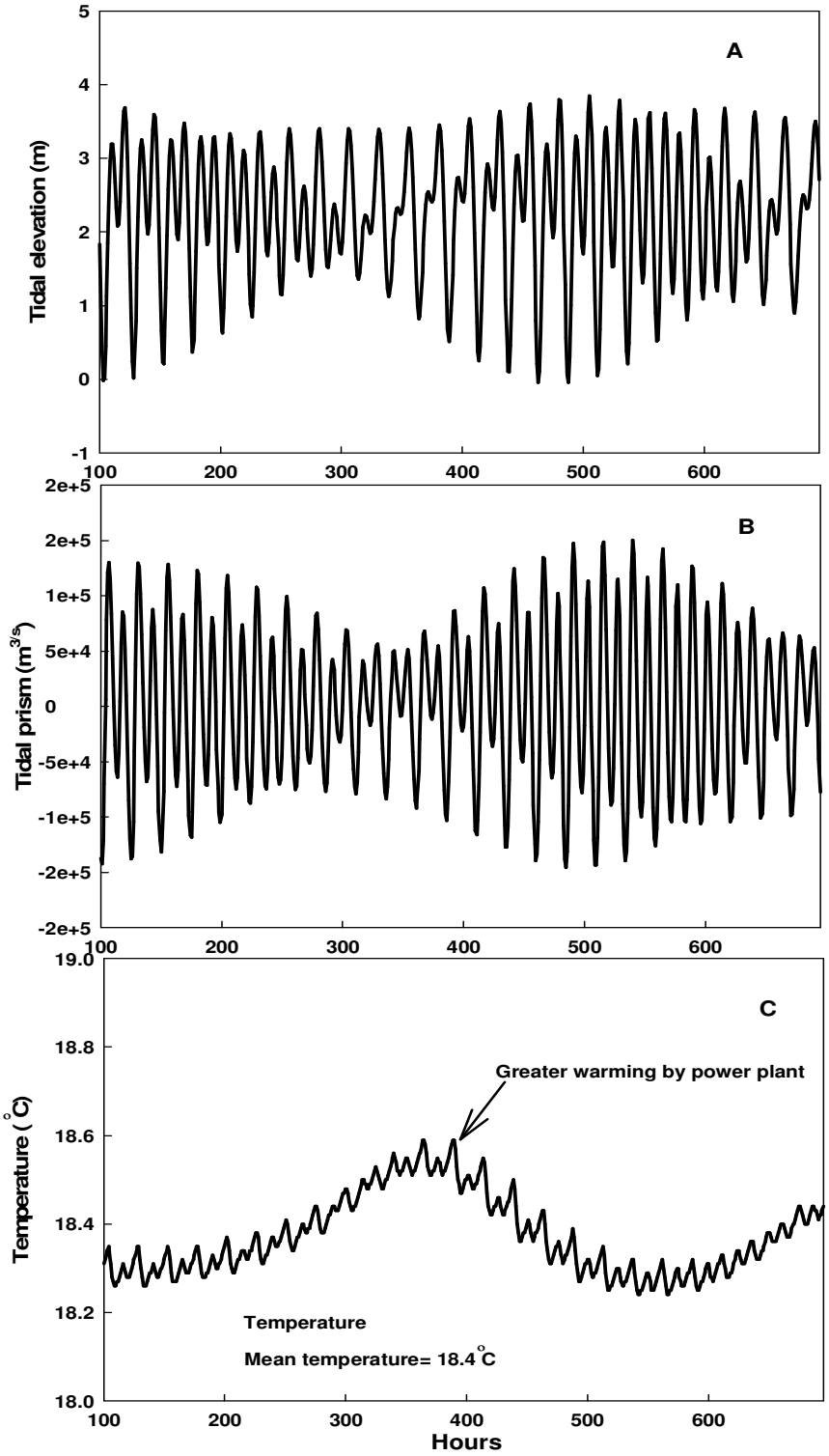

Figure 7.14: Time-series of (A) tidal elevation, (B) tidal prism and (C) estimated temperature from the heat budget model of Kuwait Bay for January 2007. The box model shows a large temperature difference on a neap tide due to greater warming by power plants. There is a two-day phase lag between the peak in temperature is two days after the minimum tide, this maybe due to mixing with the Gulf.

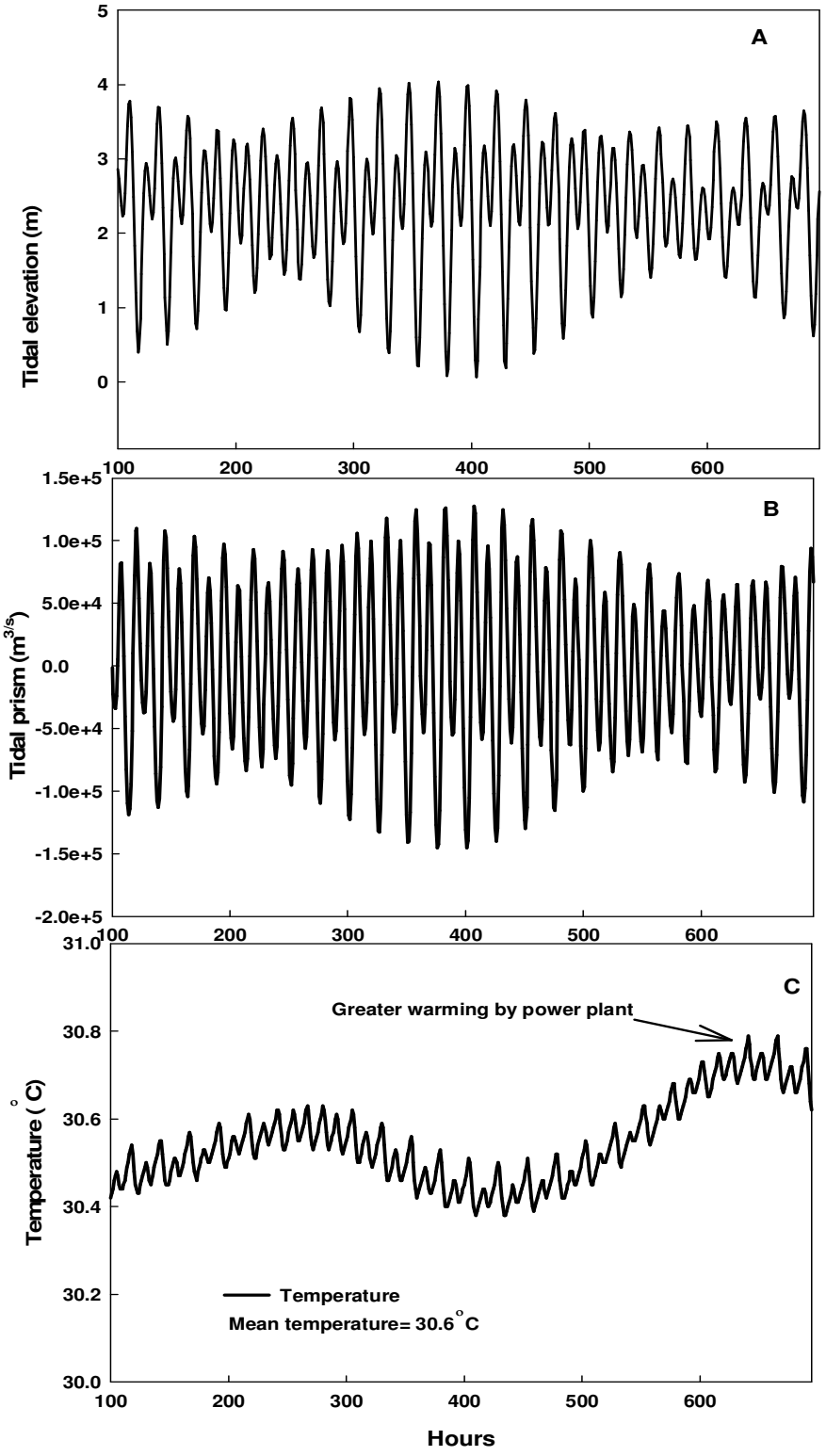

Figure 7.15: Time-series of (A) tidal elevation, (B) tidal prism and (C) estimated temperature from the heat budget model of Kuwait Bay for June 2007.

7.4 Discussion

Yanagi (2008) observed increases in seawater temperature for Tokyo Bay in Japan from 1976 to 1997 that were much higher than the global average presented in the recent IPCC report. He attributed this increase in seawater temperature to the local human activities. Al-Rashidi et al., (2009) found that the SST trend in Kuwait Bay is usually higher than the SST trend in the Arabian Gulf and in the Indian Ocean due to local drivers that are present in Kuwait Bay. This study detects the sources of local drivers of temperature change, which are mainly due to thermal discharges from power and desalination plants. Landsat images, used to detect the source of local drivers in the seawater temperature of Kuwait Bay, showed that the temperature of the seawater near the discharge points was 9 ºC above ambient. High seawater temperature was recorded near the urban centres along the south side of the bay. Al Bakri and Kittaneh (1998) also found that using seawater for cooling power and desalination plants in Kuwait Bay led to an increase the seawater temperature. This study has quantified this increase.

High seawater temperature was also recorded close to sewage outlets exist. The southern coast of Kuwait Bay is subject to sewage pollution, due to the discharge of sewage through emergency rainwater drains (Al-Mussalam, 1999; Al Bakri, 1996). The sewage water is the same temperature as the air temperature (approaching 50 ºC in summer) and hence, it can affect seawater temperature in the coastal zone.

There is a correlation between monthly SST and monthly thermal discharge from power and desalination stations in Kuwait Bay, related to the high use of electricity and fresh water in summer (time of high SST). The results of the relative thermal heat box model showed that the contribution of thermal discharge from the existing stations to seawater temperature of Kuwait Bay is 0.4 ºC in winter and 0.6 ºC in summer. These temperature increases may be considered as additive to the regional and global effects described earlier. Thermal plumes are found to have important influences on the ecosystem of marine environment (Jiang et al., 2009). In Kuwait Bay, there is an increase in demand for more electricity and fresh water due to the increasing population (Darwish et al., 2008). According a new report of the Ministry of Planning in Kuwait, the Government plans to increase the number of the

power and desalination plants in Kuwait Bay to meet the future needs from fresh water and electricity. The box model of this study predicts that the SST in Kuwait Bay will increase by 0.1 ºC for each new power plant of the Subiya station scale adds to the bay.

It is expected that the marine life in Kuwait Bay will be affected by increasing SST due to these intensive local drivers originated in the coastal zone. The future demand for fresh water and electricity due to the rapid development and increasing of population in the coastal zone of Kuwait will increase potential impacts of these local drivers on the marine environment.

7.5 Conclusions

The contribution of local drivers of seawater temperature change in Kuwait Bay has been evaluated. Landsat images were used to investigate the source and influences of coastal thermal plumes in Kuwait Bay. It is clear that the contributions of local drivers are less than the global and regional drivers. However, local drivers are the only ones that can be controlled. The major conclusions of this study are:

(1) Landsat images have detected the sources of thermal discharges along the coastline of Kuwait Bay;

(2) the distribution of SST from Landsat is Gaussian and exhibits a spread of 1.2 ºC. This spread is considered to be the spatial scatter in data due to random processes. The error of Landsat SST calibrated against EPA measurements is ±0.4 ºC and against AVHRR data the error is ±0.2 ºC. The predicted contribution of local drivers is greater than this error at seasonal time scales;

(3) SST along the north side of Kuwait Bay is less than that in the south of the bay. Low SST in the north of the bay is due to heat losses to the intertidal flats in summer. Highest SST in the south of the bay was recorded close to the urban centres, and illustrate the impact of local drivers;

(4) local drivers in Kuwait Bay are thermal discharges from power and desalination plants, sewage discharges, and intertidal flat exposure time;

(5) the difference between seawater temperature close to urban centres and seawater temperature in the central bay was 3.4 ºC in 1985 and increased to 6 ºC in 2002. This suggests that the input of local drivers to coastal seawater temperature has doubled in the 17 years covered by this study; and

(6) the average contribution of thermal discharge from the existing power and desalination stations to the seawater temperature of Kuwait Bay is about 0.4 ºC in winter and 0.6 ºC in summer. This contribution is additive to regional and global drivers of temperature change.

Chapter 8: General discussion and conclusions

8.1 Drivers of seawater temperature trends in Kuwait Bay

In this thesis, satellite SST and *in situ* measurements were used to study the distribution of seawater temperatures in the Arabian Gulf and Kuwait Bay. MODIS and Landsat SST were used to describe the horizontal distribution of SST. Vertical temperature measurements on an hourly basis were used to investigate the vertical distribution of seawater temperature. These measurements included the sea-bed temperature and the intertidal flat sediments temperature during summer and winter seasons. Results of SST distribution showed that the Arabian Gulf seawater temperature is higher in the south than in the north. Close to the shoreline, the SST is 3 ºC warmer due to local source of heat. The results showed that seawater temperature is higher in the south of Kuwait Bay than in the north. The lowest SST in northern Kuwait Bay is due to losses of heat to intertidal flat sediments; the distribution is also affected by human activities which are concentrated in the south of the bay and lead to increases in seawater temperature. Vertical temperature measurements showed that the water column is well-mixed in Kuwait Bay; the temperature varies from 15.2 ºC in winter to 37 ºC in summer. Within the sea-bed and the intertidal flat of Kuwait Bay, the temperature increases with depth in winter and decreases with depth in summer. The depth below the sea-bed at which no temperature change takes place is 140 cm. At this depth, the temperature is constant at 23.7 ºC. The depth below the intertidal flat surface at which no temperature change takes place is 125 cm. The temperature at this depth remains a constant of 25.6 ºC. Thus the intertidal flat sediments are 1.9 ºC warmer on average than those of the adjacent sea-beds. Studies of subsurface temperature profiles are limited in Kuwait. However, understanding the potential geothermal benefits of the subsurface is important (Al-Temeemi and Harris, 2001). This study has shown that there are great temperature differences within the sea-bed and intertidal flat of Kuwait Bay. The gradient in temperature changes show a potential for extracting energy from the ground for heating in winter and for cooling in summer.

This study investigates the effect of different drivers, which work together in the coastal region and examines what influences seawater temperature trends in Kuwait Bay on local, regional and global scales. The study attempts to separate the effects of global, regional and local drivers on the seawater temperature in the study region. Long-term AVHRR SST monitored at three selected sites (Kuwait Bay, the Arabian Gulf and the Arabian Sea) was used to study the trends of SST. The observed trends were proportioned to the relevant drivers in each case. In Kuwait Bay, the mean seawater temperature has increased by 0.62 (± 0.01) ºC/decade in the last two decades, which is three times greater than the global average. This increase in seawater temperature is substantiated by routine *in situ* monthly measurements of SST made in the region and was also similar to air temperature trends recorded at Kuwait airport. The observed trend is driven by global, regional and local drivers (Figure, 8.1). The contribution of global drivers was found to be 37% in the SST trend in Kuwait Bay. It appears that this contribution is growing with time, due to climate change (IPCC, 2007).

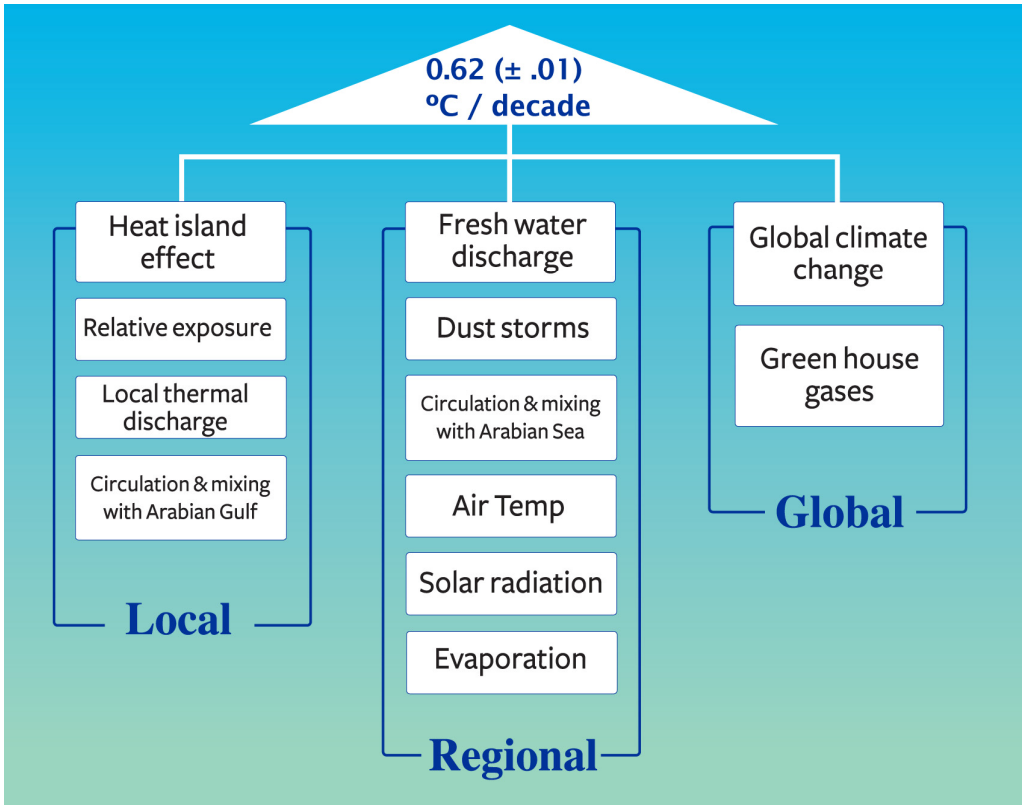

Figure 8.1: The drivers of seawater temperature of Kuwait Bay at the three different scales considered in this thesis.

The regional drivers have larger effects on seawater temperature of Kuwait Bay, contributing 50% of the signal. Regional drivers are those related to regional weather patterns, circulation and mixing with the Arabian Sea, fresh water discharge from the Shatt Al-Arab, and dust storms. It is appears that the contribution of regional drivers to seawater temperature is also increasing in time due to reduction in freshwater discharge though mitigated by an increase in dust storms.

Local drivers were found to contribute about 13% of the increase in seawater temperature in Kuwait Bay. Local drivers are those related to circulation and mixing with the Arabian Gulf, relative exposure, "heat-island" effects, and local thermal discharges. The highest temperatures were recorded in the thermal plumes from power and desalination plants, which are distributed around Kuwait Bay. The thermal discharge from power and desalination plants are 9 ºC above ambient (compared to the seawater temperature in the middle of the bay). The influences of power and desalination plants to the bay seawater temperature doubled during the time period of this study due to the increase productions of power and fresh water. This trend is likely to continue in the future. This study illustrates that the significance of local drivers in Kuwait Bay is presently less than regional and global drivers. The impact of local drivers would be greater in the flushing rate were lower (low tidal effect). To date, the concentrated "heat-island" effect has been studied in cities (González et al., 2005; Leake, 2009). This study illustrates that the heat island effect may also related to coastal water.

Figure 8.2 shows the temperature anomalies at the local, regional and global scales for the study region between 1985 and 2007. The temperature anomalies were calculated by taking the difference between the annual temperature and the mean for three selected sites in Kuwait Bay, the Arabian Gulf and the Arabian Sea (northern Indian Ocean). The temperature anomalies are not constant with time; sometimes they increase and at other times they decrease. The temperature anomalies are cyclic and the frequency seems to be two years from 1985 to 1990 and three years from 1992 until the present. The graph shows a lag between the temperature anomalies in the three studied regions. The largest temperature anomalies occurred in Kuwait Bay, they are intermediate in the Arabian Gulf, and least in the Arabian Sea. The

temperature anomalies are thus larger at local levels in the coastal region. Figure 8.2 also shows three periods in temperature anomalies at local and regional levels. The first period (between 1985 and 1992) shows a fall in temperature anomalies; the second period (between 1992 and 2004) shows a steady increase in temperature anomalies; the third period shows a further fall in temperature anomalies after 2004. The drop in temperature after 2004 may be related to the increased in dust frequency in the region that presenting 25% of the year (Alsharhan, 2009). The dust has the effect of solar dimming, which reduces seawater temperature (Kaufman et al., 2005). The movement of tanks and vehicles of US army across the desert from Kuwait to Iraq in the 2003 invasion disturbed the top layers of sand and contributed to the desertification process (Tharp, 2009). In Kuwait Bay, the lowest temperature anomaly was in 1991 during the burning of the oil fields in the second Gulf War (Al-Rashidi et al., 2009). The impact of this event was also clear in the Arabian Gulf (Husain, 1997; Khordagui and Alajmi, 1993) but did not impact on the Arabian Sea (the north Indian Ocean). The highest temperature anomaly took place in 2003, which was recorded as one of the five warmest years on record (IPCC, 2007). In this year, the fresh water discharge from the Shatt Al-Arab into the Gulf was reduced due to the restoration of the marsh land in the south of Iraq, as a result of the third Gulf War (UNEP, 2006). The effect of the third Gulf War is masked by the 2003 El Niño event. Reducing the fresh water discharge was found to be one of the regional drivers contributing to the increase in the seawater temperature of Kuwait Bay.

Linear regression analyses were used to calculate the trends in the temperature anomalies with time in the study area (Figure 8.3). The graph showed that the amplitude of the temperature anomaly has increased over time at all three scales. The greatest increase is at the local scale. It's higher in the local scale due to a rapid increase of local anthropogenic activities in the region.

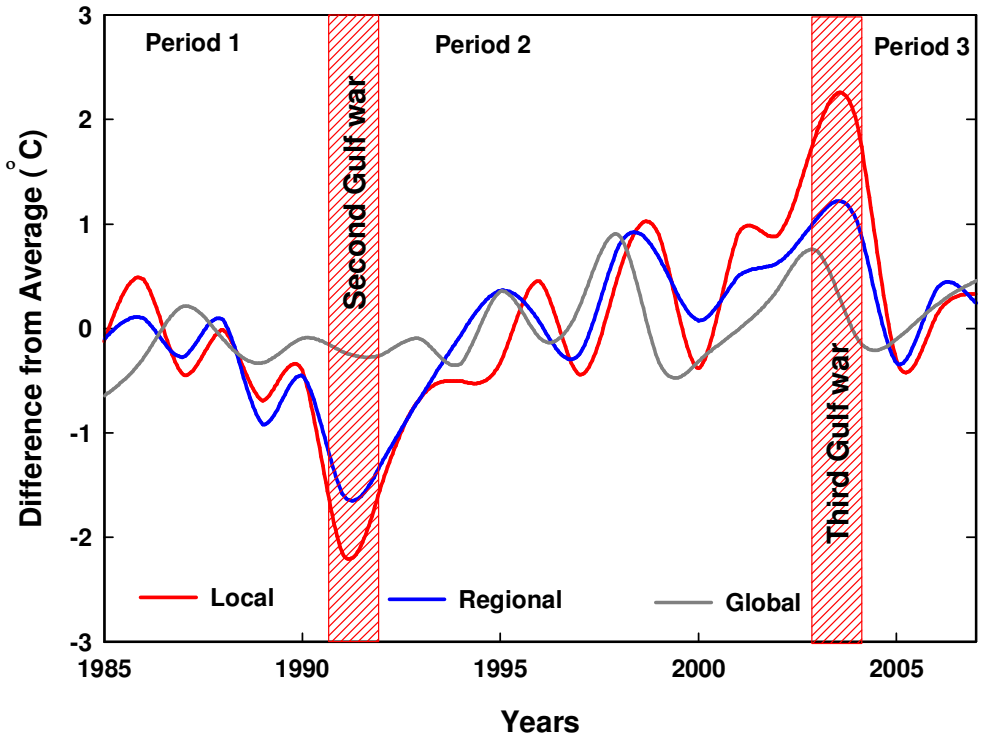

Figure 8.2: The SST anomalies at local, regional, and global levels for the study region between 1985 and 2007.

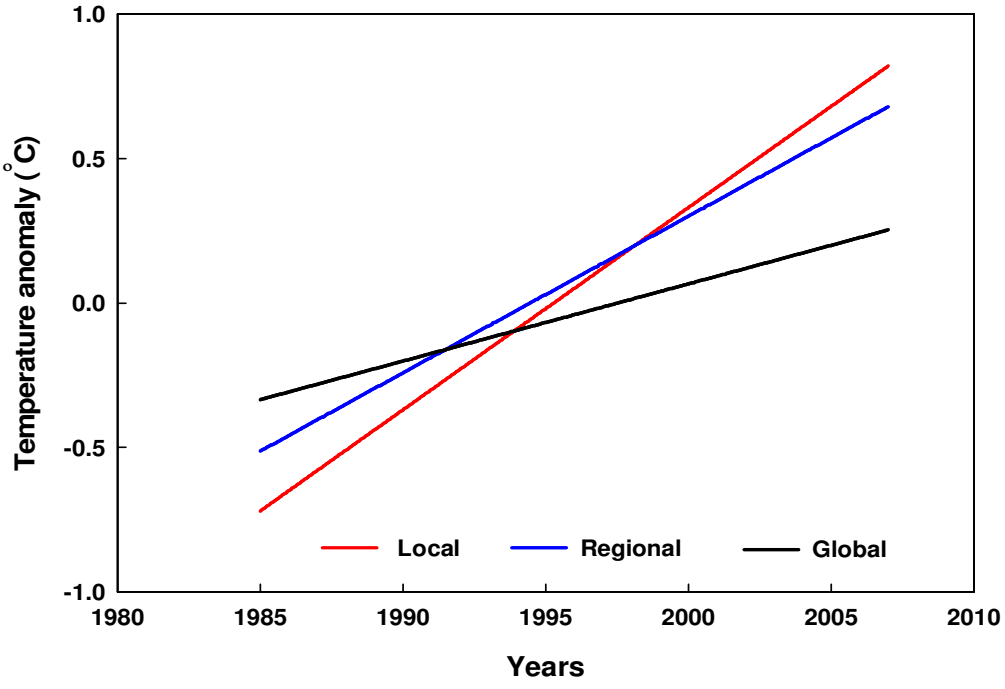

Figure 8.3: The linear trends of SST anomalies at the local, regional and global scales for the study region between 1985 and 2007.

8.2 Seawater temperature rise and the loss of habitats in Kuwait Bay

Seagrass, mangroves and areas of coral reef have disappeared over the last 20 years in response to rapid human development in the Kuwait coastal zone (Al-Awadhi ROPME; El-Sammak, KISR- *personal communications*). There are, however, certain other factors which may affect the distribution of habitats and the marine ecosystem in the region, such as the turbidity from the Shatt Al-Arab. High seawater temperatures were evident at the time of the marine ecosystem crisis in the region. Coral bleaching is documented in the south of the Gulf due to high seawater temperatures of 1998 (Riegl, 2002). Also fish kills occurred in 2001, when the sea water temperature reached 36 ºC (Glibert et al., 2002). Seawater temperature is an important factor that affects dissolved oxygen. Table 1.1 illustrates the relationship between dissolved oxygen and seawater temperature. As the seawater temperature increases, the concentration of dissolved oxygen decreases (Morton et al., 1997; Weiss, 1970). Decreasing dissolved oxygen is harmful for fish life and increases mortality rates (Burton et al., 1980).

The difference between seawater temperature, recorded in the bay recently and compared to those two decades ago, is large. The recent seawater temperature measurements taken in this study show that the seawater temperature often reaches 37 ºC in the summer time. The seawater temperatures measured at the beginning of the 1980, when seagrasses, mangroves and coral reefs existed in the bay, ranged between 30.8 ºC in summer and 16.2 ºC in winter (Jacob and Zarba, 1981). Dames and Moore (1983) recorded the hourly seawater temperature at selected stations in Kuwait Bay in 1981 and 1982; they found that the highest seawater temperature was 32.4 ºC. Thus mean seawater temperature in Kuwait Bay has increased significantly in the last 30 years.

8.3 Future sea water temperatures in Kuwait Bay

The Arabian Gulf is a unique body of water, in which the temperature is cooler than that of the waters around it. Therefore, mixing with the Arabian Sea adds heat to the Arabian Gulf rather than the reverse. The peaks in the lunar nodal cycle of the tide will contribute to the rising seawater temperature in the Arabian Gulf and

Kuwait Bay. This nodal cycle is the relationship between the gravitational effects of the sun, the earth, and the moon on the tides, that generates a 18.6-yr maximum amplitude in the tides (Yndestad, 2008). The nodal cycle was a maximum in 1987 and a minimum in 1996 (Pugh, 1996). The levels of mixing with the Arabian Sea are at their peak in the peak of 18.6-yr nodal cycle, which occured in 2006 (McKinnell and Crawford, 2007). The contribution of the exchange between the Arabian Gulf and Arabian Sea will thus reduce from the time of writing this thesis until the time of the minimum of the nodal cycle, which will be in 2016. It will then increase until 2025, when the next nodal cycle will start.

The electrical power and desalination plants in Kuwait Bay are expected to increase seawater temperature by 0.6 ºC over 600 hours. Each power plant added to the existing number will increase seawater temperature by 0.1 ºC. There is a demand for an increased production of electricity and fresh water in Kuwait due to the increase in population (Darwish et al., 2008). Therefore, the Government plans to increase the number of power and desalination plants in Kuwait Bay. There is also a plan in the near future to extend the production of the existing power and desalination plants. The potential increase in seawater temperature will affect the ecosystem in the bay (Al Bakri and Kittaneh, 1998). Thus local drivers are likely to increase in magnitude and thus have an ever-greater impact of the ecosystem of Kuwait Bay.

The fresh water discharge from the Euphrates has been affected by the South-eastern Anatolia Development Project (GAP) in Turkey. 22 dams and 19 power plants were constructed in the early 1980's to control the discharge of the Euphrates and Tigris rivers. This project has led to an 80% reduction in the flow from the Euphrates in the Iraqi territory (El-Fadel et al., 2002). The result of this study indicates that there is a relationship between the fresh water discharge from the Euphrates to the Arabian Gulf through Shatt Al-Arab and the seawater temperature. The GAP project will be completed in 2011. The critical time will be from 2016 to 2025, when the nodal cycle increases the exchange between the Arabian Gulf and the Arabian Sea. It is essential to try to alleviate the effect of these drivers at all levels. At the regional level, the Government of Kuwait must link up with the nations in the region to cooperate in reducing the effect of the regional drivers which have led to an

increase in seawater temperature in the Arabian Gulf, for example, the factors that reduced the discharge of fresh water discharge to the Arabian Gulf through the Shatt Al-Arab, such as the GAP project in Turkey.

Global warming is expected to increase with climate change (IPCC, 2007). According to this study, the seawater temperature in Kuwait Bay has increased by 0.62 (± 0.01) ºC/decade and the rate of change has been calculated to be 0.2 ºC/decade. This indicates that in the next two decades the seawater temperature will increase by 0.8 ºC/decade. This result is inevitable if the global and regional drivers continue to make the similar contributions to seawater temperature in Kuwait Bay.

The local driver contribution to the increase in seawater temperature for Kuwait Bay is presently the lowest. These drivers are expected to increase in their relative and absolute contributions. These may be controlled by reducing the impact of the power or desalination plants.

8.4 Recommendations and future work

In this study, long term satellite images off SST were used to determine the drivers of seawater temperature change in Kuwait Bay over the last two decades. Filed measurement was used to investigate the vertical distribution of seawater temperature in the bay. The following are some recommendations for future work based upon this work:

1. Satellite long-term monitoring of the seawater temperature in Kuwait Bay is recommended to continue to 2025, when the next significant peak of the nodal cycle will occur. It is also recommended to continue monitoring SST on a daily basis using the satellite images that cover Kuwait Bay. The daily SST can be used as an early warning, which will alert the decision makers in Kuwait to prevent, or reduce as far as possible, the effect of the drivers on the seawater temperature.

2. The measurements of the geothermal gradient in the intertidal flat sediments of Kuwait Bay showed a difference in the temperature during summer and winter time. This difference in temperature could be used for cooling in summer and heating in winter. It is recommended to measure the thermal gradients at different sites in the

intertidal zone of Kuwait in order to understand the heat transfer at each site. Also, the time-series of temperature at various depths could be used to cross-correlate data from the sensors in order to show the rate of heat at transfer.

3. This study has investigated the trends of seawater temperature in Kuwait Bay due global, regional, and local drivers. It is recommended to apply the same method to study the drivers of the seawater temperature in other coastal environments, in particular highly populated coastal areas such as Venice lagoon or Arabian Gulf cities such as Dubai.

9. References:

Abdelrahman, M. & Ahmad, F. (1995) A note on the residual currents in the Arabian Gulf. *Continental Shelf Research,* 15**,** 1015-1022.

Abouseida, M. M. & Alsarawi, M. A. (1990) Utilization and management of coastal areas in Kuwait *Coastal Management,* 18**,** 385-401.

Abu-Hamdeh, N. H. & Reeder, R. C. (2000) Soil Thermal Conductivity: Effects of Density, Moisture, Salt Concentration, and Organic Matter. *Soil Science Society of America Journal,* 64**,** 1285-1290.

Ahn, Y. H., Shanmugam, P., Lee, J. H. & Kang, Y. Q. (2006) Application of satellite infrared data for mapping of thermal plume contamination in coastal ecosystem of Korea. *Marine Environmental Research,* 61**,** 186-201.

Al-Asfour, T. (1981) The study of and a contribution to the geomorphology of the Arabian Gulf. *Change and development in the Middle East.* 173-188.

Al-Asfour, T. A. (1982) Changing sea-level along the north coast of Kuwait Bay. *Changing sea-level along the north coast of Kuwait Bay***,** 6-18.

Al-Bassam, E., Popov, V. & Khan, A. (2009) Impact of road traffic on air quality at two locations in Kuwait. IN Brebbia, C. A. & Popov, V. (Eds.) *17th International Conference on Modelling, Monitoring and Management of Air Pollution.* Tallinn, ESTONIA, Wit Press.

Al-Gahtani, A. & Maslehuddin, M. (2002) Characteristics of the Arabian Gulf environment and its impact on concentrate durability - An overview. *The 6th Saudi Engineering* Dhahran, Saudi Arabia King Fahd University of Petroleum and Minerals.

Al-Ghadban, A. & Salman, A. (1993) Preliminary assessment of the suspended sediment and its associated pollutants in Kuwait Bay. Kuwait, Kuwait Institute for Scientific Research.

Al-Ghadban, A. N. (2002) Geological oceanography of the Arabian Gulf. In Khan, N. Munawar, M., and Price, A.R.G (Eds.) *The Gulf Ecosystem, Health and sustainability*, Leiden, Netherlands, Backhuys, 23-40.

Al-Ghadban, A. N., Abdali, F. & Massoud, M. S. (1998) Sedimentation rate and bioturbation in the Arabian Gulf. *Environment International,* 24**,** 23-31.

Al-Ghadban, A. N. & El-Sammak, A. (2005) Sources, distribution and composition of the suspended sediments, Kuwait Bay, northern Arabian Gulf. *Journal of Arid Environments,* 60**,** 647-661.

Al-Haddad, S. (2009) The direct behind the dust. *Kuwait Times.* Kuwait, Yousuf Alyan. Available via DIALOG: http://www.kuwaittimes.net/read_news.php?newsid=MTA4NTU4MzgzOA.

Al-Majed, N. & Preston, M. R. (2004) The distribution and inventory of total and methyl mercury in Kuwait Bay. *Marine Pollution Bulletin,* 49**,** 930-937.

Al-Mussalam, F. (1999) Marine ecology and fisheries in Kuwait Bay with emphasis on the ecological impact of anthropogenic activities. In Al-Sarawi, M. & Massoud, M , (Eds.) *the impact of environmental pollution on development in the Gulf region.* Kuwait, EPA, 135-151.

Al-Muzaini, S., Beg, M. U. & Ali, L. N. (1997) Microtox assay for assessment of marine pollution in industrial discharge zone of Kuwait. *Environmental Toxicology and Water Quality,* 12**,** 109-115.

Al-Rashidi, T. B., Amos, C. L. & El-Gamily, H. I. (2007) Utilization of remotely sensed data to detect anthropogenic impacts on sea surface temperature of Kuwait Bay, Kuwait. *Oceans 2007 - Europe, Vols 1-3***,** 94-98.

Al-Rashidi, T. B., El-Gamily, H. I., Amos, C. L. & Rakha, K. A. (2009) Sea surface temperature trends in Kuwait Bay, Arabian Gulf. *Natural Hazards,* 50**,** 73-82.

Al-Sarawi, M., Al-Sarawi, M., Erich, R., Gundlach & Bart, j. (1988) Coastal Geomorphology and Resources in terms of sensitivity to oil spill in Kuwait. *Journal University of Kuwait,* 15**,** 141-184.

Al-Shemmari, H., Al Senafy, M. & Al-Fayad, K. (2002) Effects of seasonal variations on the water quality in Kuwait bay. *International Conference On Coastal Zone Management and Development.* Kuwait, EPA.

Al-Temeemi, A. A. & Harris, D. J. (2001) The generation of subsurface temperature profiles for Kuwait. *Energy and Buildings,* 33**,** 837-841.

Al-Zamel, A. Z., Al-Sarawi, M. A., Khader, S. R. & Al-Rifaiy, I. A. (2009) Benthic foraminifera from polluted marine environment of Sulaibikhat Bay (Kuwait). *Environmental Monitoring and Assessment,* 149**,** 395-409.

Al-Yamani, F. (2008) Importance of the freshwater influx from the Shatt-Al-Arab River on the Gulf marine environment In Abuzinada, A. H., Barth, H.-J., Krupp, F., Ber, B. & Abdessalaam, T. Z. A. (Eds.) *Protecting the Gulf's Marine Ecosystems from Pollution.* Verlag/Switzerland, Birkhäuser Basel, 207-222.

Al-Yamani, F., James, B., Essa, R., Al-Husaini, M. & Al-Ghadan, A. (2004) *Oceanographic atlas of Kuwait's waters,* Kuwait, KISR publication, 81-191.

Al-Yamani, F. Y., Bishop, J. M., Al-Rifaie, K. & Ismail, W. (2007) The effects of the river diversion, Mesopotamian Marsh drainage and restoration, and river

damming on the marine environment of the northwestern Arabian Gulf. *Aquatic Ecosystem Health & Management,* 10**,** 277-289.

Al-Zaidan, A. S., Jones, D. A., Al-Mohanna, S. Y. & Meakins, R. (2000) Endemic macrofauna of the Sulaibikhat Bay salt marsh and mudflat habitats, Kuwait: status and need for conservation. *International Conference of the Environment-Public-Authority on Conservation Biodiversity in the Arid Regions.* Kuwait, Academic Press Ltd Elsevier Science Ltd.

Al-Zaidan, A. S., Jones, D. A., Al-Mohanna, S. Y. & Meakins, R. (2003) Endemic macrofauna of the Sulaibikhat Bay salt marsh and mudflat habitats, Kuwait: status and need for conservation. *Journal of Arid Environments,* 54**,** 115-124.

Al-Zaidan, A. S., Kennedy, H., Jones, D. A. & Al-Mohanna, S. Y. (2006) Role of microbial mats in Sulaibikhat Bay (Kuwait) mudflat food webs: evidence from delta C-13 analysis. *Marine Ecology-Progress Series,* 308**,** 27-36.

Al Bakri, D. (1996) A geomorphological approach to sustainable planning and management of the coastal zone of Kuwait. *Geomorphology,* 17**,** 323-337.

Al Bakri, D. & Kittaneh, W. (1998) Physicochemical characteristics and pollution indicators in the intertidal zone of Kuwait: Implications for benthic ecology. *Environmental Management,* 22**,** 415-424.

Alabdulrazzaq, S. K., Shublaq, W. & Alsheikh, Z. (1982) Ostracode distribution and ecology of the Sulaibikhat Bay, Kuwait. *Marine Geology,* 47**,** 57-75.

Alawadi, F., Amos, C., Byfield, V. & Petrov, P. (2008) The application of hyperspectral image techniques on MODIS data for the detection of oil spills in the RSA. *Proceedings of the SPIE - The International Society for Optical Engineering,* 7110**,** 71100Q (12 pp.).

AlFahed, S., AlHawaj, O. & Chakroun, W. (1997) The recent air temperature rise in Kuwait. *Renewable Energy,* 12**,** 83-90.

Alhassan, L. A. J. (1987) Variations in meristic characters of *Nematalosa nasus* from Iraqi and Kuwaiti waters *Japanese Journal of Ichthyology,* 33**,** 422-425.

Alsharhan, M. (2009) The days of dust will be more than quarter of the year. *Al-Qabas Newspaper* Kuwait, Dar Al-Qabas. Available via DIALOG: http://www.alqabas.com.kw/Temp/Pages/2009/03/22/09_page.pdf.

Altinbilek, D. (2004) Development and management of the Euphrates-Tigris basin *International Journal of Water Resources Development,* 20**,** 15 - 33.

Álvarez-Robles, J. A., Zarazaga-Soria, F. J., Latre, M. A., Ruben Béjar, R. & Muro-Medrano, P. R. (2006) Water quality monitoring based on sediment distribution using satellite imagery. *9th AGILE Conference on Geographic Information Science* Visegrád, Hungary.

Amos, C. L. & Alfoeldi, T. T. (1979) The determination of suspended sediment concentration in a macrotidal system using Landsat data. *Journal of Sedimentary Research,* 49**,** 159-173.

Anderlini, V. C., Jacob, J. C. & Lee, J. W. (1982) Atlas of Physical and Chemical Oceanographic Characteristics of Kuwait Bay. Final report of the oceanographic data project. Kuwait, Kuwait Institute for Scientific Research. Report no. KISR704, 15-66.

Anderson, J. M., Duck, R. W. & McManus, J. (1995) Thermal radiometry: a rapid means of determining surface water temperature variations in lakes and reservoirs. *Journal of Hydrology,* 173**,** 131-144.

Bhat, N. R., Suleiman, M. K. & Shahid, S. A. (2004) Mangrove, *Avicennia marina*, Establishment and Growth under the Arid Climate of Kuwait *Arid Land Research and Management,* 18**,** 127 - 139.

Boyd, D. S. & Danson, F. M. (2005) Satellite remote sensing of forest resources: three decades of research development. *Progress in Physical Geography,* 29**,** 1-26.

Brekke, C. & Solberg, A. H. S. (2005) Oil spill detection by satellite remote sensing. *Remote Sensing of Environment,* 95**,** 1-13.

Burton, D. T., Richardson, L. B. & Moore, C. J. (1980) Effect of Oxygen Reduction Rate and Constant Low Dissolved Oxygen Concentrations on Two Estuarine Fish. *Transactions of the American Fisheries Society,* 109**,** 552-557.

Campbell, S. J., McKenzie, L. J. & Kerville, S. P. (2006) Photosynthetic responses of seven tropical seagrasses to elevated seawater temperature. *Journal of Experimental Marine Biology and Ecology,* 330**,** 455-468.

Chen, X., Vierling, L. & Deering, D. (2005) A simple and effective radiometric correction method to improve landscape change detection across sensors and across time. *Remote Sensing of Environment,* 98**,** 63-79.

Cho, Y.-K., Tae-Wan, K., Kwang-Woo, Y., Lae-Hwan, P., Hyung-Tae, M., Sang-Ho, L. & Yong-Hoon, Y. (2005) Temporal and spatial variabilities in the sediment temperature on the Baeksu tidal flat, Korea. *Estuarine, Coastal and Shelf Science,* 65**,** 302-308.

Coles, S. L. & Brown, B. E. (2003) Coral bleaching - Capacity for acclimatization and adaptation. *Advances in Marine Biology, 46*, 183-223.

Cox, P. M., Betts, R. A., Jones, C. D., Spall, S. A. & Totterdell, I. J. (2000) Acceleration of global warming due to carbon-cycle feedbacks in a coupled climate model. *Nature,* 408**,** 184-187.

Dames & Moore (1983) Hydraulic studies, Vol. II. Studies for Subiya area, Kuwait Bay and development of electrical networks. Ministry of Electricity and Water. Government of Kuwait, report no. MEW/CP/PGP-1113-80/81, Kuwait.

Darwish, M. A., Al-Awadhi, F. M. & Darwish, A. M. (2008) Energy and water in Kuwait Part I. A sustainability view point. *Desalination,* 225**,** 341-355.

Davies, P. A., Mofor, L. A. & Neves, M. J. V. (1997) Comparisons of remotely sensed observations with modeling predictions for the behavior of wastewater plumes from coastal discharges. *International Journal of Remote Sensing,* 18**,** 1987-2019.

Devries, A. L., Komatsu, S. K. & Feeney, R. E. (1970) Chemical and Physical Properties of Freezing Point-depressing Glycoproteins from Antarctic Fishes. *The Journal of Biological Chemistry,* 245**,** 2901-2908.

El-Fadel, M., El Sayegh, Y., Abou Ibrahim, A., Jamali, D. & El-Fadl, K. (2002) The Euphrates-Tigris basin: a case study in surface water conflict resolution. *Journal of Natural Resources & Life Sciences Educatio,* 31**,** 99-110.

El-Gamily, H. I. (2007) Utilization of multi-dates LANDSAT_TM data to detect and quantify the environmental damages in the southeastern region of Kuwait from 1990 to 1991. *Int. J. Remote Sens.,* 28**,** 1773-1788.

Elsayed, M. & Albakri, D. (1994) Geomorphology and sedimentary/ biosedimentary structures of the intertidal environment along the coast of Kuwait, north-western Arabian Gulf. *Geologische Rundschau,* 83**,** 448-463.

Elshorbagy, W. (2005) Overview of Marine Pollution in the Arabian Gulf with Emphasis on Pollutant Transport Modeling *Arabian Coast 2005 Conference "1st International Conference and Exhibition on Coastal Zone Management and Engineering in the Middle East".* Dubai, UAE.

EPA (2008) Monthly water sampling analysis reports from 1983-2007: Sea water analysis sections. Kuwait, Kuwait Environment Public Authority.

ERDAS (1999) *Earth Resources Data Analysis System,* Atlanta, Georgia, 628.

Etnoyer, P., Canny, D., Mate, B. R., Morgan, L. E., Ortega-Ortiz, J. G. & Nichols, W. J. (2004) Sea-surface temperature gradients across blue whale and sea turtle foraging trajectories off the Baja California Peninsula, Mexico. *13th Annual Meeting of the North-Pacific-Marine-Science-Organization (PICES).* Honolulu, HI, Pergamon-Elsevier Science Ltd.

Fisher, J. I. & Mustard, J. F. (2004) High spatial resolution sea surface climatology from Landsat thermal infrared data. *Remote Sensing of Environment,* 90**,** 293-307.

Fowler, J., Cohen, L. & Jarvis, P. (1998) *Practical Statistics for Field Biology,* Chichester, England, John Wiley & Sons,142-165.

Garrett, A. J. & Hayes, D. W. (1997) Cooling lake simulations compared to thermal imagery and dye tracers. *Journal of Hydraulic Engineering-Asce,* 123**,** 885-894.

Gerges, M. A. (1993) On the impacts of the 1991 Gulf War on the environment of the region: General observations. *Marine Pollution Bulletin,* 27**,** 305-314.

Giannini, A., Kushnir, Y. & Cane, M. A. (2001) Seasonality in the impact of ENSO and the north atlantic high on caribbean rainfall. *Physics and Chemistry of the Earth, Part B: Hydrology, Oceans and Atmosphere,* 26**,** 143-147.

Gischler, E., Lomando, A. J., Alhazeem, S. H., Fiebig, J., Eisenhauer, A. & Oschmann, W. (2005) Coral climate proxy data from a marginal reef area, Kuwait, northern Arabian-Persian Gulf. *Palaeogeography, Palaeoclimatology, Palaeoecology,* 228**,** 86-95.

GISS (2005) Global Temperature Trends: 2005 Summation**:** GISS Surface Temperature Analysis. New York, USA, NASA Goddard Institute for Space Studies and Columbia University Earth Institute. Available via DIALOG: http://data.giss.nasa.gov/gistemp/2005/.

Glasgow, H. B., Burkholder, J. M., Reed, R. E., Lewitus, A. J. & Kleinman, J. E. (2004) Real-time remote monitoring of water quality: a review of current applications, and advancements in sensor, telemetry, and computing technologies. *Journal of Experimental Marine Biology and Ecology,* 300**,** 409-448.

Glibert, P. M., Landsberg, J. H., Evans, J. J., Al-Sarawi, M. A., Faraj, M., Al-Jarallah, M. A., Haywood, A., Ibrahem, S., Klesius, P., Powell, C. & Shoemaker, C. (2002) A fish kill of massive proportion in Kuwait Bay, Arabian Gulf, 2001: the roles of bacterial disease, harmful algae, and eutrophication. *Harmful Algae,* 1**,** 215-231.

González, J. E., Luvall, J. C., Rickman, D., Comarazamy, D., Picón, A., Harmsen, E., Parsiani, H., Vásquez, R. E., Ramírez, N., Williams, R., Waide, R. W. & Tepley, C. A. (2005) Urban heat islands developing in coastal typical cities. *EOS,* 86**,** 397-412.

Green, E. P., Mumby, P. J., Edwards, A. J. & Clark, C. D. (2000) *Remote Sensing Handbook for Tropical Coastal Management,* Paris, UNESCO, 93-1108.

Gregory, K. & Walling, D. (1980) *Man and Environmental Processes (Studies in Physical Geography),* London, Dawson and Sons Ltd, 17-21.

Habib, K. & Fakhral-Deen, A. (2001) Risk assessment and evaluation of materials commonly used in desalination plants subjected to pollution impact of the oil spill and oil fires in marine environment. *Desalination,* 139**,** 249-253.

Han, L. & Jordan, K. J. (2005) Estimating and mapping chlorophyll-a concentration in Pensacola Bay, Florida using Landsat ETM+ data. *International Journal of Remote Sensing,* 26**,** 5245-5254.

Harrison, S. J. & Phizacklea, A. P. (1985) Seasonal changes in heat flux and heat storage forth estuary, Scotland in the intertidal mudflats of the forth estuary, scotland. *International Journal of Climatology,* 5**,** 473-485.

Harrison, S. P., Kohfeld, K. E., Roelandt, C. & Claquin, T. (2001) The role of dust in climate changes today, at the last glacial maximum and in the future. *Earth-Science Reviews,* 54**,** 43-80.

Husain, T. (1997) Terrestrial and atmospheric environment during and after the Gulf War. *Environment International,* 24**,** 189-196.

IPCC (2007) Climate Change 2007: Synthesis report, Intergovernmental Panel on Climate Change Fourth Assessment Report. Available via DIALOG: http://www.ipcc.ch/ipccreports/ar4-wg1.htm

Jacob, D. (2008) Short communication on regional climate change scenarios and their possible use for impact studies on vector-borne diseases. *Parasitology Research,* 103**,** S3-S6.

Jacob, P. G. & Zarba, M. A. (1981) Seasonal variations in plankton and related oceanographic parameters of the coastal waters of Kuwait. *Indian Journal of Marine Sciences,* 10**,** 105-111.

Jayne, S. R. & Marotzke, J. (1999) A destabilizing thermohaline circulation-atmosphere-sea ice feedback. *Journal of Climate,* 12**,** 642-651.

Jenkinson, D. S., Adams, D. E. & Wild, A. (1991) Model estimates of CO2 emissions from soil in response to global warming. *Nature,* 351**,** 304-306.

Jiang, Z.-B., Zeng, J.-N., Chen, Q.-Z., Huang, Y.-J., Liao, Y.-B., Xu, X.-Q. & Zheng, P. (2009) Potential impact of rising seawater temperature on copepods due to coastal power plants in subtropical areas. *Journal of Experimental Marine Biology and Ecology,* 368**,** 196-201.

Jones, D., Price, A., Al-Yamani, F. & Al-Zaidan, A. (2002) Coastal and marine ecology. In Khan, N. Munawar, M., and Price, A.R.G (Eds.) *The Gulf Ecosystem, Health and sustainability.* Leiden, Netherlands, Backhuys, 65-104.

K¨ampf, J. & Sadrinasab, M. (2006) The circulation of the Persian Gulf: a numerical study. *Ocean Science,* 2**,** 27-41.

Kabat, P., van Vierssen, W., Veraart, J., Vellinga, P. & Aerts, J. (2005) Climate proofing the Netherlands. *Nature,* 438**,** 283-284.

Kaufman, Y. J., Koren, I., Remer, L. A., Rosenfeld, D. & Rudich, Y. (2005) The effect of smoke, dust, and pollution aerosol on shallow cloud development over the Atlantic Ocean. *Proceedings of the National Academy of Sciences of the United States of America,* 102**,** 11207-11212.

Khalaf, F. I., Al-Kadi, A. & Al-Saleh, S. (1985) Mineralogical composition and potential sources of dust fallout deposits in Kuwait, Northern Arabian Gulf. *Sedimentary Geology,* 42**,** 255-278.

Khalaf, F. I., Alghadban, A., Alsaleh, S. & Alomran, L. (1982) Sedimentology and mineralogy of Kuwait Bay bottom sediments, Kuwait-Arabian Gulf. *Marine Geology,* 46**,** 71-99.

Khan, N. Y. (2006) Multiple stressors and ecosystem-based management in the Gulf. *1st International Conference on the State of the Gulf Ecosystems.* Al Ain, UAE, Taylor & Francis Inc.

Khan, T. M. A., Quadir, B. A., Murty, T. S. & Sarker, M. A. (2004) Seasonal and interannual sea surface temperature variability in the coastal cities of Arabian Sea and Bay of Bengal. *Natural Hazards,* 31**,** 549-560.

Khordagui, H. & Alajmi, D. (1993) Environmental impact of the Gulf War: An integrated preliminary assessment. *Environmental Management,* 17**,** 557-562.

Kloiber, S. M., Brezonik, P. L., Olmanson, L. G. & Bauer, M. E. (2002) A procedure for regional lake water clarity assessment using Landsat multispectral data. *Remote Sensing of Environment,* 82**,** 38-47.

Knauss, J. A. (1997) *Introduction to Physical Oceanography,* New Jersey, Prentice Hall, 1-12.

Kothawale, D. R., Munot, A. A. & Borgaonkar, H. P. (2008) Temperature variability over the Indian Ocean and its relationship with Indian summer monsoon rainfall. *Theoretical and Applied Climatology,* 92**,** 31-45.

Kwarteng, A. Y., Viswanathan, M. N., Al-Senafy, M. N. & Rashid, T. (2000) Formation of fresh ground-water lenses in northern Kuwait. *Journal of Arid Environments,* 46**,** 137-155.

Lardner, R. W., Alrabeh, A. H., Gunay, N., Hossain, M., Reynolds, R. M. & Lehr, W. J. (1993) Computation of the residual flow in the Gulf using the Mt. Mitchell data and the KFUPM/RI hydrodynamical models. *Marine Pollution Bulletin,* 27**,** 61-70.

Lawrence, S. P., Llewellyn-Jones, D. T. & Smith, S. J. (2004) The measurement of climate change using data from the Advanced Very High Resolution and

Along Track Scanning Radiometers. *Journal of Geophysical Research,* 109, C08017.

Leake, J. (2009) Cities to sizzle as islands of heat. *Times Online.* London, Times Online. Available via DIALOG: http://www.timesonline.co.uk/tol/news/environment/article6256520.ece

Lécuyer, C., Grandjean, P., Paris, F., Robardet, M. & Robineau, D. (1996) Deciphering "temperature" and "salinity" from biogenic phosphates: the [delta]18O of coexisting fishes and mammals of the Middle Miocene sea of western France. *Palaeogeography, Palaeoclimatology, Palaeoecology,* 126**,** 61-74.

Lillesand, T. M. & Kiefer, R. W. (1987) *Remote Sensing and Image Interpretation,* Toronto, John Wiley and Sons, 4-16.

Literathy, P. (1993) Considerations for the assessement of environmental consequences of the 1991 Gulf War. *Marine Pollution Bulletin,* 27**,** 349-356.

Mahiko ABE, A. K., Miyuki MAEGAWA, (2008) High water-temperature tolerance in photosynthetic activity of Zostera marina seedlings from Ise Bay, Mie Prefecture, central Japan. *Fisheries Science,* 74**,** 1017-1023.

Manabe, S. & Stouffer, R. J. (1980) Sensitivity of a Global Climate Model to an Increase of CO2 Concentration in the Atmosphere. *Journal of Geophysical Research.,* 85**,** 5529-5554.

Marmoush, Y. R. (1999) Environmental management of coastal development, State of Kuwait. *Water Science and Technology,* 40**,** 47-53.

Matthews, K. R. & Berg, N. H. (1997) Rainbow trout responses to water temperature and dissolved oxygen stress in two southern California stream pools. *Journal of Fish Biology,* 50**,** 50-67.

Maxwell, C. F. (2006) The role of comparative risk assessment in decision analysis Marshlands of Mesopotamia and affected riparian countries. *Environmental Security and Environmental Management: The Role of Risk Assessment,* 5**,** 59-77.

McKinnell, S. M. & Crawford, W. R. (2007) The 18.6-year lunar nodal cycle and surface temperature variability in the northeast Pacific. *Journal of Geophysical Research-Oceans,* 112.

Ministry of Planning (2005) Annual Statistical Abstract. Central Statistical office, Kuwait, 41, 47.

Moqsud, A., Shigenori Hayashi, Yan Jun Du & Suetsugu, D. (2008) Appraisal of Thermal Properties of Mud in the Ariake Sea, Japan. *American Journal of Environmental Sciences,* 4**,** 129-135.

Morton, A. J., Callister, I. K. & Wade, N. M. (1997) Environmental impacts of seawater distillation and reverse osmosis processes. *Desalination,* 108**,** 1-10.

Mubarak, A. & Kubryakov, A. (2000) Hydrological structure of waters of the Persian Gulf according to the data of observations in 1992 *Physical Oceanography,* 11**,** 459-471.

Naidu, P. D. (2006) Link between western Arabian Sea surface temperature and summer monsoon strength and high-latitude abrupt climate events. *Journal of the Geological Society of India,* 68**,** 379-385.

NASA (2009a) Landsat 7 Science Data Users Handbook. *National Eeronautics and Space Administration.* Washington, DC. Available via DIALOG: http://landsathandbook.gsfc.nasa.gov/handbook.html.

NASA (2009b) MODIS WEB. *National Eeronautics and Space Administration.* Washington, DC NASA. Available via DIALOG: http://modis.gsfc.nasa.gov/.

Nasrallah, H. A., Nieplova, E. & Ramadan, E. (2004) Warm season extreme temperature events in Kuwait. *Journal of Arid Environments,* 56**,** 357-371.

Nature (2006) Regional Climate Change. *Nature*. Available via DIALOG: http://www.nature.com/news/specials/regionalclimatechange/index.html.

NCDC (2009) National Climate Data Center *NOAA Satellite and Information Services* Asheville, USA. Available via DIALOG: http://www.ncdc.noaa.gov/oa/ncdc.html.

Nelson, S. A. C., Soranno, P. A., Cheruvelil, K. S., Batzli, S. A. & Skole, D. L. (2003) Regional assessment of lake water clarity using satellite remote sensing. *Journal of Limnology,* 62**,** 27-32.

Newson, T. A. & Brunning, P. (2004) Thermal conductivity of deepwater offshore sediments. *International Journal of Offshore and Polar Engineering,* 14**,** 310-314.

NOAA (2009) Advanced Very High Resolution Radiometer - AVHRR. *NOAA Satellite and information service* Maryland, USA, NOAA. Available via DIALOG: http://noaasis.noaa.gov/NOAASIS/ml/avhrr.html.

Notarstefano, G., Mauri, E. & Poulain, P.-M. (2006) Near-surface thermal structure and surface diurnal warming in the Adriatic Sea using satellite and drifter data. *Remote Sensing of Environment,* 101**,** 194-211.

Olthof, I., Butson, C. & Fraser, R. (2005) Signature extension through space for northern landcover classification: A comparison of radiometric correction methods. *Remote Sensing of Environment,* 95**,** 290-302.

Paula, J., Dornelas, M. & Flores, A. A. V. (2003) Stratified settlement and moulting competency of brachyuran megalopae in Ponta Rasa mangrove swamp,

Inhaca Island (Mozambique). *Estuarine, Coastal and Shelf Science,* 56**,** 325-337.

Pearce, A. & Feng, M. (2007) Observations of warming on the Western Australian continental shelf. *Marine and Freshwater Research,* 58**,** 914-920.

Piccolo, M. C., Perillo, G. M. E. & Daborn, G. R. (1993) Soil Temperature Variations on a Tidal Flat in Minas Basin, Bay of Fundy, Canada. *Estuarine, Coastal and Shelf Science,* 36**,** 345-357.

PO.DAAC (2009) Physical Oceanography Distributed Active Archive Centre, Jet Propulsion Laboratory. *Physical Oceanography Distributed Active Archive Center*. NASA. Available via DIALOG: http://poet.jpl.nasa.gov/.

Prakash, S. & Ramesh, R. (2007) Is the Arabian Sea getting more productive? *Current science,* 92**,** 667-671

Price, A. R. G. (1998) Impact of the 1991 Gulf War on the coastal environment and ecosystems: Current status and future prospects. *Environment International,* 24**,** 91-96.

Pugh, D. T. (1996) *Tides, Surges and Mean Sea-Level,* Chichester, UK, John Wiley & Sons Ltd, 486.

Rakha, K., Al-Salem, K. & Neelamani, S. (2007) Hydrodynamic Atlas for the Arabian Gulf. *Journal of Coastal Research,* SI 50**,** 550 - 554.

Rakha, K., K.Al-Banaa & Al-Rashidi, T. (2009) Modeling of Doha Power Plant Outfall in Kuwait Bay. *33nd Congress of IAHR*. Vancouver, Canada.

Ralph, P. J. (1998) Photosynthetic response of laboratory-cultured Halophila ovalis to thermal stress. *Marine Ecology Progress Series,* 171**,** 123-130.

Rao, D. V. S., Al-Yamani, F., Lennox, A., Pan, Y. L. & Al-Said, T. F. O. (1999) Biomass and production characteristics of the first red tide noticed in Kuwait Bay, Arabian Gulf. *Journal of Plankton Research,* 21**,** 805-810.

Rayner, N. A., Brohan, P., Parker, D. E., Folland, C. K., Kennedy, J. J., Vanicek, M., Ansell, T. J. & Tett, S. F. B. (2006) Improved Analyses of Changes and Uncertainties in Sea Surface Temperature Measured In Situ since the Mid-Nineteenth Century: The HadSST2 Dataset. *Journal of Climate,* 19**,** 446-469.

Readman, J. W., Fowler, S. W., Villeneuve, J. P., Cattini, C., Oregioni, B. & Mee, L. D. (1992) Oil and combustion-product contamination of the Gulf marine environment following the war. *Nature,* 358**,** 662-665.

Reinart, A. & Reinhold, M. (2008) Mapping surface temperature in large lakes with MODIS data. *Remote Sensing of Environment,* 112**,** 603-611.

Reynolds, R. M. (1993) Physical oceanography of the Gulf, Strait of Hormuz, and the Gulf of Oman--Results from the Mt Mitchell expedition. *Marine Pollution Bulletin,* 27**,** 35-59.

Reynolds, R. M. (2002) Oceanography. In Khan, N., Maunawar, M. & Price, A. (Eds.) *The Gulf Ecosystem: Health and Sustainability.* Leiden, , Netherlands, Backhuys, 41-51.

Rezai, H., Wilson, S., Claereboudt, M. & Riegl, B. (2004) Coral reef status in the Ropme Sea area: Arabian/Persian Gulf, Gulf of Oman and Arabian Sea. *Status of Coral Reefs of the World: 2004.* Townsville, Queensland, Australia, Australian Institute of Marine Science, 155-170.

Richards, J. A. (1986) *Remote Sensing Digital Image Analysis: An Introduction,* Berlin, Springer, 363.

Riegl, B. (2002) Effects of the 1996 and 1998 positive sea-surface temperature anomalies on corals, coral diseases and fish in the Arabian Gulf (Dubai, UAE). *Marine Biology,* 140**,** 29 - 40.

Riegl, B. (2003) Climate change and coral reefs: different effects in two high-latitude areas (Arabian Gulf, South Africa). *Coral Reefs,* 22**,** 433-446.

Robinson, A. & Brink, K. (2006) *The Global Coastal Ocean, Interdisciplinary Regional Studies and Syntheses. The Sea: Ideas and Observation on Progress in The Study of The Seas,* MA, USA, Harvard University Press, Cambridge, 1375-1385.

Robinson, I. (2004) *Measuring the Ocean from Space: The Principles and Methods of Satellite Oceanography,* UK, Praxis Publishing, Springer pp.280

Robinson, I. S. & Donlon, C. J. (2003) Global measurement of sea surface temperature from space: Some new perspectives. *Journal of Atmospheric & Ocean Science,* 9**,** 19 - 37.

Saad, H. R. & Al-Azmi, D. (2002) Radioactivity concentrations in sediments and their correlation to the coastal structure in Kuwait. *Applied Radiation and Isotopes,* 56**,** 991-997.

Saeed, T., Khordagui, H. & Al-Hashash, H. (1999) Contribution of power and desalination plants to the levels of volatile liquid hydrocarbons in the nearby coastal areas of Kuwait. *Environment International,* 25**,** 553-562.

Sanderson, P. G. (2009) The application of satellite remote sensing to coastal management in Singapore. *AMBIO: A Journal of the Human Environment,* 30**,** 43-48.

Sheppard, C. & Loughland, R. (2002) Coral mortality and recovery in response to increasing temperature in the southern Arabian Gulf. *Aquatic Ecosystem Health & Management,* 5**,** 395 - 402.

Sheppard, C. & Rayner, N. A. (2002) Utility of the Hadley Centre sea ice and sea surface temperature data set (HadISST1) in two widely contrasting coral reef areas. *Marine Pollution Bulletin,* 44**,** 303-308.

Signatrol (2009) Data loggers and Data Logging Solutions. Tewkesbury, UK. Available via DIALOG: http://www.signatrol.com/.

Smith, R., Purnama, A. & Al-Barwani, H. H. (2007) Sensitivity of hypersaline Arabian Gulf to seawater desalination plants. *Applied Mathematical Modelling,* 31**,** 2347-2354.

Smith, T. M., Reynolds, R. W., Peterson, T. C. & Lawrimore, J. (2008) Improvements to NOAA's historical merged land-ocean surface. Temperature analysis (1880-2006). *Journal of Climate,* 21**,** 2283-2296.

Smith, W. L., Knuteson, R. O., Revercomb, H. E., Feltz, W., Howell, H. B., Menzel, W. P., Nalli, N. R., Brown, O., Brown, J., Minnett, P. & McKeown, W. (1996) Observations of the infrared radiative properties of the ocean - Implications for the measurement of sea surface temperature via satellite remote sensing. *Bulletin of the American Meteorological Society,* 77**,** 41-51.

Stenseth, N. C., Mysterud, A., Ottersen, G., Hurrell, J. W., Chan, K.-S. & Lima, M. (2002) Ecological effects of climate fluctuations. *Science,* 297**,** 1292-1296.

Stuart-Menteth, A. C., Robinson, I. S. & Challenor, P. G. (2003) A global study of diurnal warming using satellite-derived sea surface temperature. *Journal of Geophysical Research-Oceans,* 108**,** 16.

Subrahmanyam, B., Heffner, D. M., Cromwell, D. & Shriver, J. F. (2009) Detection of Rossby waves in multi-parameters in multi-mission satellite observations and HYCOM simulations in the Indian Ocean. *Remote Sensing of Environment,* 113**,** 1293-1303.

Sverdrup, H. U. (1945) *Oceanography for Meteorologists,* London, George allen Unwin LTD, 10-35.

Sverdrup, H. U., Johnson, M. W. & Fleming, R. H. (1942) *The Oceans, Their Physics, Chemistry, and General Biology,* New York, Prentice Hall, 54.

Swift, S. A. & Bower, A. S. (2003) Formation and circulation of dense water in the Persian/Arabian Gulf. *Journal of Geophysical Research,* 107**,** 4-1-21.

Tharp, M. (2009) Sandstorms plague Iraq and are getting worse. *McClatchy Newspapers* Washington, DC, McClatchy's Washington Bureau. Available via DIALOG: http://www.mcclatchydc.com/iraq/story/71277.html

Thomas, A., Byrne, D. & Weatherbee, R. (2002) Coastal sea surface temperature variability from Landsat infrared data. *Remote Sensing of Environment,* 81**,** 262-272.

Trenberth, K. E., P.D. Jones, P. Ambenje, R. Bojariu, D., Easterling, A., Klein Tank, D., Parker, F., Rahimzadeh, J. A., Renwick, M. R. & Zhai, B. S. a. P. (2007) Observations: Surface and Atmospheric Climate Change. In: *Climate Change 2007: The Physical Science Basis*. Contribution of Working Group I to the Fourth Assessment Report of the Intergovernmental Panel on Climate Change [Solomon, S., D. Qin, M. Manning, Z. Chen, M. Marquis, K.B. Averyt, M. Tignor and H.L. Miller (eds.)]. Cambridge University Press, Cambridge, United Kingdom and New York, NY, USA.

UNEP (2006) International workshop on sustainable management of the Iraqi marshlands- summery report. United Nations Environment Programme. Available via DIALOG: http://marshlands.unep.or.jp/default.asp?site=marshlands&page_id=0A4BF2ED-34A8-4E86-A296-98C13E473D7D

USGS (2009) Landsat Missions. *US Geological Survey*. Reston, USA . Available via DIALOG: http://landsat.usgs.gov/

Vicente-Serrano, S. M., Pérez-Cabello, F. & Lasanta, T. (2008) Assessment of radiometric correction techniques in analyzing vegetation variability and change using time series of Landsat images. *Remote Sensing of Environment,* 112**,** 3916-3934.

Weiss, R. F. (1970) The solubility of nitrogen, oxygen and argon in water and seawater. *Deep Sea Research,* 17**,** 721-735.

Wilkie, D. S. & Finn, J. T. (1996) *Remote Sensing Imagery for Natural Resources Monitoring,* New York, Columbia University Press, 295.

Wilkinson, C. (2000) *Status of Coral Reefs of the World: 2000,* Townsville, Australia, Australian Institute of Marine Science, and Global Coral Reef Monitoring Network, 363.

Yanagi, T. (2008) Great water temperature changes of 1.5 ºC per decade in Tokyo Bay, Japan - its causes and consequences. *Journal of Disaster Research,* 3**,** 113-118.

Yndestad, H. (2008) The influence of long tides on ecosystem dynamics in the Barents Sea. *Deep Sea Research Part II: Topical Studies in Oceanography,* In Press, Corrected Proof.

Zafiratos, C. (1976) *Physics,* New York, John Wiley & Sons, 398-401.

Ziervogel, G., Downing, T. E. & Patwardhan, A. (2003) Linking Global and Local Scenarios under Climate Change Stockholm, Sweden, Stockholm Environment Institute, 1-5.